Final Report

Bio-Sorption Activated Media Filtration to Reduce Nutrients and Algal Mass

Florida Department of Environmental Protection:

Project Agreement No. INV008

Submitted by

Principal Investigator: Ni-Bin Chang

Co-Principal Investigators: Debra Reinhart and AHM Anwar Sadmani

Andrea Valencia, Wei Zhang, Diana Ordonez, Jinxiang Cheng, Mohamad Odeh, Touhidul Islam, Alejandra Robles Lecompte, and Rohan Gudla

Staff and Students:

Feb., 2024

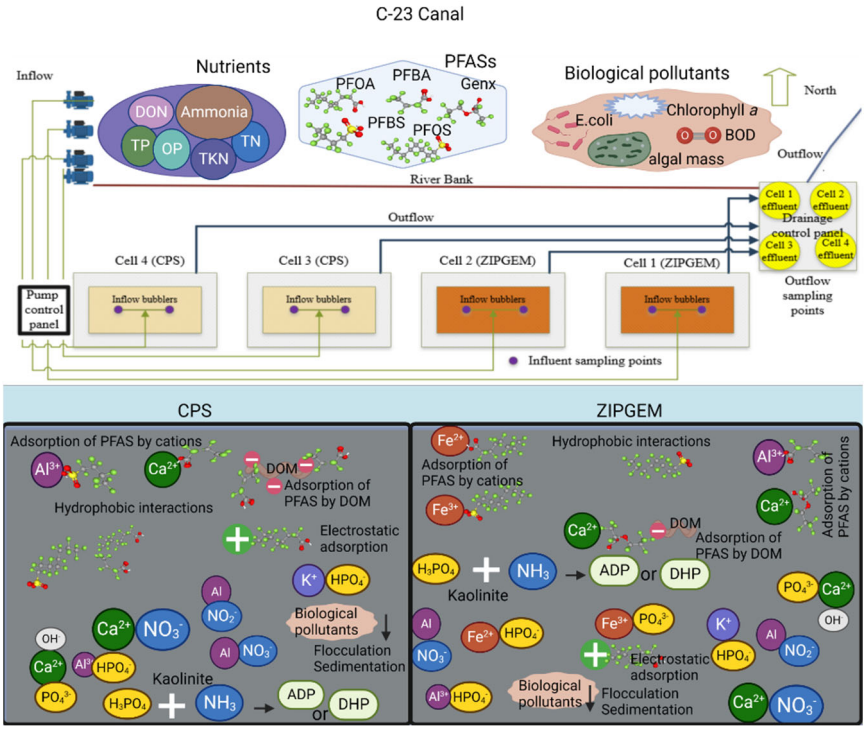

This report was funded under the Innovative Technologies for Harmful Algal Blooms Program through a grant agreement from the Florida Department of Environmental Protection. The views, statements, findings, conclusions, and recommendations expressed herein are those of the author(s) and do not necessarily reflect the views of the State of Florida or any of its subagencies.

Table of Contents

Lists of Figures

Lists of Tables

Executive Summary

The goal of this project is to demonstrate the laboratory-scale development and field-scale applications of two green sorption media (GSM) for multipollutant removal via a biofiltration system to treat the water in Canal 23 within the St. Lucie River Basin. C-23 has been classified as impaired waterbody linked to high TP by the State Impaired Rule. The quality of the canal water was impacted by upstream agricultural discharge and urban stormwater runoff. These specialty adsorbents (i.e., GSM) mixed with natural and recycled materials such as iron filings are cost-effective, sustainable, scalable, and adaptable for water treatment. Funding of $2 million was awarded for this project by the Florida Department of Environmental Protection under the FY 20-24 solicitation. The project supports the existing total maximum daily load (TMDL) program in which the endpoints in the St. Lucie River Basin are to achieve TN target (0.72 $mg \bullet L^{-1}$), TP target (0.081 $mg \bullet L^{-1}$), and biochemical oxygen demand (BOD) target (2.0 $mg \bullet L^{-1}$).

This report presents the performance assessment of a new filtration system containing two GSM, including clay-perlite-sand (CPS) and zero-valent iron (ZVI) and perlite green environmental media (ZIPGEM) when treating C-23 canal water, followed by estimations of the life expectancy of the filtration cells based on laboratory test results. The removal efficiencies of nutrients and algal mass by ZIPGEM and CPS were the focus; however, both biological pollutants and per- and polyfluoroalkyl substances (PFAS) that are persistent and less mobile in the environment result in public health and ecological risks. The removal efficiencies of biological pollutants (e.g., E. coli, Chlorophyll a, and algal mass) and long-chain PFAS [e.g., Perfluorooctanoic acid (PFOA); and Perfluorooctanesulfonic acid (PFOS)] were also evaluated in this project.

The field work of this project included site screening and planning, design, permitting, construction, testing, operation, and decommissioning. Ten field campaigns for manual sampling during the operation stage were conducted to verify the basic functionality of the filtration cells and assess their performances under field conditions in both dry and wet seasons in 2023. Four filter cells were installed, containing two types of green sorption media: ZIPGEM in Cells 1 and 2 and CPS in Cells 3 and 4. CPS served as a control for the performance assessment facilitating statistically significant comparison of data obtained from the filter cells of ZIPGEM. The first field campaign was conducted on Wednesday, March 1, 2023, followed by the remaining nine field campaigns through July 3, 2023 in accordance with the work plan of this project. All field campaigns involved the collection of water samples at the filter influent and effluent locations and media samples, which were analyzed in accordance with the QAPP. The available results for collected water samples in all field campaigns support the performance assessment of treatment cells and confirmed the efficacy of the two GSM.

Research findings indicate that the performance of ZIPGEM is better in comparison to CPS, achieving concurrent removal of nutrients, including total nitrogen (TN), total Kjeldahl nitrogen (TKN) (the sum of organic nitrogen and ammonia nitrogen), total phosphorus (TP), dissolved organic nitrogen (DON), and orthophosphate (OP). Based on a total of the ten sampling events, the average removal rates of TN, TKN, ammonia, ZIPGEM represents an effective media mix in comparison to CPS, achieving concurrent removal of nutrients, including total nitrogen (TN), total Kjeldahl nitrogen (TKN) (the sum of organic nitrogen and ammonia nitrogen), total phosphorus (TP), dissolved organic nitrogen (DON), and orthophosphate (OP).58%, and 73.16%, respectively. ZIPGEM demonstrated average removal rates of 53.86% for TN, 69.77% for TKN, -118.52% for ammonia, 75.43% for DON, 79.58% for TP, and 73.16% for OP. These removal

efficiencies significantly surpassed those achieved by CPS. The negative removal rate of ammonia can be attributed to the degradation of DON, particularly through processes such as photoammonification and mineralization, occurring within the filter, especially during the wet season. However, the performance of both green sorption media in the proposed filtration system at the field scale exhibited comparability for E. coli (80%) and chlorophyll a (95%), showcasing considerable potential for environmental remediation and watershed restoration. Moreover, ZIPGEM exhibited a high removal efficiency for Perfluorooctane sulfonic acid (PFOS), a long-chain per- and polyfluoroalkyl substances (PFAS) species, in canal water, suggesting its suitability for PFOS removal.

To ascertain the longevity of the media for the removal of nutrient, PFAS, and algal toxin (e.g., microcystin, if present in the canal water) removal, laboratory-scale isotherm and column tests were conducted. The media adsorption capacity for target pollutants, including TN, TP, microcystin, and two PFAS species were determined. The adsorption capacity indicates the mass of media needed per milligram of pollutant to be removed and serves as the basis for estimating filter media life expectancy given the current water matrix in C-23. The highest life expectancy values were observed for TP removal, with ZIPGEM exhibiting a service life of 88.7 years compared to CPS's 11.0 years, based on the current media volume at the field-scale filter in the St. Lucie River Basin. is driven mainly by the presence of microorganisms and their involvement in the nitrogen cycle. Considering the renewable life expectancy for TN removal, attributable to the dominance of microorganisms and their involvement in the nitrogen cycle, the nitrification and denitrification processes within the filter media were elucidated through microbial population dynamics, as determined by real-time polymerase chain reaction. Based on the life expectancy estimation, a cost-benefit analysis was conducted for CPS and ZIPGEM separately.

ACKNOWLEDGEMENT

The University of Central Florida research team appreciates the funding support and technical guidance from the Florida Department of Environmental Protection (FDEP). The funding provided the opportunity to support students and faculty in their pursuit of knowledge and data related to the use of two green sorption media for water quality improvement at the St. Lucie River Basin, Florida. In addition, the authors recognize the administrative assistance from the project and program managers at FDEP offered immense help with the contract amendments owing to the COVID-19 pandemic and on-campus lock down, change of media recipes, adjustment from sole source to open bidding, permit applications, sporadic hurricane landfalls, media supply chain issue during the inflation impact, and on-campus hiring freeze due to the Florida Foreign Influence Act in the project period. The authors are grateful for Dr. Del Bottcher (the President of the Soil and Water Engineering Technology Inc.) who provided excellent consulting services during permitting, design, and construction oversight. The authors also acknowledge the professional services provided by Enviro-Tech Systems, Inc., including the construction, maintenance, and decommissioning of the filter, especially during the two hurricane landfall events in fall 2022. The University of Central Florida provided Shared Research Facilities Fund for material characterization and administrative coordination for financial management, project management, and laboratory safety training for algal toxin analysis.

Chapter 1: Introduction

1.1 Research Motivation

The production of clean water is emphasized under the United Nations goals for sustainable development (SDGs), recognizing the acute need of developing new sustainable technologies in all disciplines. SDGs call for all engineers in the 21st century to design systems which mitigate pollution of drinking water sources and prevent all receiving waterbodies from the impact of agriculture discharge, wastewater effluent, and stormwater runoff. Given that 21% of lakes in the United States suffer from excessive phosphorus and nitrogen loading, the United States Environmental Protection Agency (USEPA) has established comprehensive quality criteria for water usage in human health, aquatic life, wildlife, agricultural, and industrial sectors (Giri, 2021). Consequently, the USEPA has devised "Best Management Practices (BMPs)" to mitigate elevated nutrient concentrations (Wen, 2019; Wen et al., 2020). However, water matrix constituents that may be of concern include not only nutrients [i.e., total nitrogen (TN) and total phosphate (TP)], but also natural organic matters [e.g., total organic carbon (TOC), tannic acid], heavy metals (i.e., copper, calcium), harmful algae toxins (e.g., microcystin), and contaminants of emerging concern [i.e., Per- and polyfluoroalkyl substances (PFAS), pharmaceuticals, endocrine disrupting chemicals, personal care products]. Existing water treatment technologies for the removal of the above pollutants, such as activated carbon, ion exchange, and membrane filtration, are too expensive to be applied at the watershed scale. This study presents the latest advancements in a suite of in-situ cost-effective, scalable, and fit-for-purpose green sorption media (GSM) – specialty adsorbents – designed to simultaneously remove PFAS, TN, TP, and biological pollutants [e.g., E. coli, Chlorophyl a, biochemical oxygen demand (BOD), algal toxins, and algal mass] through synergistic effects of different specialty ingredients.

Biofiltration media, such as GSM mixed with natural and recycled material, has been applied for nutrient removal from water for over a decade (Ordonez et al., 2023). Various media recipes employed enables physical, chemical, and microbiological mechanisms for pollutant removal from stormwater runoff, wastewater effluent, and agricultural discharge. The media mix employed enables physical, chemical, and biological mechanisms for stormwater pollutant removal. For instance, Ca, Al, K, and Fe filings facilitate phosphorus removal through chemical adsorption and precipitation (Xuan et al., 2009; Wen et al., 2020), while the activities of certain nitrifying and denitrifying bacteria contribute to ammonia, nitrite, and nitrate removal (Chang et al., 2010a). Consequently, the composition of the media, with its synergistic effects, plays a crucial role in controlling nutrient removal rates and efficiency, warranting further in-depth research.

1.2 Literature Review

The Stormwater Management Academy at the University of Central Florida (UCF) has developed a series of GSM which have been continually updated and enhanced to increase pollutant removal rates and cost-effectiveness of the media. These recipes of GSM vary in their features, such as physical particle properties, chemical composition, and microorganism growth for nitrification and denitrification. Figure 1-1 summarizes the history of the GSM developed by the Stormwater Management Academy at the UCF. As of Dec. 2022, these media have been applied to over 300 sites in southeast United States for the treatment of stormwater runoff, wastewater effluent, and agricultural discharge via both lab-scale tests and field-scale studies as the world needs cost-effective and sustainable solutions for surface water and groundwater treatment continuously.

1.2.1 Stage 1: Early development of the GSM

Wanielista and Chang (2008) proposed the first recipe of GSM composed of seven components (peat, sandy loam, sawdust, wood chip, tire crumb, crushed limestone, and crusted oyster) for nutrient removal from stormwater runoff and groundwater. To improve the removal efficiency of nutrients, researchers explored different combination of adsorption ingredients for nutrient removal. To obtain the baseline information, Lin et al. (2008) used nanoscale zero-valent iron (NZVI) for nitrate removal at laboratory scale for nitrite and nitrate removal from water and the nitrite and nitrate removal efficiencies using NZVI were found 65-83% and 51-68%, respectively based on three different initial concentrations. Ryan et al. (2009) proposed a GSM recipe composed of 45% expanded clay, 45% recycled tire crumb, and 10% sawdust with removal efficiencies of 37% Total nitrogen (TN), 79% Ortho-phosphorus, and 69% TP. Chang et al. (2010b) developed two GSM (i.e., expanded clay growth and pollution control media) that were applied to a subsurface upflow wetland for nutrient and pathogen removal. In combination with Cannas plants, the wetland removed 97% TN, 98% TP, 99% E. coli, and 100% in wastewater effluent. Such media mix was known as biosorption activated media (BAM). In the same year, Hossain et al (2010) explored the effect of sand particle size (between fine and coarse) to avoid clogging the media, and obtained the highest removal efficiencies of 60% ammonium, 49% total Kjeldahl nitrogen (TKN), 42% TN, 92% soluble reactive phosphorus (SRP) and 87% TP.

Chang et al. (2011) explored two new media mixes with fine sand, crumb, sawdust, and limestone under different temperatures (10°C, 23°C, and 28°C) and obtained 63~70%, 78~80%, and 94 ~ 95% of nitrate removal efficiencies, respectively. According to Chang et al. (2016), an upflow floating reactor was conducted to analyze TN and TP removal efficiency using a new GSM, composed of 50% fine sand, 20% fine expanded clay, 20% recycled tire crumb, and 10%

limestone. The removal efficiencies varied between -91% to 30% for TN and 25% to 69% for TP, and the negative results were a response to storm events flushing nutrients into the pond.

1.2.2 Stage 2: Recent development of the GSM

Wen (2019) updated the recipes of GSM with the inclusion of iron filings (i.e., zero-valent-iron (ZVI), recycled materials) and proposed two new recipes (IFGEM-1 and IFGEM-2) for nutrient removal under different field conditions. These new recipes were denoted as iron filings-based green environmental media (IFGEM) (Wen et al., 2020). IFGEM-1 was composed of 96.2% fine sand and 3.8% iron filings, whereas IFGEM-2 consisted of 80% sand, 10% tire crumb, 5% pure clay, and 5% iron filings with removal efficiencies of 40 to 91% for nitrate, 50 to 80% for TP, 91% for nitrate, and 25 to 80% TP, respectively. This finding of 91% removal for nitrate is comparable with the laboratory-scale results in Zhang et al. (2011) that over 90% of nitrate was removed from the stormwater runoff by nanoscale ZVI coated on pillared clay. However, the use of iron filings is much cheaper than nanoscale ZVI particles.

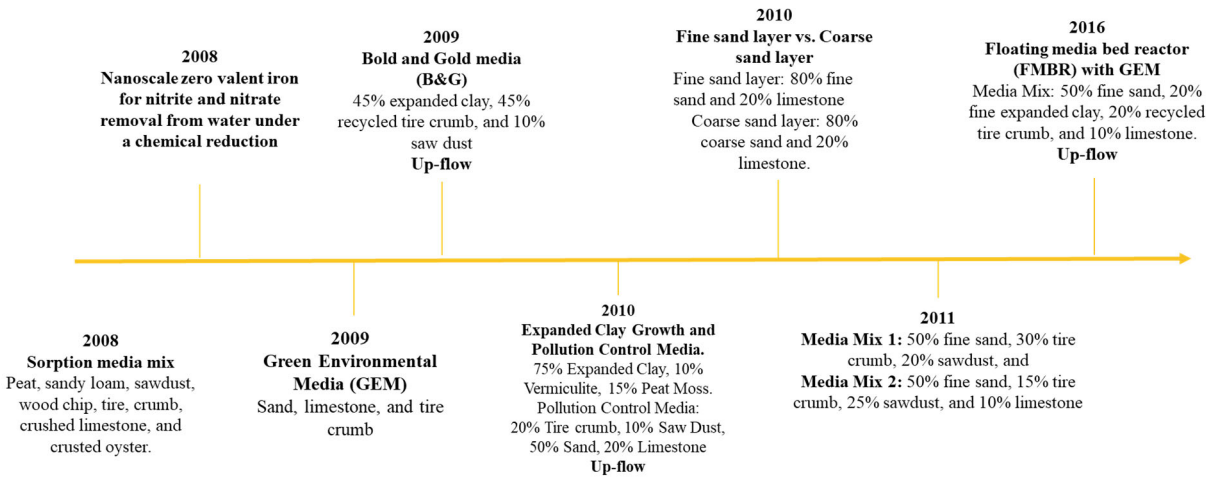

(a) Stage 1: Early development of the GSM

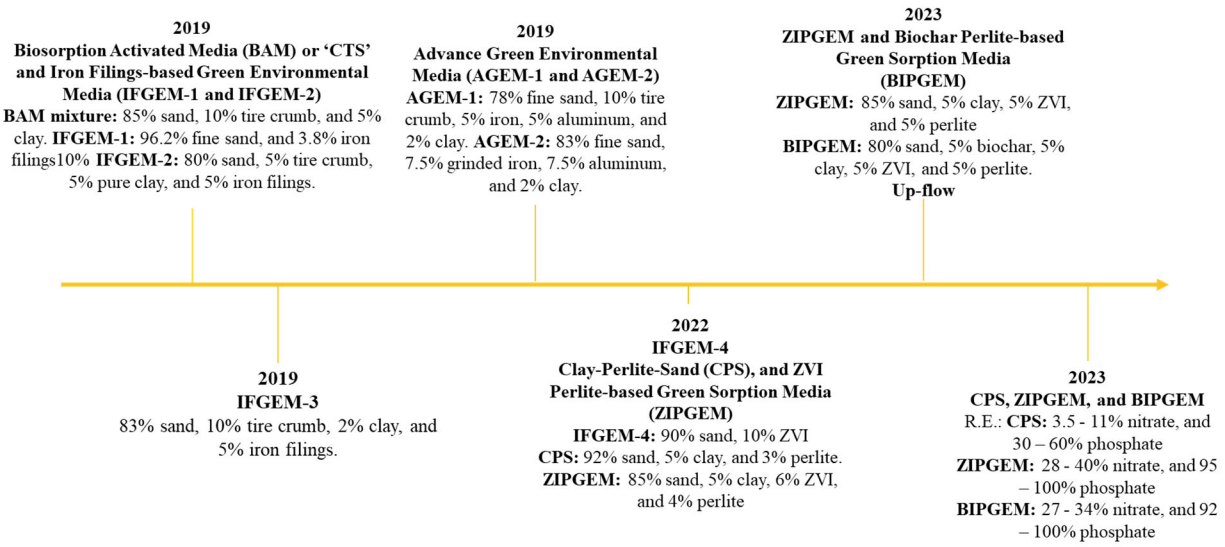

(b) Stage 2: Recent trend of the GSM

Figure 1-1: Chronological development of GSM at UCF.

Then IFGEM-3 media mix (with 83% sand, 10% tire crumb, 2% clay, and 5% iron filings) was tested by Valencia et al. (2019) after testing similar media mixture at varying clay percentages (2%, 4%, 6%, and 8%). IFGEM-3 with 2% clay resulted in the highest removal efficiencies for TN and ammonia (95~98% ammonia, 91~94% TN). The relationship between dissolved organic nitrogen (DON) removal and microbial abundance in IFGEM for stormwater treatment was investigated for both physicochemical and microbiological processes (Valencia et al., 2020). Many similar recipes were tested and analyzed in subsequent studies. For example, new media mixtures known as advanced green environmental media (AGEM) were tested at UCF, in which AGEM-1 and AGEM-2 were tested for nitrogen, phosphorus, and ammonia removal simultaneously (Ordonez et al., 2020a). AGEM-1 was composed of 78% fine sand, 10% tire crumb, 5% iron fillings, 5% aluminum fillings, and 2% clay, whereas AGEM-2 consisted of 78% fine sand, 10% tire crumb, 7.5% grinded iron fillings, 5% aluminum powder fillings, and 2% clay (Elhakiem, 2019). It is notable that 30~40% TN and 96~100% TP removal by AGEM-1 was

achieved, whereas 71~85% TN and 97-98% TP removal was achieved by AGEM-2. Extended studies of GSM were conducted to address pollutant removal from stormwater runoff and groundwater during the last few years (Chang et al., 2018a, 2018b, 2019; Wen et al., 2020).

To enhance the IFGEM recipe, Ordonez et al. (2022a) tested three different media mixtures, including IFGEM-4, clay-perlite-sand (CPS), and zero valent iron and perlite-based green environmental media (ZIPGEM). IFGEM-4 was composed of 90% sand, and 10% ZVI as a control for comparison to CPS; CPS consisted of 92% sand, 5% clay, and 3% perlite, ZIPGEM of 85% sand, 5% clay, 6% ZVI, and 4% perlite. These media mixtures were explored originally only for color (tannic acid) removal from drinking water sources; ZIPGEM was ranked the best GSM for color removal followed by IFGEM-1, IFGEM-4, BAM, and CPS (Ordonez et al., 2022a). The efficacy of adsorption by the three green sorption media of phosphorous removal from river water was explored further by Ordonez et al. (2023). Sometimes, clogging issues present in the downflow filtration systems reduced the hydraulic loading rate and an upflow filtration design was proposed as an alternative. Thus, Kilgus-Vesely (2023) explored a cascade upflow biofiltration system filled with biochar-ZVI-perlite integrated green environmental media (BIPGEM) in parallel with ZIPGEM for phosphate removal in stormwater runoff and obtained phosphate removal efficiencies of 83~91% for BIPGEM and 86~100% for ZIPGEM, respectively.

1.3 Project Implementation and Management

1.3.1 Goals and Objectives

The overarching goal of this study is to develop cost-effective, scalable, adaptable, sustainable, and fit-for-purpose GSM (i.e., specialty adsorbents) for treating stormwater runoff and agricultural discharge within a canal corridor via a biofiltration system. The project objectives

are to: 1) conduct lab-scale and field-scale pilot tests to demonstrate the applicability of the two new GSM in surface water treatment; 2) determine the removal efficiency of the target pollutants via the two GSM in a field-scale biofiltration system; and 3) educate and train next generation engineers of future sustainable engineering technologies to meet the real world needs of an interdisciplinary sustainability solution for surface water treatment.

1.3.2 Project Scope, Activities, and Timelines

Sustainable development goals addressed by the United Nations require cleaner production of water for living and cost-effective water pollution control. The scope of this project was to evaluate the efficiency of two novel filtration media, named Clay-Perlite-Sand (CPS) media and Zero-valent iron and perlite-based green environmental media (ZIPGEM), in preventing eutrophication of the St. Lucie River and Estuary by reducing nutrients, algal mass, and algal toxins from the C-23 canal. CPS served as a control and facilitated the comparison of data obtained from the filter media. The research motivation of applying these filtration media is to reduce nutrient levels including TP and TN, which can otherwise lead to algal blooms and result in the release of associated toxins such as microcystin. In addition, the project aims to remove a range of typical surface water pollutants or constituents including pathogens (E. coli), BOD, and Chlorophyll a as a surrogate for algal mass, as well as contaminants of emerging concern including algal toxins and PFAS.

A series of lab-scale batch tests, adsorption tests, and continuous column tests was conducted to optimize the design parameters for the full-scale filter cells. Field-scale activities for the pilot plant study include planning, design, permitting, construction, operation, and decommissioning of the biofiltration system at a river corridor of the Canal 23 in the St. Lucie River Basin, South Florida. The total maximum daily load (TMDL) goals for TN, TP, and BOD are set at 0.72

mg•L^{-1}, 0.081 mg•L^{-1}, and 2.0 mg•L^{-1}, respectively in the St. Lucie River and Estuary region and are expected to be achieved by the four treatment cells along the C-23 waterbody.

The original project duration was Aug. 2020 to July 2022. The project team encountered some issues that caused a delay in the completion of the design and construction tasks. The revised project timeline is now Aug. 2020 - July 2024, after multiple contract amendments. After the final report submission on Nov. 30 2023, there is a need to have 3 months for peer review and revision. The filter can then be decommissioned within 3 months and the landscape of the test bed must be restored fully before May 2024 right after the final approval of the project report. The final 2 months before July 31 2024 are needed to compete the accounting process for project closure. Further details can be seen in Section 1.3.4.

1.3.3 Project Resources and Methodology

This project (INV008) investigates the efficiency of novel GSM in a field-scale biofiltration system for removing TN, TP, and biological pollutants (e.g., E. coli, Chlorophyll a, BOD, algal toxins, and algal mass), and selected PFAS species. While several lab-scale batch and column studies employing recently developed GSM have indicated the feasibility for a field-scale investigation, the field-scale biofiltration system has further validated the concept derived from the lab-scale study. This validation is particularly noteworthy that considers the complex field environment, characterized by fluctuating weather patterns, temperature variations, moisture levels, pH values, sunlight, and varying water quality matrices across seasons. This research project received funding of $2 million from the Florida Department of Environmental Protection (FDEP) under the fiscal year 2020-2024 solicitation. Additionally, the University of Central Florida provided support through the Shared Research Facilities Fund, contributing $2,000 to facilitate material characterization and image analysis.

1.3.4 Challenges Faced in This Project

During the project period, the UCF team encountered a series of challenges owing to the following events: 1) the impact of COVID-19 and on-campus lockdown (from March 2020 to May 2021), 2) modification of media recipes due to the determination that tire crumb was unsuitable, 3) transition from a sole-source procurement model to open bidding due to budget constraints (from September 2021 to November 2021), 4) delays in the permit application process (from January 2022 to May 2022), 5) sporadic hurricane landfalls (from September 2022 to November 2022), 6) disruptions in the media supply chain during the period of inflation impact (from November 2022 to February 2023), and 7) an on-campus hiring freeze, resulting from the Florida Foreign Influence Act effective on July 1 2021, which impeded all recruitments of new international graduate students (from July 2021 to May 2022). Consequently, due to these factors, the project timeline was extended from two years to four years. The UCF research team cautiously navigated the project and got through these challenges mentioned above, ultimately achieving the project objectives.

1.4 Project Report Organization

The project report outlines the project's objectives, scope, methodology and tasks, findings, and outcomes. The rest of the report is organized into 6 chapters with the following content: Chapter 2 addresses site screening and filter design; Chapter 3 presents the filter construction details; Chapter 4 describes the sampling and data analysis for the field performance assessment of the filtration system across dry and wet seasons in 2023; Chapter 5 investigates physicochemical and microbiological removal mechanisms of the target pollutants when using CPS and ZIPGEM; Chapter 6 discusses the lab-scale experiments and life expectancy evaluation; Chapter 7

includes a cost-benefit analysis and explains the TMDL implications of this project; and Chapter 8 concludes the whole study.

This page intentionally left blank.

Chapter 2: Site Planning and Filter Design

2.1 Site Selection

The project team visited five possible sites within the Canal-23 (C-23) corridor region of the St. Lucie River Basin (see Figure 2-1), including: 1) I- 95 and the City of Port St Lucie, 2) City of Port St Lucie, 3) Boat Ramp and Canal Lock, 4) Turnpike Site, and 5) Cobblestone Martin County. The following site screening and selection criteria was finalized: 1) land availability requirements, 2) land ownership, 3) power source and access, 4) transportation condition, 5) construction maneuverability, and 6) site security. Based on these site screening and selection criteria, Site 5 (Cobble Stone Community in Martin County) was selected for construction of the filter cells. The Cobble Stone Community in Martin County is located along C-23, south of Port St. Lucie, just east of I-95, on the south side of the C-23 in South Florida; the selected site is within the right-of-way owned by the South Florida Water Management District (SFWMD).

2.2 Land Survey and Geotechnical Survey

The land survey map (Figure 2-2) of the south side right-of-way of the C-23 canal bank in Martin County is shown in Figure 2-2. According to information obtained from the United States Geologic Survey (USGS) "Indian Town NW, Florida" quadrangle map, the native ground surface elevation across the site area ranges from approximately +30 to +35 feet National Geodetic Vertical Datum (NGVD). The subject site is located due south of C-23. Based on the USGS map, C-23 has a normal high-water elevation of +28 feet NGVD.

As part of this limited exploration, two (2) Standard Penetration Test (SPT) borings, designated B-1 and B-2 on the attached Boring Location Plan (Figure 2-3), were performed in accordance with the ASTM D 1586 "Standard Method for Penetration Test and Split-Barrel

Sampling of Soils." The consultant (UES) located the test borings by using the provided site plan, measuring from existing on-site landmarks shown on an aerial photograph, and by using handheld GPS (global positioning system devices). No survey control was provided.

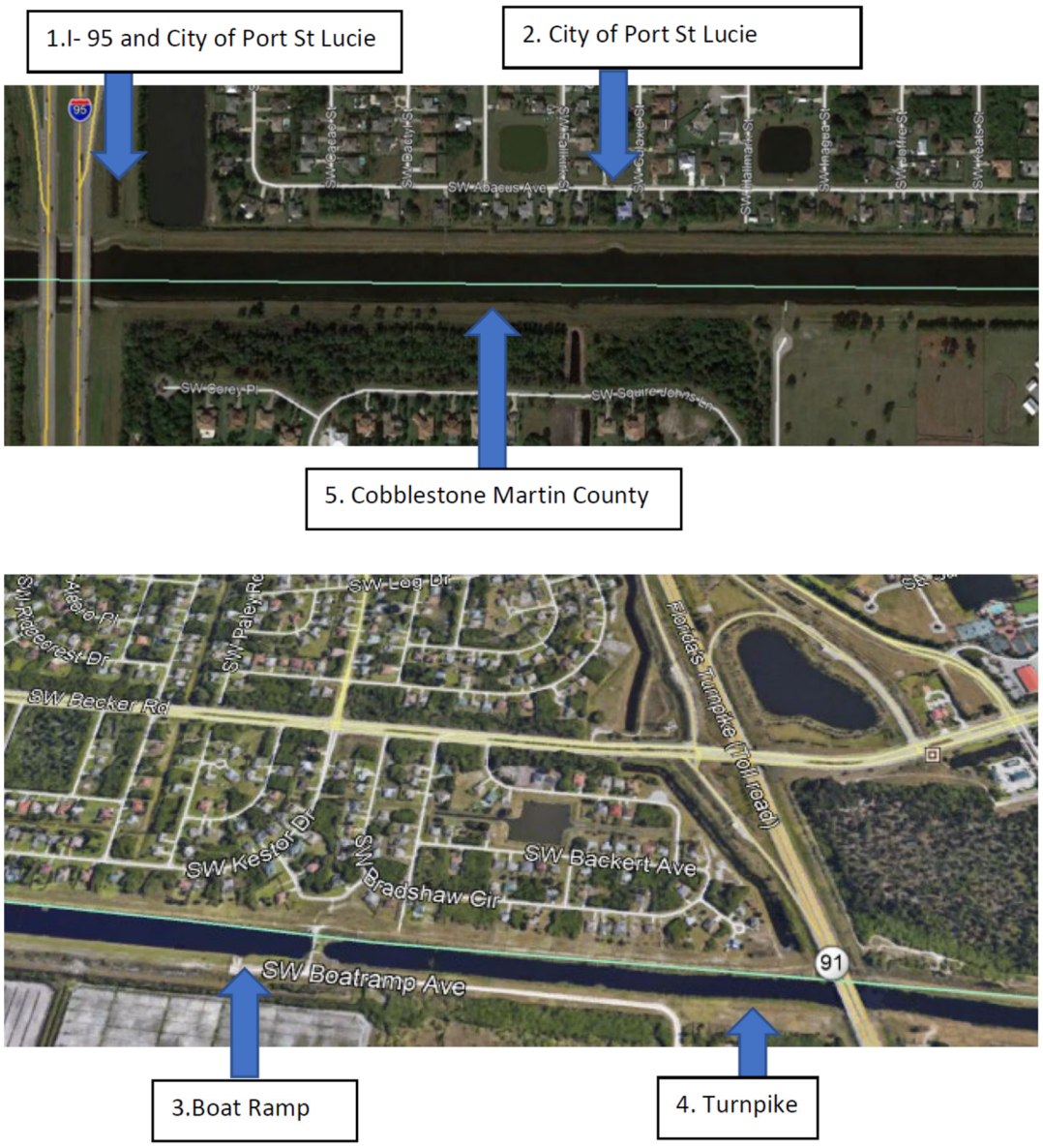

Figure 2-1: Site screening and selection

(a) Study site

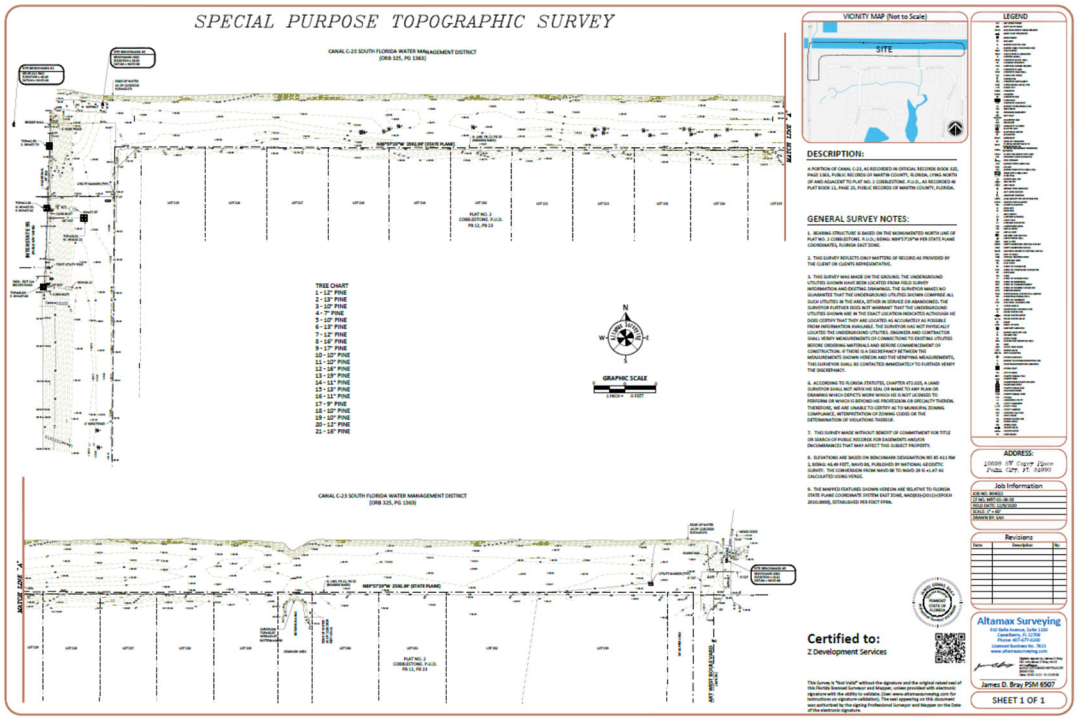

(b) land survey map

Figure 2-2: (a) Site condition before construction and (b) land survey map within the south side of the R/W of the C-23 canal bank in Martin County

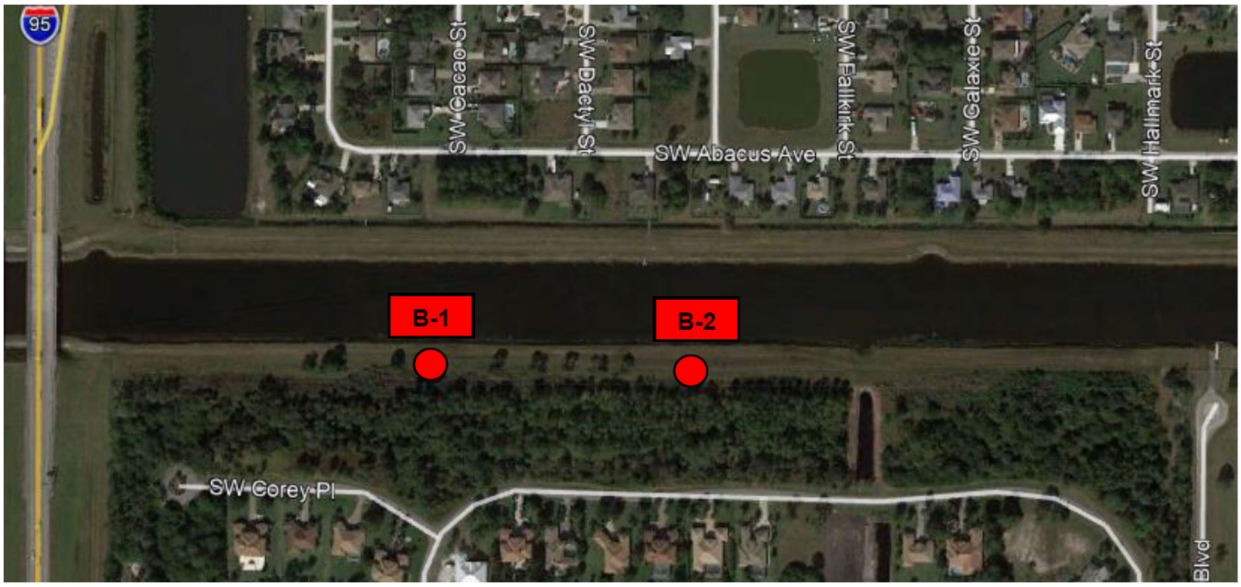

Figure 2-3: Borehole plan of the study site

Soil samples recovered from the field exploration were returned to the UCF laboratory, and visually classified by a geotechnical engineer in general accordance with the Unified Soil Classification System (ASTM D 2487). Then, the soil profiles were prepared from the field logs. The majority of the soils obtained from the boring locations consist of fine sands [SP, SP-SM, SP-SC] to the maximum depth of drilling, 20 feet bls. On the date of our field exploration, the groundwater table was encountered in the borings at depths of approximately 8.2 to 8.3 feet below the existing ground surface. The groundwater table fluctuated seasonally depending on local rainfall and other site specific and/or local influences. Brief ponding of stormwater may occur across the site after heavy or extended rainfall events. The results of our limited exploration, along with pertinent information obtained from the soil borings are shown on the boring logs for B-1 and B-2 sites in Figure 2-4.

Universal Engineering Sciences
607 NW Commodity Cove
Port Saint Lucie, Florida 34986
(772) 924-3575

LOG OF BORING B-1

PAGE 1 OF 1

CLIENT Z Development Services
PROJECT NAME UCF Algae Bloom Project
PROJECT NUMBER 0730.2000099.0000
PROJECT LOCATION C-43 SFWMD Canal, Palm City, Florida
DRILLING CONTRACTOR GFA International Inc.
HOLE DEPTH 20 ft
HOLE DIAMETER 3 in
DRILLER PM/TG/MJ
DATE STARTED 1/17/21
COMPLETED 1/17/21
DRILL RIG CME-45
GROUND WATER LEVEL: ▽ **AT TIME OF DRILLING** 8.20 ft
METHOD SPT
LATITUDE
LONGITUDE
NOTE:
HAMMER TYPE

DEPTH (ft)	SAMPLE	SAMPLE NUMBER	BLOW COUNTS	N VALUE	GRAPHIC LOG	MATERIAL DESCRIPTION	MOISTURE CONTENT (%)	FINES CONTENT (%)	ORGANIC CONTENT (%)
	X	1	3 4 4 5	8		Gray-brown mixed fine sand, trace clay (SP)			
						2.0			
	X	2	3 4 6 7	10		Gray fine sand (SP)			
						5.0			
5	X	3	4 5 6 7	11		Dark gray organically stained fine sand with silt (SP-SM)			
						7.0			
	X	4	5 6 6 8	12		Brown fine sand with clay (SP-SC)			
						8.5 ▽			
	X	5	6 5 4 6	9		Dark brown fine sand (SP)			
10									
	X	6	6 6 8	14					
15									
						18.5			
	X	7	3 3 4	7		Light brown fine sand (SP)			
20						20.0			

Bottom of borehole at 20.0 feet.

Figure 2-4(a): Borehole log report of B-1

Universal Engineering Sciences
607 NW Commodity Cove
Port Saint Lucie, Florida 34986
(772) 924-3575

LOG OF BORING B-2

PAGE 1 OF 1

CLIENT Z Development Services
PROJECT NAME UCF Algae Bloom Project
PROJECT NUMBER 0730.2000099.0000
PROJECT LOCATION C-43 SFWMD Canal, Palm City, Florida
DRILLING CONTRACTOR GFA International Inc.
HOLE DEPTH 20 ft **HOLE DIAMETER** 3 in
DRILLER PM/TG/MJ
DATE STARTED 1/17/21 **COMPLETED** 1/17/21
DRILL RIG CME-45
GROUND WATER LEVEL: ▽ **AT TIME OF DRILLING** 8.30 ft
METHOD SPT
LATITUDE **LONGITUDE**
NOTE:
HAMMER TYPE

DEPTH (ft)	SAMPLE	SAMPLE NUMBER	BLOW COUNTS	N VALUE	GRAPHIC LOG	MATERIAL DESCRIPTION	MOISTURE CONTENT (%)	FINES CONTENT (%)	ORGANIC CONTENT (%)
	X	1	4 5 6 8	11		Brown fine sand (SP)			
	X	2	4 5 4 4	9					
						4.0			
5	X	3	6 6 10 10	16		Gray fine sand (SP)			
	X	4	6 5 6 6	11		7.0			
	X	5	4 5 8 8	13		Dark gray organically stained fine sand (SP) ▽			
						9.0			
10						Brown fine sand (SP)			
						13.5			
	X	6	10 11 14	25		Dark brown organically stained fine sand (SP)			
15									
	X	7	4 7 9	16					
20						20.0			

Bottom of borehole at 20.0 feet.

Figure 2-4(b): Borehole log report of B-2

2.3 Filter System Design

The system design in the corridor of C-23 canal located at the St. Lucie River basin, Florida (Figure 2-5) included the treatment volume/pumping system, power and control system, land survey and filter size, geotechnical survey, piping layout, impervious liner system, balance cut, and water quality monitoring devices. These design drawings, provided in Appendix A, were certified by a professional engineer (Dr. Del Bottcher) from Soil and Water Engineering Technology (SWET) Inc., and served as supporting materials for permit applications. The filter system was designed to extract water from the C-23 canal using four 30-gpm (0.048 MGD) submersible pumps and deliver it to four (22'W x 133'L bottom dimension) infiltration cells. See Sheets 2 and 4 in Appendix A.

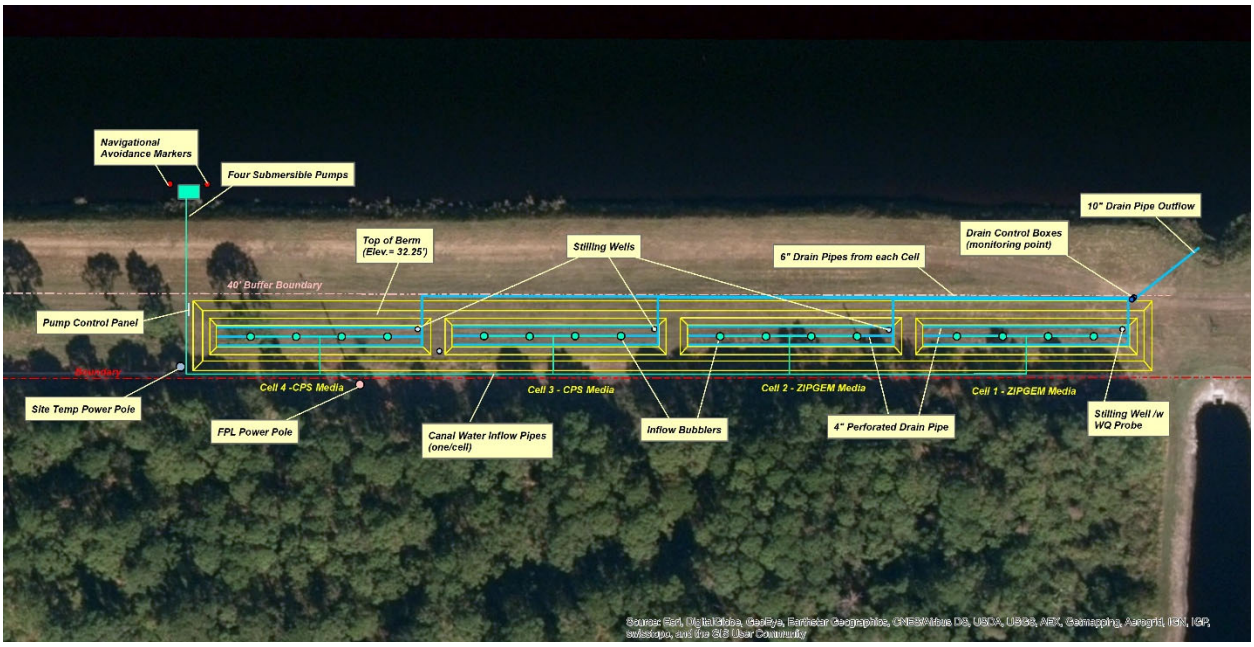

Figure 2-5: Aerial exhibit of C-23 canal filter project in Martin County, FL

Each cell has a dedicated pump and float controls to maintain a 6 ± 2 inches water depth over the media. A flowmeter is placed on each cell's inlet pipeline and enables us to read remotely via a cellular telemetry system. This telemetry system also provides remote viewing of the infiltration pond water levels, flow volumes to and from the ponds, and real-time water quality data, enabling the ability to turn pumps on or off remotely. These cells are 4 feet deep and have a berm height of 1.85 feet based on the cut-fill estimate. The perimeter berm has 3:1 exterior side-slopes and 1:1 interior side-slopes. The canal water is delivered into each cell via multiple energy dissipating bubbler inlets to prevent scouring of the media. Please note that the 40-foot buffer from the top of the C-43 canal berm is kept unobstructed as seen in the design drawings as required by the US Army Corps of Engineers and the SFWMD.

Cells 1 and 2 contain ZIPGEM, and Cells 3 and 4 contain CPS media with a depth of 2 feet. The media are underlain with about 6 inches of gravel with a series of perforated plastic drainpipes embedded to collect and deliver the infiltrated (treated) water back to the C-23 canal approximately 600 feet east (downstream) from where water is extracted from the canal. This separation is necessary to reduce recycling of treated water within the canal during low flow periods. Low flow periods occur about 50% of the time, based on the flow data from the S-97 structure located approximately 3.3 miles to the east. Water levels in C-23 range from about 14 to 21.5 feet (NAVD88), and the top of the berm of the filtration cells are about 32.25 feet (NAVD88) (Sheet 4 in Appendix A), to ensure sufficient water head above the media for maintaining the design flows. Each of the outlets from the cell underdrain systems has a sampling port (Sheets 4 and 6 in Appendix A). Using the flowmeter readings and the inlet and outlet flow weighted nutrient (nitrogen and phosphorus) concentrations, the treatment efficiency

and total nutrient loads removed by each of the cells can be calculated daily over the duration of the project.

2.3.1 Canal Pumping, Piping System, and Inflow Ports in Ponds

Four individual low head "chopper" style electric submersible pumps were installed as shown in Sheets 2 and 9. Each pump has the following specifications: 30 gpm with optimal efficiencies between 15 to 25 feet of total dynamic head and a 3-Phase 240VAC electric motor. The pumps maintain a water depth of 6-inches over the media in the ponds by using float switches mounted in stilling wells in each pond (Sheets 2, 8, 9, & 10) that are wired to the pump control panel (Sheet 12 in the Appendix A). An example of wiring in the electrical control panel for the pumps is provided in Sheet 12 in the Appendix A. All pumps, pipes, valves, and electrical components meet SFWMD minimum specifications. The pumps are mounted such that their inlets are located at or below an elevation of 12.5 feet (17 feet below top of bank @ 29 feet-NAVD88) and at least 12 inches from the canal side slope or the bottom of the canal (Sheet 9 in the Appendix A). Pumps are placed as close as possible to each other along the canal bank. Two non-corrosive (stainless steel or PVC over treated mounting post) navigation avoidance posts of at least 8 inches in diameter were installed as shown on Sheet 2. The pump discharge pipe (3-inch Schedule 40 PVC or equivalent) has a disconnect flange just before where the horizontal pipe enters the berm (Sheet 9 in the Appendix A). The pipes in the berm are buried to a depth of at least 24 inches (Sheet 9 in the Appendix A). The power cable from the control panel is buried with the pipes in an armored and anchored conduit between the pump and the buried pipe.

All pipelines from the pumps to the ponds are Schedule 40 2-inch diameter PVC or equivalent. Sheets 2, 4, and 9 in the Appendix A show the general layout of the pipelines. Pipelines outside of the ponds are buried to a depth of at least 24 inches. Within the ponds, the

pipes are laid on top of the media. To endure heavy vehicular traffic, all PVC pipe joints are cemented. The flowmeters for all the pipelines from each pump are located where the inlet pipes cross over the top of the south berms (Sheets 7, 8a and 8b in the Appendix A). An air release valve is placed on the inlet pipe as shown in Sheet 7.

Each infiltration pond has four evenly spaced energy dissipating bubbler inflow ports to provide even distribution of the canal water within the ponds in addition to preventing any erosion/disturbance of the media. The blowup of the proposed inflow port is shown on Sheet 9 where a 3-foot diameter 6-inch-high pile of small riprap is placed on top of permeable fabric around the riser pipe. Besides dissipating energy to prevent erosion, this configuration also prevents any possible backflow from the ponds toward the pumps, even if a check valve failure were to occur.

As indicated above, each pipeline into the infiltration ponds has its own flowmeter. The flowmeters (2-inch diameter) with accumulative flow volume reading visible on each flowmeter is capable of sending wired digital/pulse signals to the Eurika Telemetry Panel installed, so that the flowmeter readings can be read remotely at any time. The flowmeters are placed at least ten pipe diameter lengths from anything that can cause turbulence, such as fittings (Sheet 7 in the Appendix A). An air release valve is attached to the inlet pipe as shown in Appendix A.

2.3.2 Water Depth Transducers

Each infiltration pond has a water level sensor or pressure transducer located within a stilling well located in its NE corner approximately three feet in from the bottom of the perimeter. Sheets 2, 8a, 8b, 9, and 10 show the location and a blowup of the recommended 10-inch diameter PVC stilling well that is perforated with numerous ¼-inch holes including its bottom to allow water to

equilibrate between the pond and inside the well (Sheet 9 and 10). To prevent media from flowing through the ¼ -inch holes, the outside of the well pipe is wrapped with a screening material. The stilling well is installed 6 inches into the media (see Sheets 9 and 10) so that the depth (pressure) sensor can be located below the top of the media. The pressure sensor has a depth range of at least 0 to 2 feet (24 inches) with an accuracy of ±0.1 inches. Note, Cell 1 (Sheet 10) has a pressure transducer as part of its water quality probe while the other three cells only have a depth transducer (Sheet 9). The wires from the stilling wells outside the pond are buried at least 6 inches deep. Note, 18-inch extended mounting legs attached to the side of the stilling wells are used to properly anchor the wells in the media.

2.3.3 Pump Power Panel and Cellular Linked Programmable Logic Controller and Datalogger (PLC-D)

This section will present the required specifications for the control system for the four pumps as well as how remote control of the pumps will be achieved. Sheet 12 shows an example of a control system that will meet the minimum requirements of this project, but alternative control systems are acceptable if they meet the following minimum requirements:

1. All electrical and control system components are located in a weather and vandal proof enclosure/panel that is mounted at eye level and can be securely locked. The panel should be located at NW end of the Cell # 4 infiltration pond (Sheets 2, 4b, and 9).
2. FPL placed a 240VAC single-phase transformer on their power pole as shown in Sheet 14, which has a power drop to the project's temporary power pole with a meter box. This meter pole is placed near their transformer pole (see Sheets 4b and 14).

3. A buried power line within a conduit from the meter pole to the pump control panel was needed with a 100-amp rating and buried to a minimum depth of 24". The distance from the temporary meter pole to the panel is approximately 30 feet (see Sheets 4b and 14). The power to the pump control panel is single-phase 240VAC requiring a single-throw power disconnect.
4. Separate 20-amp breakers are provided for each of the four 240VAC pumps.
5. An 120VAC power outlet is provided at the Control Panel.
6. 120VAC power is provided to the Eureka Telemetry Panel from the pump control panel via a ~200-foot buried (minimum of 24") wire.
7. A 120 VAC to 12 VDC transformer is provided to lower voltage power for relays and float switches (Sheet 12).
8. 600VAC 20-amp contact power relays are provided for each of the four pumps. A 12 VDC coil activation voltage is recommended, as shown in Sheet 12, but not required if an alternative relay activation voltage is shown to provide equivalent performance and safety.
9. Four manual pump control switches are required within the panel that will allow any pump to be manually set to "Off", set to "On", or set to "Auto", which will allow remote control of the pumps via a cellular control module.
10. A cellular control module within the pump control panel is required to provide remote control by UCF staff of the four pumps (see Sheet 12). The contractor for construction, maintenance, and site restoration (decommissioning) of the filter will be responsible for setting up and paying for the cellular service to the cellular control module and electricity bills as part of the maintenance fees.

2.3.4 Filter Construction

The pond was constructed as shown in Sheets 2 through 11. The berm elevation of 33' is the same for all ponds, which is set to provide an even cut and fill ratio as close as possible. The above ground berms are compacted according to standard STMP specifications. Each pond is lined with a minimum of a 40 mil HDPE plastic liner, which is anchored at the top using an anchor trench (Sheets 4a, 4b, 5, and 7). Each cell required approximately 1,704 ft^2 of liner material (about 6,814 ft^2 for all the ponds). A liner boot is required at the bottom NE corner of each cell to allow the 4" diameter manifold pipe in the ponds to be connected watertight to the 4" solid drainpipes that deliver water to the drainage control boxes.

Each of the ponds has 4-inch diameter perforated plastic drainpipes embedded in 6 inches of gravel (~10 yd^3 per pond or ~40 yd^3 for all four ponds) at the bottom of the ponds (Sheets 4a, 4b, and 5). A geotextile porous fabric material is placed on top of the gravel to prevent media intrusion. A 4-inch diameter perforated plastic drainpipe serves as the collector manifold for the three 4-inch drainpipes (Sheets 4a, 4b, and 5). A 4-inch liner boot at the bottom NE corner of each cell is used to ensure a watertight connection between the internal 4-inch manifold and the 4-inch diameter solid drainpipe (sewer grade acceptable) that delivers the drainage water to four drainage control boxes located at the NE corner of Cell # 1 (Sheets 4a, 4b, 5, and 6). These control boxes allow the discharge head for each of the cells to be set independently and allow the flowrates to be controlled and measured via a water depth probe / pressure transducer providing the head over a V-notch weir within the control box (i.e., this part was changed to be a set of orifices in the later stage before construction). The 4-inch discharge drainpipes from these control boxes are connected to an 8-inch solid drainpipe that delivers all of the cells' drainage water back to the C-23 canal (Sheets 2, 4a, and 10 in the Appendix A).

Two different types of green sorption media were placed in the four cells on top of the gravel level at a depth of 2 feet. Cells 1 and 2 contained ZIPGEM media and Cells 3 and 4 contained CPS media. Each cell was filled with ~50 yd^3 of these sorption media, totaling ~100 yd^3 of ZIPGEM and ~100 yd^3 of CPS. The mixing recipes for the two media types are provided in Table 2-1.

Table 2-1: Recipe of the green sorption media by volume to be tested in this project.

Name	Sand (%)	Clay (%)	Tire Crumb (%)	Iron Filings (%)	Perlite (%)	Biochar (%)	Natural Soil (%)
CPS	92	5	--	--	3	--	--
ZIPGEM	85	5	--	5	5	--	--

2.3.5 Remote and In-situ Automatic Monitoring and Data Acquisition System

A weather station was installed and connected to the Eureka Telemetry Panel so that local rainfall, temperature, wind, and solar radiation could be continuously measured and recorded. Please see location in Sheets 2 and 4a. Measuring Inflow and Outflow Rates: As indicated above, the canal inflow to each cell was measured using flowmeters. These flowmeters were read and recorded manually by the UCF team during each site visit. The outflow from each cell was measured using the pressure transducer on the Eureka water quality probes located in the drainage control boxes. The probes provided the water depth/head over the weir plate in the control box, which was used to calculate the flowrate.

The control boxes are equipped with Eureka water quality probes to collect continuous water quality data remotely. One additional water quality probe is placed in stilling well in Cell #1 in order to obtain the same water quality data for the canal inflow water. In addition, water samples were collected manually from one of the ponds and the outflow boxes to validate the remotely

obtained data. The project team carried out field campaigns on a monthly basis to manually sample water at the outlet well of each cell in addition to a common set of samples at the inlet close to the pumping station to analyze selected physical (inflow vs. outflow, temperature, DO, turbidity), chemical (ammonia, TKN, nitrate, nitrite, orthophosphate, total nitrogen, total phosphorus, dissolved iron and aluminum, chlorophyll-a, BOD, pH, conductivity, PFAS, DON, and ABON) and microbiological (E. Coli and Microcystin) properties of the water. The project team also installed a set of *in situ* multi-probe automatic sensors to measure physical (infiltration rate, inflow vs. outflow, Temp, pH, ORP, DO, turbidity), chemical (N, ammonia, conductivity) and microbiological (algal mass, Phycocyanin (Blue-green algae)) properties of the water in addition to the meteorological conditions (air temperature, relative humidity, precipitation intensity, air pressure, wind direction and speed). The measurements were stored in a data logger and transmitted to the cloud via a wireless communication network for remote access.

This page intentionally left blank.

Chapter 3: Facility Construction and Testing

3.1 Managerial Background

The media preparation and filter construction tasks were originally assigned to Environmental Conservation Solution Inc. (ECS) (sole source). At the onset of COVID-19 pandemic (late 2020), ECS suddenly increased the total cost from $Ele1.35 million to $2.25 million, exceeding the total budget ($2 million) of this project. UCF then decided to switch to an open bidding option. UCF sent contract amendment #3 to the Florida Department of Environmental Protection (FDEP) to revise the project timeline and design to reduce the filter size and proceed with the rebidding, which was approved by FDEP in late May 2022. The second design modification to downsize the filter from 0.3 acre to 0.06 acre was completed by the vendor - Soil and Water Engineering Technology Inc. (SWET) - on June 6, 2022. The first open bidding (due on April 21, 2022) was not successful due to budget constraints. UCF Department of Purchasing Services launched a market survey in May 2022 and identified two more companies for the next bidding (i.e., rebidding). Based on the modified design drawings, the second open bidding was successfully concluded on July 21, 2022. The construction company, Enviro-Tech Systems, Inc. (ETS hereafter) won the bid. The construction work began in early Sept. 2022 after receiving the approval with permits from the SFWMD, the Army Corps of Engineers, and the FDEP Southeast Division. It took about six months to acquire four permits. Two permits that were issued by the Army Corps of Engineers; one permit was issued by the FDEP Southeast Division, and one was issued by the SFWMD.

3.2 Facility Construction

Prior to construction, ETS conducted a field survey for Gopher Tortoise Burrows. Due to the presence of Gopher Tortoise Burrows (Figure 3-1) near the new construction site, it was shifted 20 ft to the West (Figure 3-2). This did not change any approved design (Figure 3-3) by FDEP. The construction work started in early Sept. 2022 after receiving the right-of-way permit (site access permit) from the South Florida Water Management District.

Figure 3-1: Recent survey of Gopher Tortoises Burrows in late Sept. 2022.

Figure 3-2: Final construction site shifted 20 ft to the west based on the original design map.

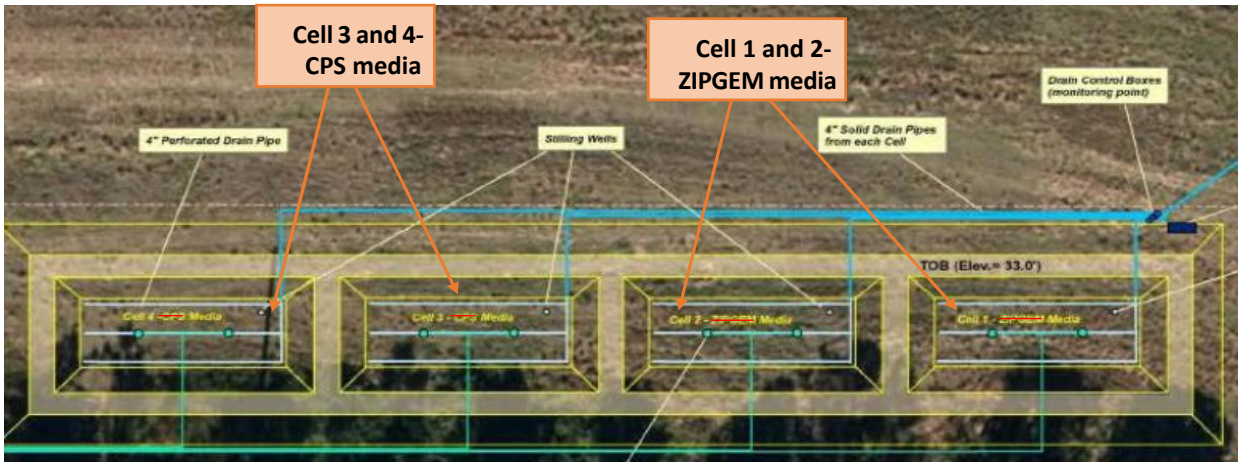

Figure 3-3: Final construction of four cells, inlet, and outlet.

The filter cells were constructed in Sept. and Oct. 2022 following this sequence: site clearance, precise site surveys, excavation, liner placement and welding, pumping station installation, wiring, and drainage box installation. The control panel was tailored to support the control scheme of each pump via a float valve. Balanced cut and fill were achieved with the assistance of precise site surveys. In early February 2023, after completing media mixing and

installation, inlet pipes for all cells were finally installed. FP&L installed new transformers and electronic poles in the same month.

Media preparation commenced in early January using a 4-auger mixer for Cell #4 but encountered a transmission and control issue. ETS subsequently transitioned to two overhead excavators and a dumpster to continue media mixing for the remaining three cells through late January 2023. During the scheduled field visits from January 3 to January 27, 2023, the UCF research team collected both raw and mixed media samples. By creating gradation curves of mixed media for comparison against lab-based gradation curves, team members confirmed the effectiveness of on-site media preparation and mixing in the field. On-site sieve analysis, powered by a generator (Figure 3-4), facilitated this confirmation.

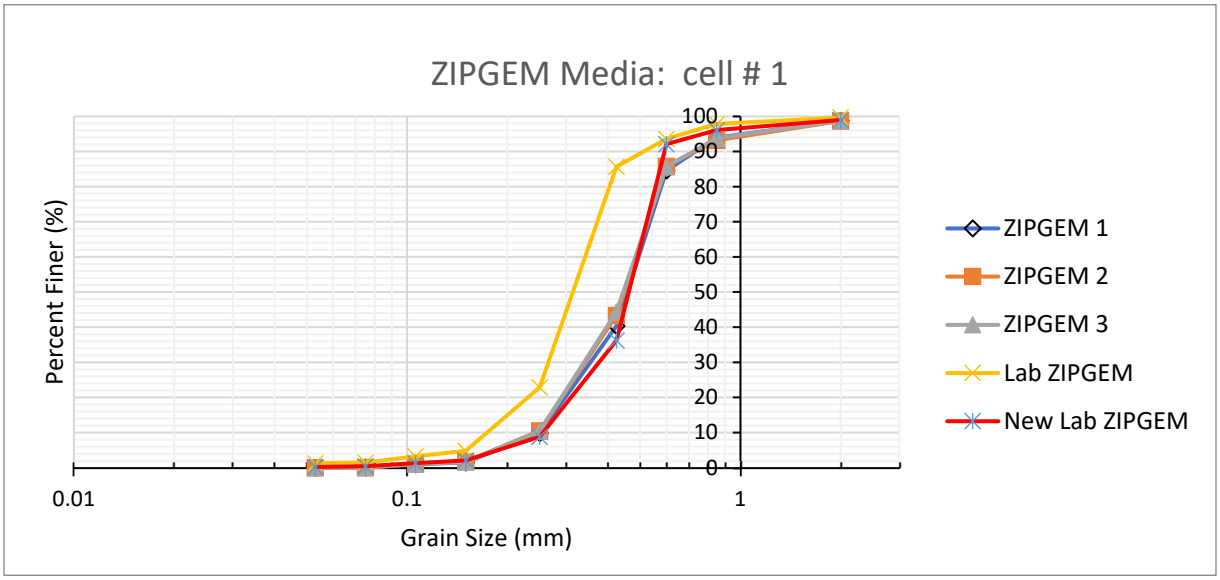

(a) Cell #1 (ZIPGEM)

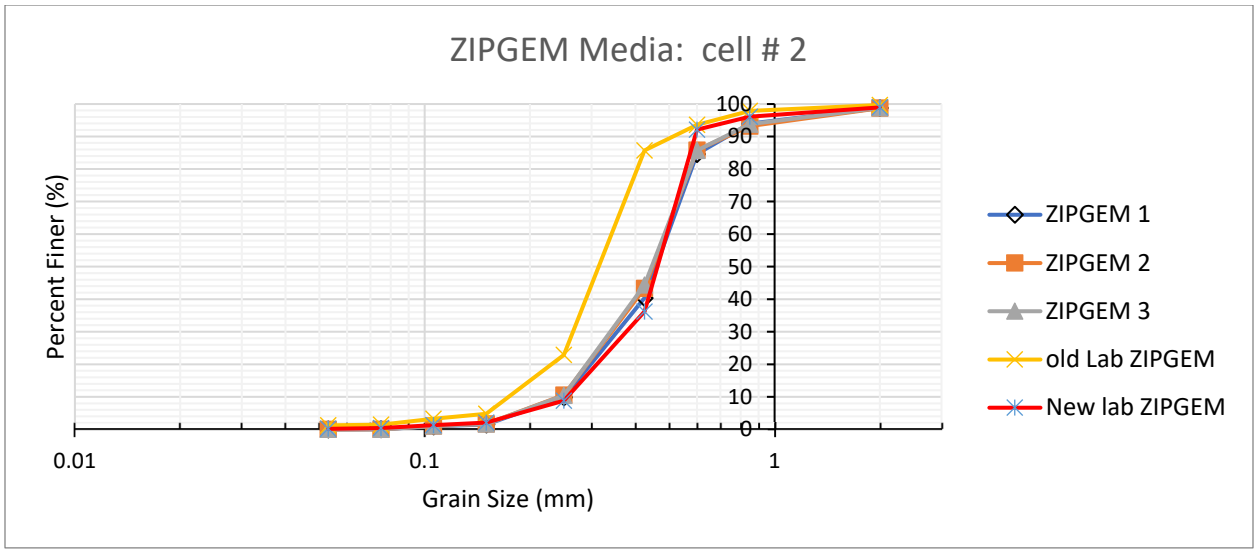

(b) Cell #2 (ZIPGEM)

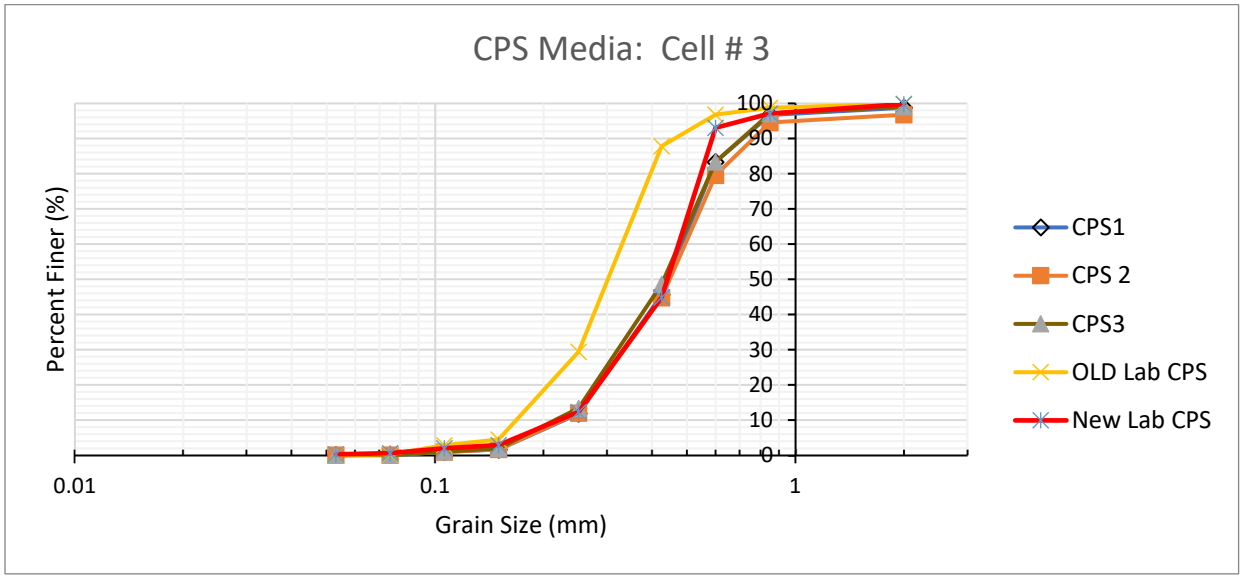

(c) Cell #3 (CPS)

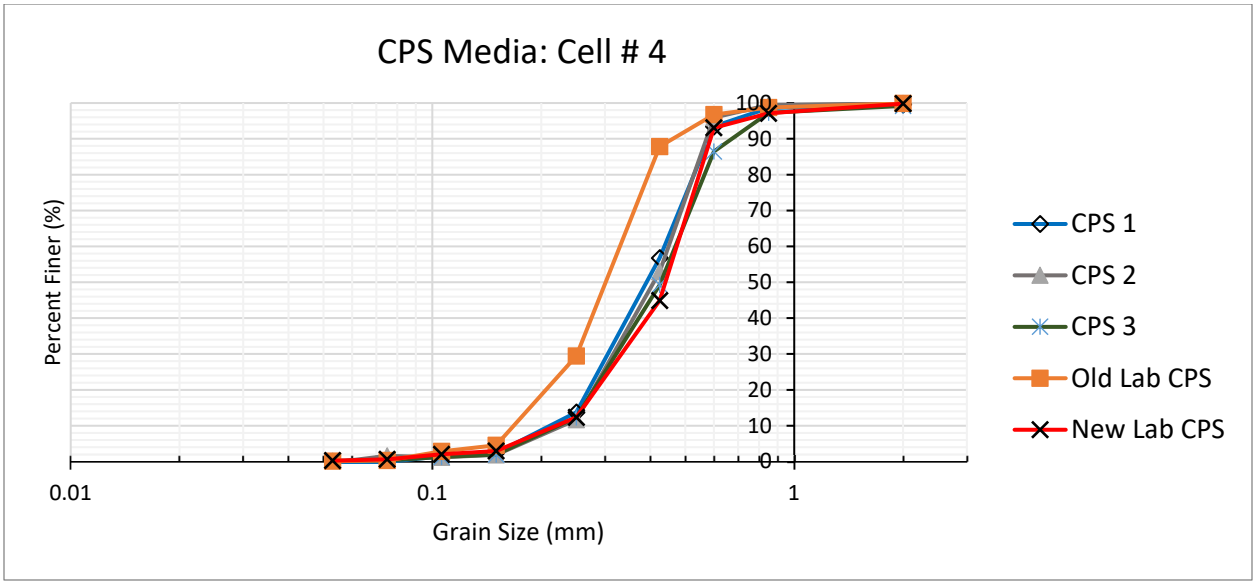

(d) Cell #4 (CPS)

Figure 3-4: Comparison of media particle size distribution by gradation curves for four cells.

To undertake a comprehensive comparison of the composition between field and laboratory media for both CPS and ZIPGEM, the chemical characterization of these media mixes was meticulously examined. The X-ray fluorescence spectrophotometer (XRF) data, as presented in Table 3-1 (Ordonez et al., 2023), revealed that silicon (Si) constitutes the predominant element in both the field media matrices of CPS and ZIPGEM, with approximate proportions of 79% and 67%, respectively. In contrast, Si proportions in the corresponding laboratory media for CPS and ZIPGEM are approximately 80% and 70%, respectively. There are similar proportions of aluminum (Al)—the second most abundant element—in the field and laboratory media of CPS and ZIPGEM. These observations substantiate the validity of the media mixing during the construction stage, pointing to the consistency between the field and laboratory compositions **of the GSM**. Furthermore, these data contribute to a more profound understanding of the impact of media composition on the mechanisms involved in PFAS removal, as elucidated in Chapter 5.

Table 3-1(a): Chemical element composition of CPS and ZIPGEM raw media mixed in the field via the XRF analysis (elements detected at tracer level were excluded)

Element	CPS	ZIPGEM	Unit
AI	9.7	6.5	%
Si	78.8	67.1	%
P	2.8	2.8	%
CI	1.8	3.0	%
K	2.7	3.5	%
Ca	2.4	2.7	%
Ti	0.8	0.5	%
Fe	0.7	13.2	%
Sn	——	0.2	%
S	——	0.5	%

Table 3-1(b): Chemical element composition of CPS and ZIPGEM raw media mixed in the UCF laboratory via the XRF analysis (elements detected at tracer level were excluded)

Element	CPS	ZIPGEM	Unit
Al	10.5	8.4	%
Si	80.1	70.3	%
P	2.1	1.9	%
S	0.6	0.0	%
Cl	1.8	2.0	%
K	2.9	2.8	%
Ca	1.1	1.0	%
Ti	0.4	1.3	%
Fe	0.4	12.1	%

Five water quality probes and one weather station (Table 3-2) were installed on Feb. 3, 2023. Four out of five water quality probes were installed beside the drainage boxes to monitor effluent from each cell (Figure 3-5). The fifth one was installed in the stilling well at cell 4 that provided a combined measurement at the inlet of all cells (Figure 3-6). A sensor network (Figure 3-7) was installed for automatic monitoring allowing the UCF research team to remotely monitor the pumps, water quality parameters, and weather conditions via the Eureka cloud system.

Table 3-2: In situ automatic water quality probes

Sensor		**Parameter**
Manta + 35A	Regular sensors	Temperature, conductivity (salinity and TDS), pH, ORP, optical dissolved oxygen, turbidity
	ISE sensor	Nitrate Ammonium
	Fluorometric sensor	Chlorophyll, Phycocyanin (Blue-green algae)
	Trimeter	Soil water pressure for infiltration rate destination. BP reading, temperature and water level depth
Luff Weather Station	Luff WS-600 with sensor	Air temperature, relative humidity, precipitation intensity, air pressure, wind direction and speed

Note: TDS stands for total dissolved solid; ORP stands for oxidation reduction potential

Figure 3-5: Water quality monitoring (circular enclosures) wells and drainage boxes (square boxes).

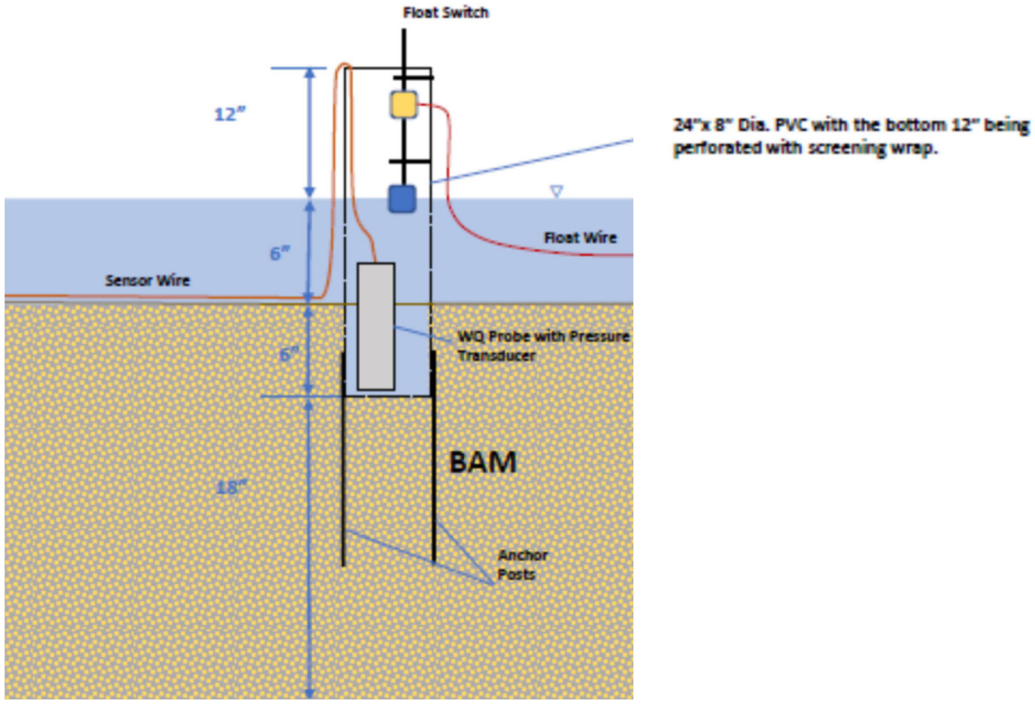

Figure 3-6: Stilling wells and water quality probe (BAM stands for Biosorption Activated Media representing CPS and ZIPGEM in this project).

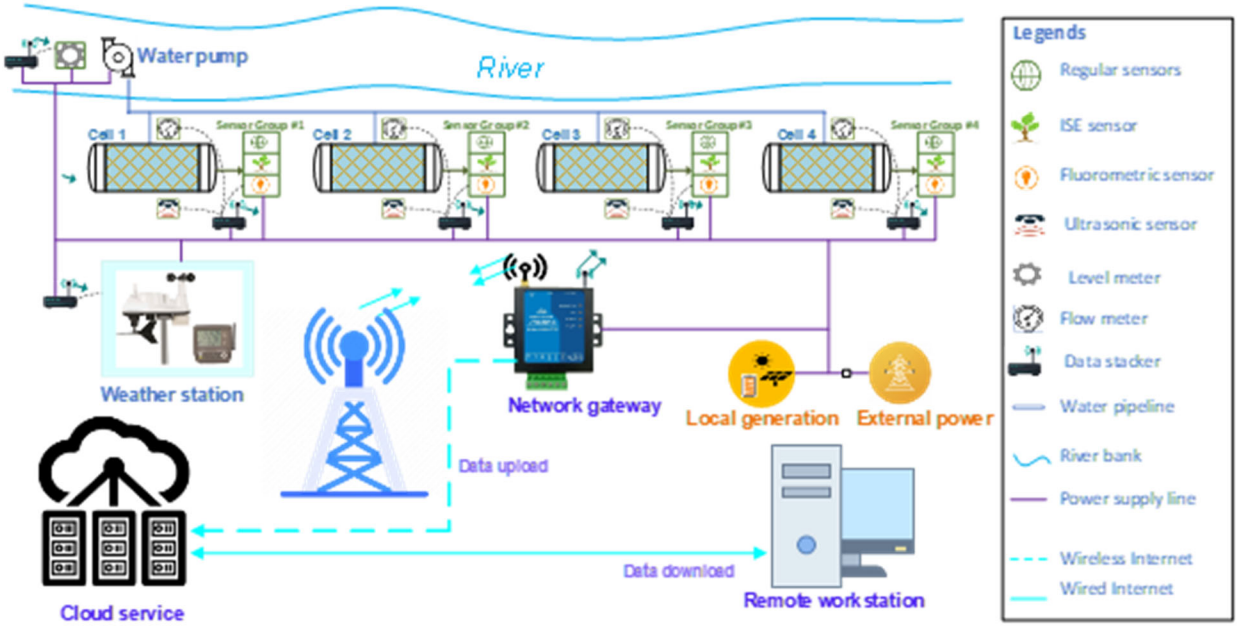

Figure 3-7: The designed sensor network.

The construction work was completed on Feb. 17, 2023. The filter will be decommissioned at the end of the project (Figure 3-8), as summarized in Table 3-3 associated with photo numbers. The construction work completion and the planned decommissioning are certified by two professional engineers, including Mr. Richard Jones and Dr. Del Bottcher. The photos of the site before, during, and after construction, as summarized in Table 3-3, are provided in APPENDIX B.

(a) Site condition before construction

(b) Site condition after construction (new electric poles are shown in the background)

Figure 3-8: Site condition change to show four completed cells, inlet pipes, a stilling well, and a few new electric poles that the FPL installed for this project.

Table 3-3: Construction summary of the parentage of completion

Item No.	Description	%	Additional Details*	Photos No.	Engineer Verification	Date
1	Cut/Fill Earthwork to construct 4 cells	100	Equipment: Komatsu Mini-Excavator	001, 002, 006, 011	RAJ	11/1/2022
2	Supply/Install Pond Liner, 40 mil HDPE min., w/anchor trench	100	Vendor for liner: Comanco	003, 004	RAJ	11/1/2022
3	Supply/Install 4" Pipe Boot for pond liners	100	Vendor for boot: Comanco	005	RAJ	11/3/2022

4	Supply/Install 4" perforated drainpipe in all cells	100	Pipe Vendor: Somers Irrigation	007, 008, 009, 010	RAJ	11/16/2022
5	Supply/Install 4" drainpipes from cells to Drainage Control Boxes	100	Pipe Vendor: Somers Irrigation	015, 017	RAJ	11/17/2022
6	Supply/Install Drainage Control Boxes (4" inlets)	100	Vendor: Agri Drain Corporation	014, 015, 016	RAJ	11/17/2022
7	Supply/Install 8" drainpipe to canal outlet	100	Pipe Vendor: Somers Irrigation	021, 022	RAJ	11/17/2022
8	Supply/Install #57 double washed gravel in cells over drainpipes	100	Gravel Vendor: T.Disney Trucking Equipment: Kobelco Long Reach Excavator	012, 013	RAJ	11/16/2022
9	Supply/Install geotextile porous fabric over gravel in all cells	100	R.H. Moore & Associates	033	RAJ	11/18/2022
10	Supply/Install CPS media	100	See note	035, 036, 037	ANE	2/6/2023
11	Supply/Install ZIPGEM-2 Media	100	See note	038, 039, 040	ANE	2/6/2023
12	Supply/Install 30 gpm submersible pumps w/ 1" mesh screen enclosure with check valve in the C-23 Canal	100	Somers Irrigation	022-027	RAJ	11/17/2022
13	Supply/Install "No Anchorage" warning posts by pumps	100	Okeechobee Sign Company, Bass Pro, Taylor Made	041	ANE	2/6/2023
14	Supply/Install Pumps Control Panel w/ pump controllers	100	Control by Web	028, 043, 044	ANE	2/6/2023
15	Supply/Install Cellular Control Module in Pump Control Panel for remote	100	Sierra Wireless	043, 044	ANE	2/6/2023

	pump control					
16	Install temporary power line from meter pole to Pump Control Panel	100	Vendor: City Electric Supply	029, 043	ANE	2/6/2023
17	FP&L Service Connection Fee	100	FP&L	Receipt Provided	MKM	2/1/2023
18	Install buried power line from meter pole to Pump Control Panel	100	ETS Electrical Crew	018, 019, 030, 031, 043	ANE	2/6/2023
19	Supply/Install 2" PVC pipelines from pumps to inlet bubblers	100	ETS Pipe Crew	035, 036, 037, 038, 039, 040	ANE	2/6/2023
20	2" flowmeter on inflow line to each cell	100	Somers Irrigation	033, 034	RAJ	11/18/2022
21	2" air release valve on inflow line to each cell	100	Somers Irrigation	033, 034	RAJ	11/18/2022
22	Supply/Install 8 inlet bubblers with rip rap energy dispensing	100	ETS Pipe Crew	035, 036, 037, 038, 039, 040	ANE	2/6/2023
23	Power supply to Eurika Panel	100	ETS Electrical Crew	032		
24	Install Stilling Wells in each cell with float controls	100	Vendor: Florida Equipment And Restoration, Inc. and Grainger	033, 035, 036, 037, 038, 039, 040	ANE	2/6/2023
25	Supply/Install Pressure Transducers in cells 2, 3, 4	100	UCF, ETS Electrical Crew	035, 036, 037, 038, 039, 040	ANE	2/6/2023
26	System Startup and Performance Certification by Contractor	100	ETS Supervisor	045, 046	RAJ	2/10/2023
27	Routine Site Maintenance (mowing at least 5 times/year)	0	ETS Crew			
28	Setup and pay monthly electric bill (will be	0	ETS			

	<$500/month)					
29	Setup and pay monthly cellular service for remote pumps control module	0	ETS			
30	Obtain "Temporary Access Permit" from the SFWMD	100	ETS, SFWMD		MKM	1/4/2023

* Materials/Equipment/ Labor Source

**
Note: Masonary Sand - Palmdale Sand Mine

Perlite - Diamond R Fertilizer

Clay - Edgar Minerals

Iron Filings - Connelly-GPM, Inc

Mixing Machine - Botanics Wholesale

3.3 Facility Testing

3.3.1 Stage I Testing

On Feb. 10, 2023, the ETS engineer turned on the pumps and controls powered by a generator. To test whether the float switches and pumps operate properly, ETS plugged a temporary cable into the generator providing 240 VAC power to the system. Then, the ETS engineer supplied power to the system and then set the Hand-off-Auto (HOA) switch to AUTO for one pump at a time (Figure 3-9). Water began to flow into the cells after about 15 seconds. To test the float switches, the ETS engineer set the control to AUTO and walked to the stilling well to access the float switch where the engineer manually lifted the floats to duplicate its typical function. When both the floats were lifted (pond full), the pumps stopped. When both the floats were placed back in their original positions, the pumps restarted in all cases. The pumps can be remotely controlled by a similar system. The ETS engineer also found that the Eureka sensors in some cases were too close to the float switches and could possibly interfere with their operation, so the engineer

devised a fastening system to keep them away from the float switches. After checking the various functions of the control system and float switches, the engineer tested the pumps and recorded pumping rates via the flow meters (Table 3-4).

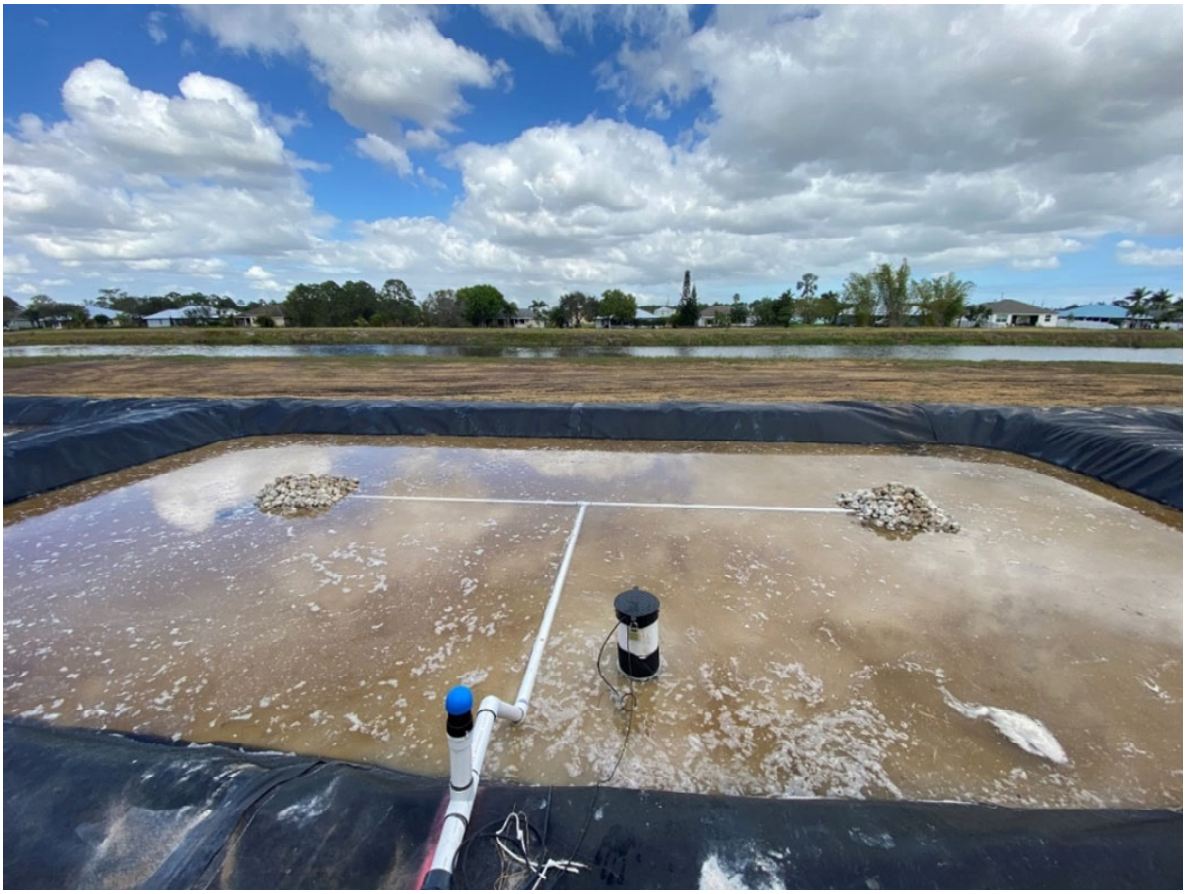

Figure 3-9: Test run at cell #4 (CPS) with the stilling well in the middle.

Table 3-4: Flow rates in pumping system test

PUMP ID	LINE 1 (amps)	LINE 2 (amps)	FLOW (gpm)
P1	1.48	1.49	34
P2	1.62	1.64	42
P3	1.60	1.60	48
P4	1.68	1.66	52

All electrical tests were completed at 244 VAC output from the generator. The increase in the flow rates resulted from the head losses associated with different pipe lengths from the pump to

each cell. The design flow was 30 GPM. The parameters reported in the above table were obtained from a digital meter with amp readings, which fluctuated over a range, and hence, the flowrates reported in Table 3-4 are the averages of the readings observed. It is to be noted the amp readings for all four pumps were consistent and the currents were appropriately influenced by the flow rates. The ETS engineer and the UCF research team members met again on Feb. 16, 2023, to continue the test run for the outlet weir and check the flow conditions of effluent in each cell. As all cells were tested, the switch flows worked fine. The ETS engineer fabricated outfall weirs for the discharge structures and adjusted the water level in the cells to 6" as per the design and installed the adjustable orifice for all the drainage boxes to control the outflow.

3.3.2 Stage II Testing

Each cell has a multicore probe at both inlet and outlet for water quality monitoring providing online real-time measurements every 5 minutes. Water quality constituents that are measured on site include temperature, conductivity (salinity and total dissolved solids), pH, oxidation-reduction potential, optical dissolved oxygen, turbidity, nitrate, ammonium, phycocyanin (blue-green algae), chlorophyll a, and soil water pressure for infiltration rate. All data collected by each multicore probe (IoTs) can be transmitted and stored in the cloud for machine learning with big data analytics via cell telemetry system including cellular modem (The Global System for Mobile Communications, GSM), battery, solar charge controller, solar panel connection cable, and pole mounting kits. Pumping rates can be adjusted to optimize the treatment efficiency based on the measured parameters. This biofilter system can be modularized and mobilized for different field applications. The data streams in the current cyber physical network as shown in Figure 3-10 enable us to support real-time reinforcement of machine learning with big data analytics. The optimal patterns in relation to pumping rate, infiltration rate, and treatment

efficiency were obtained with the aid of digital transformation in a real-time simulator incorporating signal conditions, data acquisition, and even plant digital twin. These efforts helped identify the optimal operation strategies. We may use Azure Digital Twins (an IoT platform) to further optimize operations.

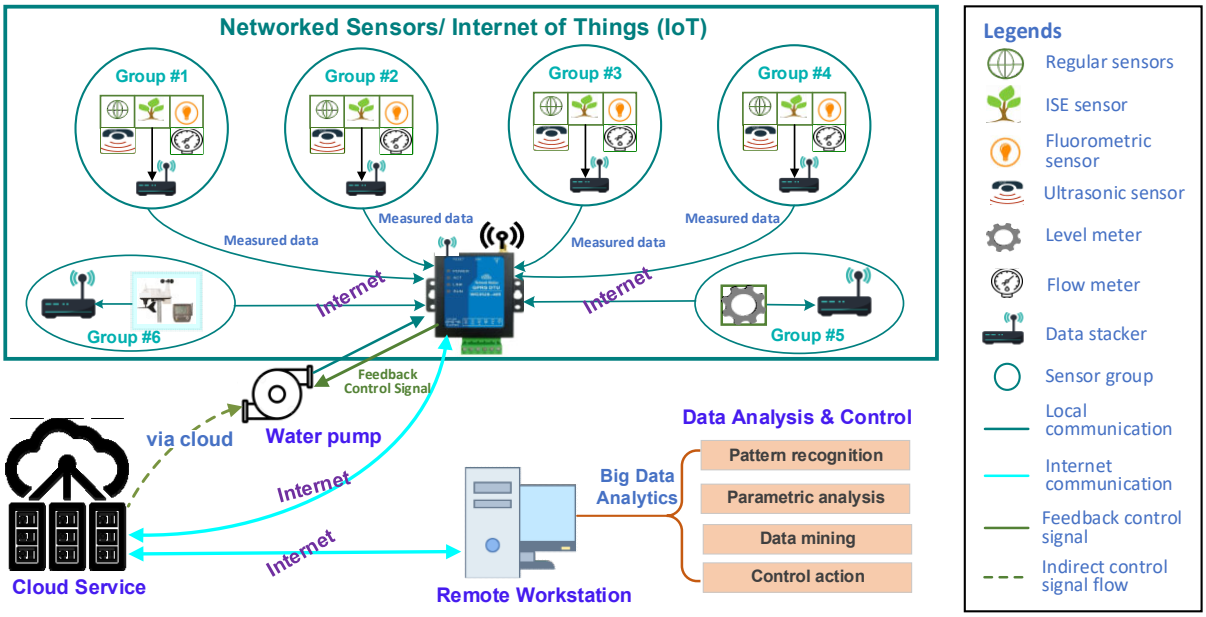

Figure 3-10: The final sensor and communication framework with big data analytics for operation.

On Feb. 16, 2023, the ETS engineers and the UCF research team members met to test the water probes using power generators on site as per the following steps: 1) Connecting 12 v battery, 2) Checking water probes signal, 3) Checking Eureka cloud storage, and 4) Checking UCF Cloud storage as a backup. UCF research team members had also added all parameters of the station (i.e., Global Radiation, Humidity, Precipitation, Temp (°F), Wind) to the Eureka cloud. By using the laptop for on-site testing, UCF research team members read out all measurements collected from the five water quality probes [as the example in Table 3-5(a)] and the weather stations [as the example in Table 3-5(b)] via the Eureka cloud. Serving as a back-up, the UCF cloud has been receiving data since Feb. 16, 2023. The cyberinfrastructure system of this filter is up and running as per the design as tested in Tables 3-4 and 3-5.

On Feb. 24, 2023, FP&L provided power supply on site and the facility was formally transferred from ETS to UCF for the forthcoming field campaigns. The UCF research team conducted the first field campaign started on March 1, 2023.

3.4 Background Water Characteristics of C-23 Canal

Two sampling activities at the study site were performed at Location 3 (Figure 3-11) during the dry season (January 27, 2021) and wet season (June 2, 2021). Field water quality parameters were analyzed based on the methods listed in Table 3-6.

Table 3-5(a): Measurements of water quality constituents from water quality probe via cloud

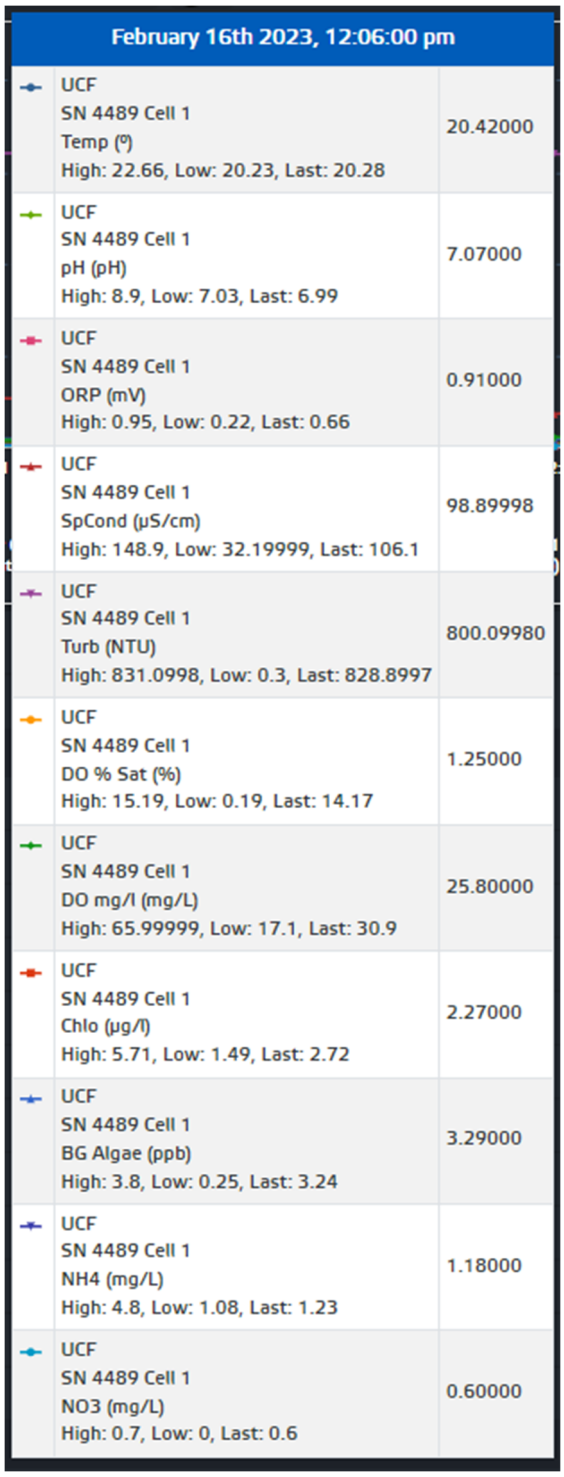

February 16th 2023, 12:06:00 pm	
UCF SN 4489 Cell 1 Temp (°) High: 22.66, Low: 20.23, Last: 20.28	20.42000
UCF SN 4489 Cell 1 pH (pH) High: 8.9, Low: 7.03, Last: 6.99	7.07000
UCF SN 4489 Cell 1 ORP (mV) High: 0.95, Low: 0.22, Last: 0.66	0.91000
UCF SN 4489 Cell 1 SpCond (µS/cm) High: 148.9, Low: 32.19999, Last: 106.1	98.89998
UCF SN 4489 Cell 1 Turb (NTU) High: 831.0998, Low: 0.3, Last: 828.8997	800.09980
UCF SN 4489 Cell 1 DO % Sat (%) High: 15.19, Low: 0.19, Last: 14.17	1.25000
UCF SN 4489 Cell 1 DO mg/l (mg/L) High: 65.99999, Low: 17.1, Last: 30.9	25.80000
UCF SN 4489 Cell 1 Chlo (µg/l) High: 5.71, Low: 1.49, Last: 2.72	2.27000
UCF SN 4489 Cell 1 BG Algae (ppb) High: 3.8, Low: 0.25, Last: 3.24	3.29000
UCF SN 4489 Cell 1 NH4 (mg/L) High: 4.8, Low: 1.08, Last: 1.23	1.18000
UCF SN 4489 Cell 1 NO3 (mg/L) High: 0.7, Low: 0, Last: 0.6	0.60000

Table 3-5(b): Measurements of the weather station via cloud

February 16th 2023, 12:12:00 pm		
	UCF Weather Station Temp (°F) High: 82.2, Low: 76.1, Last: 80.3	81.50000
	UCF Weather Station Wind () High: 12, Low: 0, Last: 5	11.50000
	UCF Weather Station Precipitation () High: 0, Low: 0, Last: 0	0.00000
	UCF Weather Station Humidity () High: 67.2, Low: 52.3, Last: 56.1	54.30000
	UCF Weather Station Air Pressure () High: 1022.3, Low: 1020.4, Last: 1020.4	1021.20000

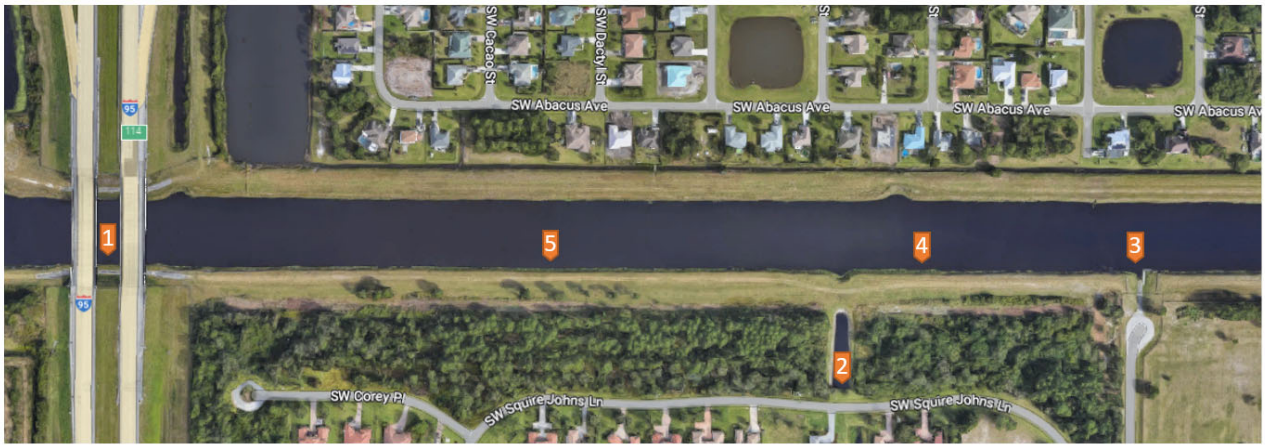

Figure 3-11: Canal water sampling locations.

(Source: Google maps retrieved March 28, 2023)

Table 3-6: Field water quality parameters and methods of water quality analysis

Parameter	Analysis/ Method	Laboratory
PFOS	Modified EPA 537.1	Eurofins Lancaster
PFOA	Modified EPA 537.1	Eurofins Lancaster

Total Nitrogen	EPA 351.2	Eurofins Environment Testing
Ammonia	EPA 350.1	Eurofins Environment Testing
Nitrate or Nitrite	EPA 353.2	Eurofins Environment Testing
Nitrate + Nitrite as N	EPA 353.2	Eurofins Environment Testing
Kjeldahl Nitrate	EPA 351.2	Eurofins Environment Testing
Orthophosphate	EPA 365.1	Eurofins Environment Testing
Total Phosphorus	EPA 365.1	Eurofins Environment Testing
Chlorophyll-a	SM10200H	Eurofins Environment Testing
E. Coli	SM 9223B	Eurofins Environment Testing
Biological Oxygen Demand (BOD)	SM 5210B	Eurofins Environment Testing
Dissolved Iron	EPA 200.7	Eurofins Environment Testing
Dissolved Aluminum	EPA 200.8	Eurofins Environment Testing
Bioavailable Organic Nitrogen (BDON)	HACH 10242 HACH 10205	University of Central Florida
Dissolved Organic Nitrogen	FT-ICR-MS	Florida State University
pH	pHTestr®30	University of Central Florida
ORP	HACH instrument HQ40D portable multi meter	University of Central Florida
DO	HACH instrument HQ40D portable multi meter	University of Central Florida
Turbidity	Aqua Fluor fluorometer	University of Central Florida

3.4.1 Dry Season Sampling and Water Quality

A dry season sampling event was conducted on January 27, 2021 to obtain background water quality data from 5 different locations around the construction site (Table 3-7). The parameters pH, temperature, ORP and DO were measured onsite using Hach kits.

Table 3-7: Summary of sampling locations and basic water quality parameters

Sample ID	Latitude	Longitude	pH	Temp (∘C)	Time	ORP (mV)	DO ($mg•L^{-1}$)
Location 1	27.205676	-80.400518	8.7	26.9	11:41 AM	127.2	9.2
Location 2	27.204614	-80.39424	8.2	24.8	11:55 PM	139.3	9.0
Location 3	27.205674	-80.391727	8.4	27.9	12:28 PM	142.6	9.0
Location 4	27.205596	-80.393131	8.57	31.4	1:04 PM	145.2	8.3
Location 5	27.205731	-80.396402	8.6	30.5	1:17 PM	143.0	8.9

Additional water samples were collected and delivered for PFAS analysis, conducted at Eurofins Lancaster laboratories (Table 3-8). Water samples for microcystin and phycocyanin were analyzed at Green Water laboratories and McGlynn laboratories, respectively (Table 3-9). The nutrients (TN, organic nitrogen, nitrate, nitrate, TKN, ammonia, phosphate, and TP), metals (dissolved iron and aluminum), chlorophyll a, E. coli, and BOD_5 were measured at Eurofins Environment Testing laboratories (Table 3-10).

Table 3-8: Canal background information of PFAS

Sample ID	PFAS	
	PFOA ($ng•L^{-1}$)	PFOS ($ng•L^{-1}$)
Control	--	1.6 J*
Location 1	15	16
Location 2	3.4	4.5
Location 3	14	14

*J: under the reporting limit but greater or equal to the MDL, and the concentration is an approximate value.

Table 3-9: Algal mass and algal toxin background information

Sample ID	Microcystin ($\mu g \cdot L^{-1}$)	Phycocyanin ($\mu g \cdot L^{-1}$)	Chlorophyll-a ($\mu g \cdot L^{-1}$)	E. Coli (mpn•100 ml^{-1})	BOD_5 ($mg \cdot L^{-1}$)
Location 1	*ND	0.9	12.8	20	2 U
Location 2	ND	0.6	2.82	10 **U	2 U
Location 3	ND	1.1	14.3	10	2.56
Location 4	ND	1.6	--	--	--
Location 5	ND	1.0	--	--	--

*ND stands for not detected above the method detection limit (MDL).

** U means that the compound was analyzed for but not detected.

Table 3-10: Nutrient and metal concentrations.

Sample ID	Organic Nitrogen ($mg \cdot L^{-1}$)	Total Nitrogen ($mg \cdot L^{-1}$ as N)	Nitrate ($mg \cdot L^{-1}$ as N)	Nitrite ($mg \cdot L^{-1}$ as N)	Total Kjeldahl Nitrogen ($mg \cdot L^{-1}$ as N)	Ammonia ($mg \cdot L^{-1}$ as N)	Phosphate ($mg \cdot L^{-1}$ as P)	Total Phosphorus ($mg \cdot L^{-1}$ as P)	Aluminum, Dissolved ($mg \cdot L^{-1}$)	Iron, Dissolved ($mg \cdot L^{-1}$)
Location 1	0.980	1.01	0.02 *U	0.0259 **I	0.98	0.0100U	0.0178	0.0476	0.01 *U	0.0806
Location 2	0.912	1.02	0.0785	0.0245 I	0.912	0.0100 U	0.005 U	0.0191	0.0120 **I	0.114
Location 3	1.04	1.06	0.02 U	0.0256 I	1.04	0.0100 U	0.0182	0.0566	0.0120 I	0.0832

*U means that the compound was analyzed for but not detected.
** "I" signifies that the reported value is between the laboratory MDL and the laboratory quantitation limit.

3.4.2 Wet Season Sampling and Water Quality

A similar sampling event was conducted on June 2, 2021 to collect water quality data during the wet season. The results are summarized in Tables 3-11~3-14.

Table 3-11: Summary of sampling locations and basic water quality parameters.

Sample ID	Latitude	Longitude	pH	Temp (∘C)	Time	ORP (mV)	DO ($mg \cdot L^{-1}$)
Location 1	27.205676	-80.400518	8.63	28.9	11:50 am	133.1	11.38
Location 2	27.204614	-80.39424	8.66	29.9	11:00 am	141	11.31
Location 3	27.205674	-80.391727	8.45	30.1	10:43 am	148.1	11.63
Location 4	27.205596	-80.393131	8.70	--	12:08 pm	140.7	12.08
Location 5	27.205731	-80.396402	8.43	--	12:39 pm	136.3	9.24

Table 3-12: PFAS concentrations in the Canal water

Sample ID	PFAS	
	PFOA (ng•L^{-1})	PFOS (ng•L^{-1})
Location 1	14	19
Location 2	3.6	5.5
Location 3	9.7	14

Table 3-13: Algal mass and algal toxin background data

Sample ID	Microcystin (µg•L^{-1})	Phycocyanin (µg•L^{-1})	Chlorophyll-a (µg•L^{-1})	E. Coli (mpn•100 ml^{-1})	BOD_5 (mg•L^{-1})
Location 1	ND*	2.2	51.9	50.4	2.56
Location 2	0.27	1.1	4.83	2420	2.00 U**
Location 3	ND	1.8	33.2	435	3.22
Location 4	ND	2.3	--	--	--
Location 5	ND	2.1	--	--	--

* ND stands for not detected.
** U means that the compound was analyzed for but not detected.

Table 3-14: Nutrient and metal concentrations.

Sample ID	Organic Nitrogen (mg•L^{-1})	Total Nitrogen (mg•L^{-1} as N)	Nitrate (mg•L^{-1} as N)	Nitrite (mg•L^{-1} as N)	Total Kjeldahl Nitrogen (mg•L^{-1} as N)	Ammonia (mg•L^{-1} as N)	Phosphate (mg•L^{-1} as P)	Total Phosphorus (mg•L^{-1} as P)	Aluminum, Dissolved (mg•L^{-1})	Iron, Dissolved (mg•L^{-1})
Location 1	1.22	1.33	0.110	0.0200U	1.22	0.01U*	0.100U	0.081	0.0889	0.292
Location 2	0.881	0.942	0.0613	0.0200U	0.881	0.01U	0.100U	0.048	0.0589	0.0399
Location 3	1.03	1.07	0.0416	0.0200U	1.03	0.01U	0.100U	0.082	0.0243	0.0279

* U means that the compound was analyzed for but not detected.

This page intentionally left blank.

Chapter 4: Field Sampling and Performance Assessment of the Filtration System

4.1 Sampling Events and Media Characteristics

The primary goal of applying filtration media is to reduce nutrient levels including Total Phosphorus (TP) and Total Nitrogen (TN), which can lead to algal blooms and result in the release of associated toxins such as microcystin. In addition, the project aims to remove a range of typical surface water pollutants including pathogens (E Coli), biochemical oxygen demand (BOD), and algal mass, as well as contaminants of emerging concern including algal toxins and per- and polyfluoroalkyl substances (e.g., PFAS). The total maximum daily load (TMDL) goals for TN, TP, and BOD are set at 0.72 mg•L^{-1}, 0.081 mg•L^{-1}, and 2.0 mg•L^{-1}, respectively in the St. Lucie River and Estuary region and are expected to be achieved by the four treatment cells along the C-23 canal.

The filtration system was designed to extract water from the C-23 canal using submersible pumps and deliver it to four treatment cells (22’ W x 43.5’ L each) to evaluate the efficiency of CPS and ZIPGEM media in removing the above-mentioned pollutants. Cells 1 and 2 contained ZIPGEM media and Cells 3 and 4 contained CPS media, as shown in Figure 4-1. The filter is located at 27°12'19.8"N (Latitude) and 80°23'47.8"W (Longitude).

The experimental protocol, along with the manual sampling activities enabled a direct comparison of the effectiveness of the two media in mitigating eutrophication and reducing the levels of target pollutants. Process schematic is shown in Figure 4-2. Ten manual sampling and monitoring events at a frequency of approximately every two weeks have been summarized in Table 4-1. Each sampling event included collection of water (influents and effluents) and media samples from each of the filtration cells (Figure 4-2), manual recording of basic water quality

parameters, and maintaining in situ automated water quality sensors. All field water sampling events were conducted according to Florida Department of Environmental Protection Standard Operating Procedures (FDEP SOP: FT1000, FS1000, FS2000 and FS2100). Table 4-1 also shows that average flow rate decreases in wet season. This is mainly due to particle deposition and capture (Pinheiro et al., 1999, Todisco et al., 2023) within ZIPGEM and CPS. During the wet season, more complex water matrix may imply more physicochemical reactions, which can cause biofilm fouling inside the media, thereby reducing the average flow rate.

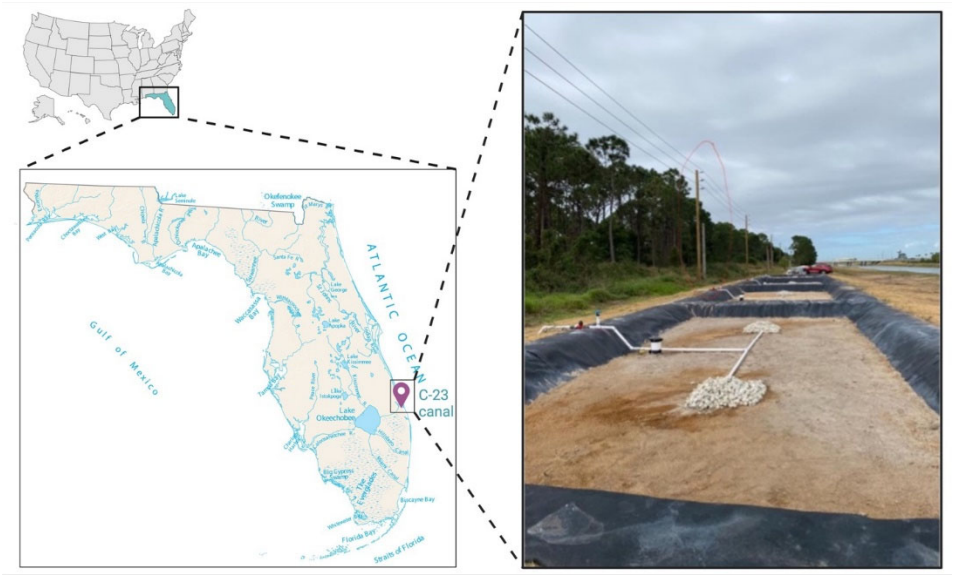

(a) Study location at canal 23 corridor

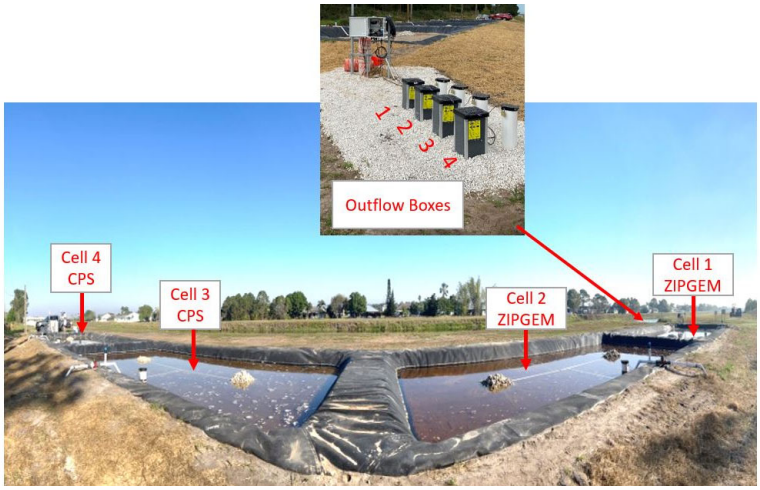

(b) Panoramic view of four pilot-scale filter cells with influent and effluent sampling locations.

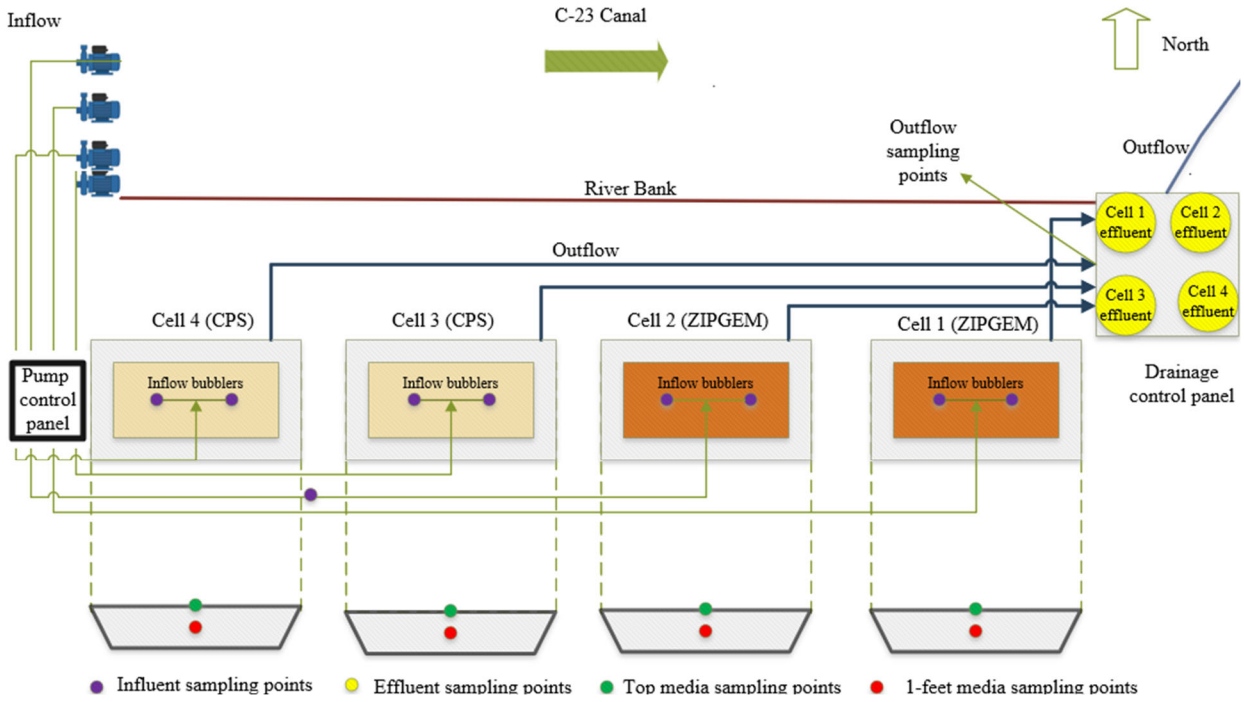

(c) Process schematic

Figure 4-1: Study location and sampling locations of ZIPGEM cells (cells 1 and 2) and CPS cells (cells 3 and 4) filtration cells.

(a)

(b)

Influent Sample Collection Point

Effluent Sample Collection Point

Figure 3: (a) Panoramic view of four filter cells with influent and effluent sampling locations, and (b) Effluent water sampling locations next to the drainage box.

Table 4-1: Sample collection events and weather conditions during field campaigns.

Event	Date	Season	Temp. (F)	average flowrate		Rainfall (mm)	Hydraulic loading rate (GPD/ft^2)
				(CMD)	(GPM)		
1	**3/1/2023**	Dry	71.43	65.41	12	0	18.06
2	**3/14/2023**	Dry	69.96	65.41	12	0.01	18.06
3	**3/28/2023**	Dry	79.13	54.51	10	0	15.05
4	**4/11/2023**	Dry	72.95	54.51	10	0.09	15.05
5	**4/25/2023**	Dry	73.35	43.61	8	0.46	12.04
6	**5/9/2023**	Wet	74.89	43.61	8	0.28	12.04
7	**5/23/2023**	Wet	77.68	38.16	7	0.09	10.53
8	**6/6/2023**	Wet	75.84	38.16	7	1.13	10.53
9	**6/20/2023**	Wet	74.96	32.71	6	0.64	9.03
10	**7/3/2023**	Wet	81.02	32.71	6	0.99	9.03

The filtration system receives water from C-23 canal via four 30-gpm (0.043-MGD) submersible pumps. Four pipes in parallel configuration deliver water to four filtration media beds. Each treatment (filtration) cell has a dedicated pump and float switch to maintain a 6 (±2) inch water depth over the media. Inlet pipelines for each treatment cell are equipped with flowmeters that can be remotely read via a telemetry system, as illustrated in Chapter 3. The filtration media beds are equipped with a telemetry system to aid in remote data collection. The telemetry system provided readings of different parameters including infiltration pond water levels, flowrates to and from the ponds, real time water quality data, etc. In addition, the telemetry system in the project supports the monitoring of water levels in cells and real-time water quality data, as well as the ability to control the pumps remotely. Each cell has a dedicated float control to maintain a 6 (±2)-inch water depth over the media. Each cell's inlet pipeline has a flowmeter for continuous reading of flowrate. The cells have a maximum depth of 4 feet with 3:1

exterior and 1:1 interior side-slope of the perimeter berm. Each outlet is connected to a drainage control box that allows the outlet head of the cell to be set via an orifice to control outflow rate. The outlet pipe contains the water quality and depth pressure probes. Each orifice in the box has a diameter of 1 inch, and all orifices have been configured to discharge at a predetermined flow rate by adjusting the water depth in the drainage boxes.

Multiple energy dissipating bubblers are used to deliver canal water to each cell while avoiding the scouring of the media. Cells 1 and 2 contain CPS media while cells 3 and 4 contain ZIPGEM media. The filtration media in each cell was placed over a 6-inch gravel layer and a permeable geo-textile sheet. The drainage network in each treatment cell consists of three 4" perforated plastic drainpipes embedded in the gravel layer to collect and deliver the treated water into an 8- inch PVC main outlet pipe and then back to the C-23 canal approximately 200 feet east (downstream) from where the water is extracted. The thickness of media bed in each cell is 2 feet. As shown in Figure 4-3, we studied two specialty adsorbents, including CPS and ZIPGEM, to determine their potential to remove nutrients via physiochemical interactions.

ZVI used for this study was procured from a manufacturer of iron aggregate, Connelly-GPM, Inc. (Chicago, IL). The manufacturer's ZVI is known as ETI CC-1004 (-8 + 50). The ZVI contained 87%–93% metallic iron. The perlite used in this study was procured rom Miracle-Go®, containing 99.44% perlite. The physical characteristics, including BET surface area and density, were determined at the EMSL Analytical, Inc. laboratories. Density and BET surface area were measured following ASTM D854 and ASTM B922 methods. The saturated hydraulic conductivity was measured using the constant head permeability test at the UCF Geotechnical Laboratory.

Figure 4-3: Media mixes and media components (Ordonez et al., 2023)

The treated water was collected via gravity through three 4-inch perforated plastic drainpipes and then delivered back to the C-23 cannel 200 feet east (downstream) from the influent collection point. This distance between inflow collection and drainage was maintained to avoid recycling treated water during low flow periods. The four effluents that were collected from the drainage control box are denoted by numbers 1, 2, 3, and 4. In addition to housing the water quality probe and depth pressure probe, the drainage control box allows the adjustment of outlet head of each cell as designed. The four probes at the outlet were connected to a telemetry system that facilitates continuous and remote monitoring of various water quality parameters and water depth. An additional water quality probe was placed in cell 1 to monitor the inflow water quality parameters. The samples collected during each field campaign were sent to the certified laboratories for the analyses of water constitutes of concern. The effluent samples are collected

in triplicate to ensure reliability of data measurements. Additionally, manual samples were collected from the canal directly for the validation of the background concentrations and quality control of our data analysis.

4.2 Sampling and Analysis Protocol

The first field campaign conducted on March 1st, 2023, involved collecting water and media samples, as listed in Table 4-2. Following the QA/QC protocols, all sample containers were properly cleaned, labeled, and packed for transport the day prior to the field trip (Table 4). During the campaign, a waterproof notebook was utilized to accurately document all relevant information. Additionally, both a hard copy and an online copy of all chain of custodies were securely stored in Eng. 1 Room 322 at UCF and a dedicated Dropbox folder, respectively. Figure 4-2 shows the typical locations from which water and media samples were collected at each treatment cell.

Table 4-2: Sampling locations and number of samples collected during each field trip

	Cell 1 CPS Media		Cell 2 CPS Media		Cell 3 ZIPGEM Media		Cell 4 ZIPGEM Media		Set / Campaign	#Samples/ Campaign
Media	Top	1 ft	Top	1 ft	Top	1 ft	Top	1 ft	4	16
	2	2	2	2	2	2	2	2		
Water/field trip	Inf	Eff	Inf	Eff	Inf	Eff	Inf	Eff	16	187
	1	3	1	3	1	3	1	3		
Blank	1								1	

During each sampling event, a set of triplicate water samples was collected for each water quality parameter from the inlet (canal water) and the outlet of each treatment cell. All water samples were collected at similar locations at the inlet and outlet of each cell and preserved and delivered to the corresponding laboratories in accordance with the methods and the FDEP SOPs listed in Table 4-2 and Table 4-3. Blank samples were collected for analyzing for nutrients including TN, TP, ortho-phosphate (PO_4^{3-}), ammonia (NH_3), TKN, nitrate (NO^{3-}) and nitrite

(NO^{2-}), and metal ions including iron and aluminum in accordance with DEP SOP FQ 1000. All sample containers and intermediate containers were prepared at UCF laboratory according to FDEP SOP FC-1000. PFAS samples were processed by the Eurofins Lancaster Environmental Lab. Nutrient and biological pollutants were processed by Eurofins Environmental Testing Southeast Laboratories (formerly Flowers).

Table 4-3: Summary of water quality parameters, analytical methods, and detection limits

Due to 508 compliance requirements, Table 4-3 was removed from this document. To access the full document, which does not meet 508 compliance standards, please reach out to InnTech_HAB@FloridaDEP.gov

The point of zero charge (PZC) for each medium was also measured using the salt addition method (Mahmood et al., 2011) at UCF. The salt addition method determines the pH when the surface of the adsorbent is at ionic equilibrium, the condition when the numbers of H^+ and OH^- at the surface of the particle are equal. The protocol followed in this study was presented in detail in Ordonez et al. (2020b); The protocol used 0.2 M $NaNO_3$ solution and NaOH or HNO_3 for pH adjustment. The results are presented in Figure 4-4.

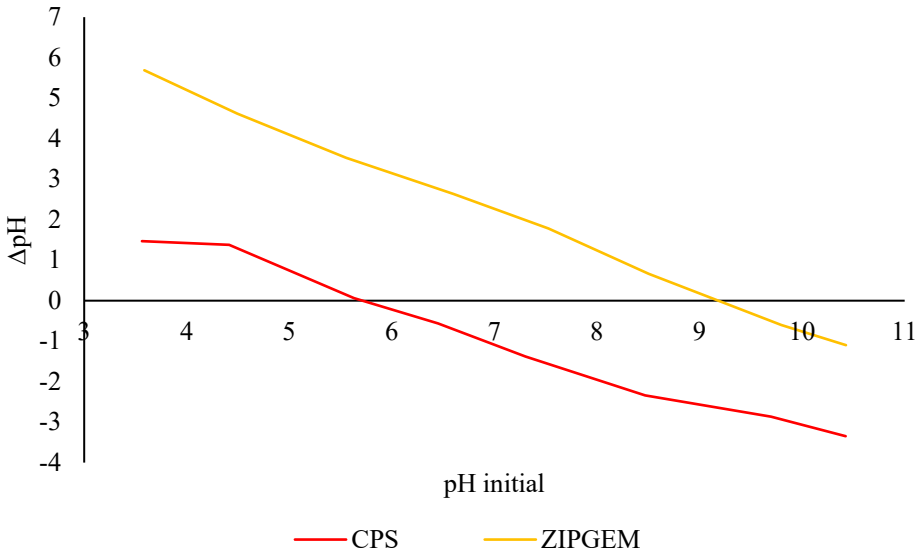

Figure 4-4: Location of PZC for CPS and ZIPGEM (Ordonez et al., 2023)

4.3 Environmental Monitoring and Data Collection and Storage

The water quality probes installed in the drainage boxes are also connected to the telemetry panel to provide continuous and remote monitoring of water quality parameters and water depth, which can be used to estimate outflow rates through the orifice in each drainage box. The site is equipped with one CCTV monitoring camera to support the monitoring and management of the filter system in case of any technical issues.

A weather station is installed at the site and connected to the Eureka Telemetry Panel to gather local rainfall, temperature, wind, and humidity data continuously, as presented in Figure 4-5 and Table 4-4. The data were utilized in the system water balance calculations as well as in future hydrological studies. Additionally, the weather station data can help identify the trends in water quality parameters related to the weather conditions, which can be utilized in future design decisions and operational performance evaluation of the treatment cells.

The telemetry system, the Stevens eTracker, has been successfully uploading the water quality data to the cloud storage since the installation of the automatic water quality monitoring system. As recommended by the Eureka team, the logging interval has been adjusted to 15 minutes and the reporting interval has been set to 1 hour. The collected data set is uploaded to a cloud service at stevens-connect.com. Moreover, the uploaded data set is being automatically forwarded to the dedicated cloud storage at UCF as a backup. However, the received backup data in the UCF cloud are still in raw form, and UCF technical support is currently constructing an interface to present the data in a similar format as Eureka's cloud storage for better data management and analysis.

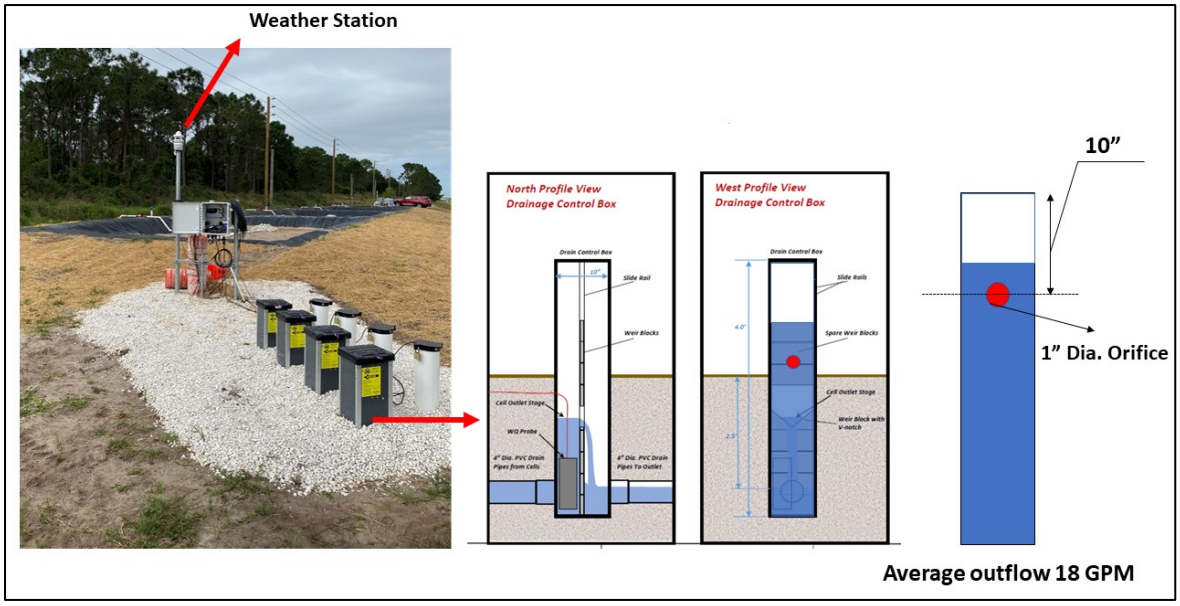

Figure 4-5: Weather station and drainage box's locations.

Table 4-4: Samples for the station records of weather conditions in the site via Eureka Cloud

	Weather Station				
Date/Time	**Temp °F**	**Wind**	**Precipitation (in)**	**Humidity**	**Air Pressure**
3/15/2023 22:45	60.8	2.9	0.05	76.2	1022
3/15/2023 22:30	61.4	6.1	0.05	75	1022.1
3/15/2023 22:15	61.9	4	0.05	74.9	1022.1
3/15/2023 22:00	62.3	5	0.05	73.4	1022.1
3/15/2023 21:45	63	5.1	0.05	73.6	1022
3/15/2023 21:30	63.2	4.2	0.05	73.3	1021.8
3/15/2023 21:15	63.4	4.8	0.05	73.3	1021.6
3/15/2023 21:00	63.4	4.5	0.05	73.1	1021.4
3/15/2023 20:45	63.9	2.1	0.05	70.7	1021.4
3/15/2023 20:30	64.5	4	0.05	66.5	1021.3
3/15/2023 20:15	64.8	3.2	0.05	64	1021
3/15/2023 20:00	65.5	5.1	0.05	62.3	1021.1
3/15/2023 19:45	65.5	3	0.05	62.2	1021

4.4 Performance Assessment of Green Sorption Media and Seasonality Effect

4.4.1 Nutrient Removal

The average efficiencies of ZIPGEM and CPS in removing six water contaminants collected over ten sampling events are shown in Table 4-5, emphasizing the seasonality effects at first. Event-based performance evaluation was discussed later. These contaminants include TN, TKN, ammonia, dissolved organic nitrogen (DON), TP, and Orthophosphate (OP). Note that TKN is the sum of nitrogen in the forms of ammonia [un-ionized (NH_3) and ionized (NH_4^+)], soluble organic nitrogen, and particulate organic nitrogen. Contaminants of emerging concern such as PFAS were considered as well. It is expected that the changes in climatic conditions, characterized by wet and dry weather transitions and the stimulation of denitrification during the wet season, can reveal that the microbial-assisted filtration processes led to high nutrient removal performance.

As shown in Table 4-5, ZIPGEM demonstrated significantly higher (40–60%) Orthophosphate as P removal efficiency when compared to CPS, with an average removal rate of 73.16% for ZIPGEM and -134.97% for CPS. Since ZVI is included in ZIPGEM and ZVI may be dissolved and oxidized partially or completely to various forms of Fe oxides (i.e., Fe^{2+} and Fe^{3+}), phosphate can precipitate with Fe^{2+} and Fe^{3+} iron in accordance with the following equations ($Fe^{2+} + H_2PO_4^- \rightarrow Fe_3(PO_4)_2 + H^+$; $Fe^{3+} + PO_4^{3-} \rightarrow FePO_4$), further contributing to phosphate removal. The precipitation reaction of Fe^{3+} salts in the presence of OP in water was so fast [i.e., less than 1 s and may be instantaneous (Recht and Masood, 1970)] such that the simple crystalline precipitate, namely $Fe(PO_4)\cdot 2H_2O$, was formed. Based on the adsorption capacity values obtained through the isotherm studies as shown in Table 6-7, it is indicative that ZIPGEM has more than 10 times the capacity for phosphate removal than CPS (i.e., 1.796mg·g^{-1} for

ZIPGEM and 0.14mg·g^{-1} for CPS), confirming that ZIPGEM is better than CPS to remove phosphate. It is known that the field-mixed and lab-mixed raw media samples for CPS and ZIPGEM had similar percentages of elemental phosphorus as detected via the XRF analysis [Tables 3-1(a) & (b)] and the higher absolute volume of sand in CPS than that in ZIPGEM (~92yd^3>~85 yd^3), the amount of the negative removal rate of OP by CPS may be partly due to the release of OP from raw materials such as sand and geological origin of sandy soil because Florida's sand is primarily originated from ancient marine deposits, including phosphate minerals (Jasinski, 2013), and the extensive agriculture practices with a long history of phosphate-mining in Florida (Duan et al., 2021).

In line with such findings, ZIPGEM was better than CPS in removing TN and TP. The overall TN and TP removal rate by ZIPGEM was 53.86% and 79.58%, respectively, which was much higher than that of CPS. The negative values of ammonia removal may be attributed to the production of ammonia during the photoammonification, ammonification via microbial activities, and mineralization of dissolved organic nitrogen. In general, nitrification should be driven by the microbial species AOB and NOB leading to consume NH_3 and decrease NH_3. Integrated actions of photoammonification, ammonification, and mineralization might have caused negative ammonia removal rates, but those ammonia will be consumed by the microbial community finally.

Table 4-5: The average removal rate of nutrients by ZIPGEM and CPS overall and in dry and wet season

	ZIPGEM			CPS		
	dry season	wet season	Overall	dry season	wet season	Overall
TN	57.89%	40.67%	49.28%	45.57%	18.37%	31.97%
TKN	64.82%	69.45%	67.13%	62.47%	57.73%	60.10%
Ammonia	-16.44%	-220.59%	-118.52%	-33.65%	-475.53%	-254.59%
DON	68.31%	77.48%	72.90%	66.14%	72.11%	69.13%

TP	73.43%	85.72%	79.58%	9.18%	21.80%	15.49%
OP	74.42%	71.89%	73.16%	-220.20%	-49.74%	-134.97%

Figure 4-6 further presents the event-wise comparative performance evaluation of the two green sorption media. For ZIPGEM, TN removal efficiencies were below 50% during only three sampling events, events 6, 9, and 10. For CPS, however, the TN removal efficiency was lower than 50% during seven sampling events. For sampling event 9, ZIPGEM and CPS showed the lowest total nitrogen removals of 15.39% and 3.49%, respectively. However, ZIPGEM was significantly better than CPS in removing TN in general.

Figure 4-6: The removal efficiency of (a) TN, (b) TKN, (c) Ammonia, (d) DON, (e) TP, and (f) OP by ZIPGEM and CPS

TKN removal efficiency of ZIPGEM was higher than CPS. Moreover, ZIPGEM had only one sampling event with removal efficiency below 50%, while CPS had two sampling events

with removal efficiency below 50%. Sampling event 5 exhibited the lowest point of TKN removal for both ZIPGEM and CPS, which may be related to seasonal change. The efficiency of ammonia removal by both ZIPGEM and CPS was influenced by seasonal variation. During the first four sampling events, CPS appeared to remove slightly more ammonia than ZIPGEM, but the difference was small. From the fifth event onward, both ZIPGEM and CPS had negative efficiencies in removing ammonia. But this does not indicate the inefficiency of ZIPGEM and CPS in removing ammonia. The negative values may be because ammonia nitrogen concentration of influents is less than that of effluent since ammonia is continuously released due to photoammonification, bacteria ammonification, and mineralization of DON (Davis et al., 2006; Liu et al., 2010; Shrestha et al., 2018). Nevertheless, ZIPGEM exhibits superior adaptability to seasonal variations compared to CPS.

ZIPGEM demonstrated significantly higher (30–60%) TP removal efficiency when compared to CPS. TP removal efficiency by ZIPGEM was greater than 70% and only slightly lower in the first sampling event. In comparison, the removal rate of CPS only reached 60% during the tenth sampling event. The average TP removal rate by ZIPGEM was 79.58%, while that for CPS was only 15.49%. Even in the 10th sampling event, ZIPGEM still achieved 96.22%, while the removal rate of CPS was only 61.04%. ZIPGEM demonstrated significantly higher (40–60%) OP removal efficiency when compared to CPS in each sampling event, with an average removal rate of 73.16% for ZIPGEM and -134.97% for CPS. The latter may be due to the release of orthophosphate from raw materials such as sand because of the geological origin of sandy soil (Jasinski, 2013) and the extensive agriculture practices (Duan et al., 2021) in Florida.

4.4.2 Biological Pollutant Removal

As listed in Table 4-6, the average efficiency of ZIPGEM and CPS in removing E. coli was similar (around 80%), indicating that ZIPGEM and CPS have a wide range of practical applications as green sorption media. The results of Chl-a and algal mass removal by ZIPGEM and CPS are also promising, especially during the wet season. However, BOD removal by ZIPGEM and CPS was not high because these specialty adsorbents mainly promote sorption processes with limited biofilm activity on the surface of the media. The biofilm activity was limited due to algal organic matter released from algal blooms, especially in wet season (i.e. removal rate of BOD in event 10 was negative), because the large portion of labile organic compounds in AOM and its continuous load may significantly decrease the diversity of biofilm community structure at the top layer (surface) of media (Jeon et al., 2020; Prest et al., 2016).

Table 4-6: Average removal rate of biological pollutants over seasons

	ZIPGEM			CPS		
	dry season	wet season	Overall	dry season	wet season	Overall
E. coli	73.04%	86.46%	79.75%	82.04%	82.77%	82.40%
Chlorophyll a	95.05%	98.78%	96.92%	87.08%	99.47%	93.27%
Algal mass	95.49%	98.77%	97.13%	89.06%	99.47%	94.26%
BOD	40.47%	5.32%	22.90%	41.64%	-6.63%	17.50%

As shown in Figure 4-7(a), the removal efficiency of E Coli varied from event to event. Seven events showed very good removal efficiencies. As shown in Figure 4-7(b), the results of chlorophyll-a removal by ZIPGEM and CPS were very close to each other during each sampling event, and both ZIPGEM and CPS were able to remove chlorophyll-a very well, with an average removal rate exceeding 90%. As shown in Figure 4-7(c), both ZIPGEM and CPS exhibited large fluctuations in BOD removal, which can be attributed to the weather effects such as heavy rainfall, although their removal efficiencies were relatively close to each other during each

sampling event. As shown in Figure 4-7(d), both ZIPGEM and CPS exhibited good algal mass removal efficiency.

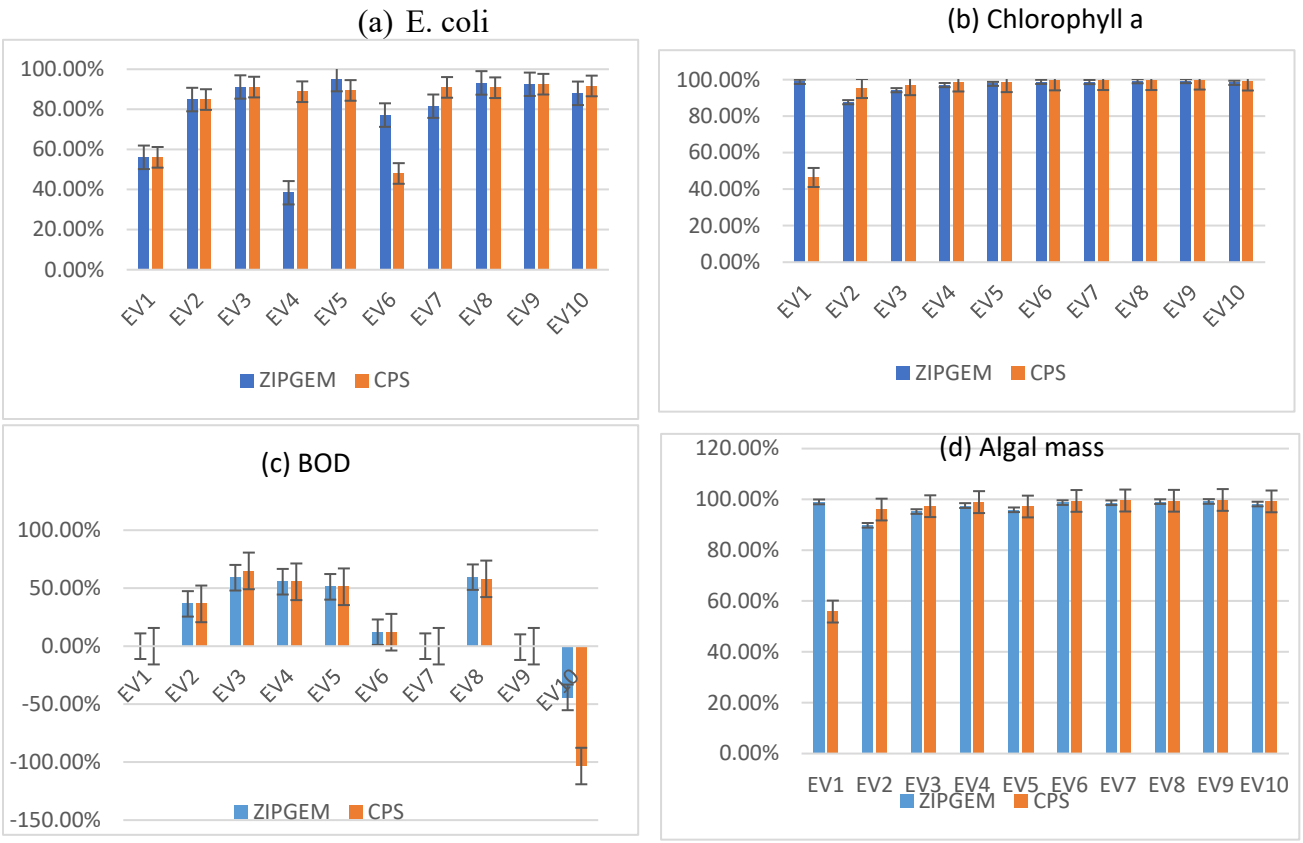

Figure 4-7: The removal efficiency of (a) E. coli, (b) Chlorophyll-a, (c) BOD, and (d) algal mass by ZIPGEM and CPS.

Both the event-based assessment and the seasonality-based assessment in above reveal the process reliability between ZIPGEM cells and CPS cells with respect to the varying temporal scale. Figures 4-8 and 4-9 clearly revealed that the cell-based assessment can exhibit a unique temporal pattern for ZIPGEM cells, which indicates the photoammonification and mineralization was predominant in the wet season and ammonia removal rates were always negative in the wet season. However, Figures 4-10 and 4-11 shows both OP and ammonia cannot be removed efficiently in both seasons for CPS cells. As for the removal of biological pollutants in Figures 4-

12~15, both ZIPGEM and CPS cells exhibited equal performance. Other than BOD, both can remove E. coli, Chlorophyll-a, and algal mass efficiently. Overall, ZIPGEM cells performed much better than CPS cells. More details of the event- or cell-based analysis can be found from Tables C1~C4 in Appendix C.

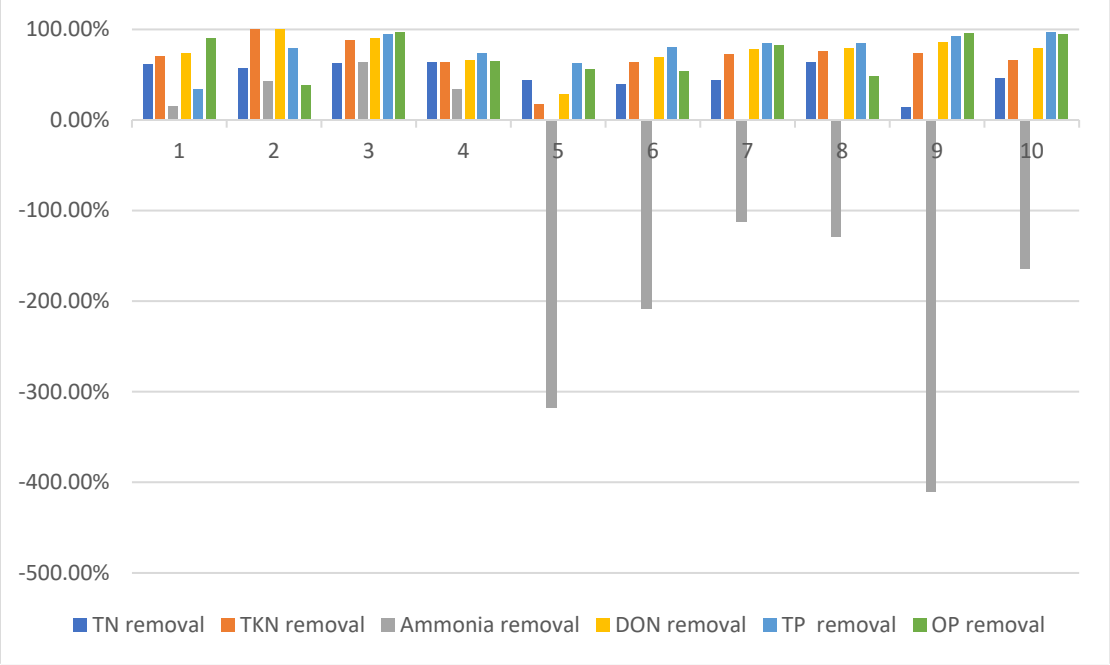

Figure 4-8: The removal rate of nutrients by ZIPGEM in cell 1.

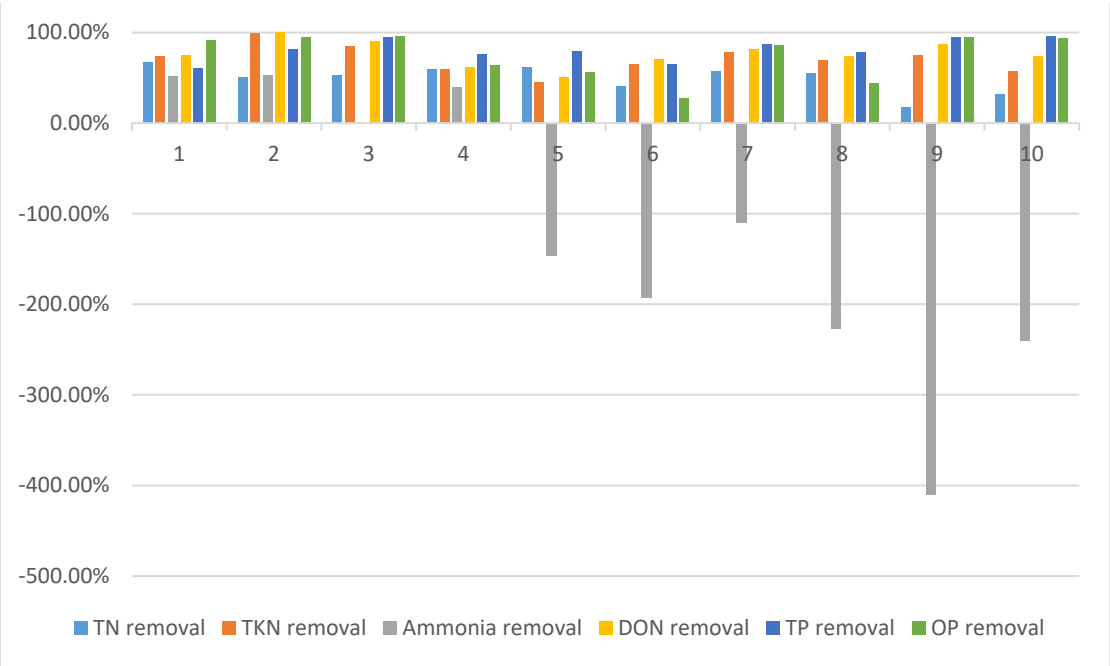

Figure 4-9: The removal rate of nutrients by ZIPGEM in cell 2.

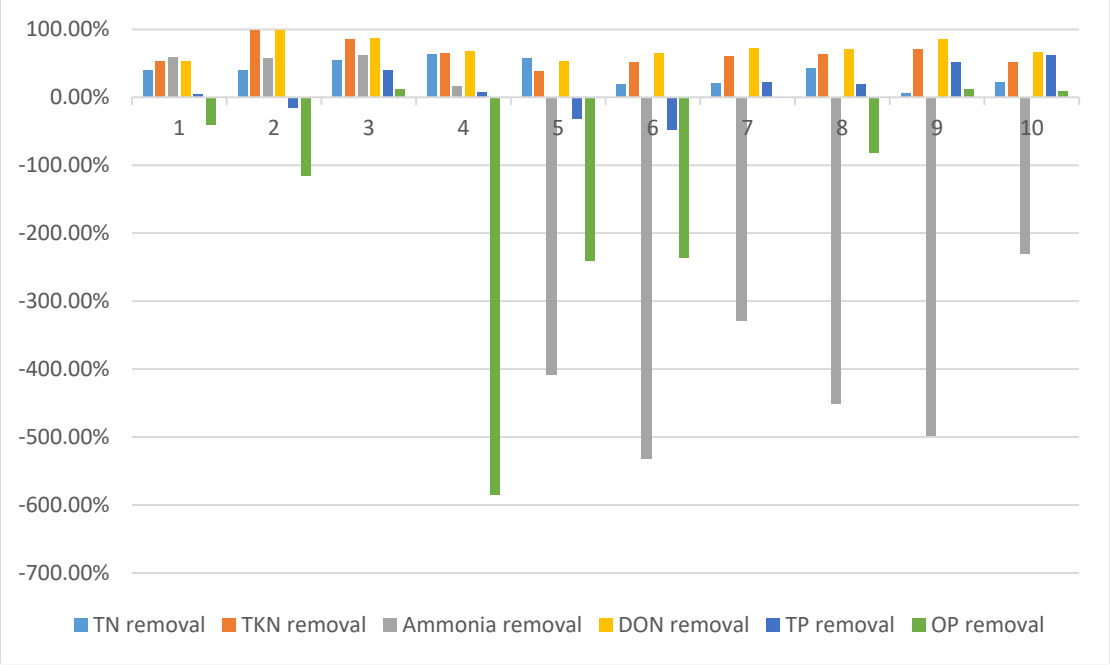

Figure 4-10: The removal rate of nutrients by CPS in cell 3.

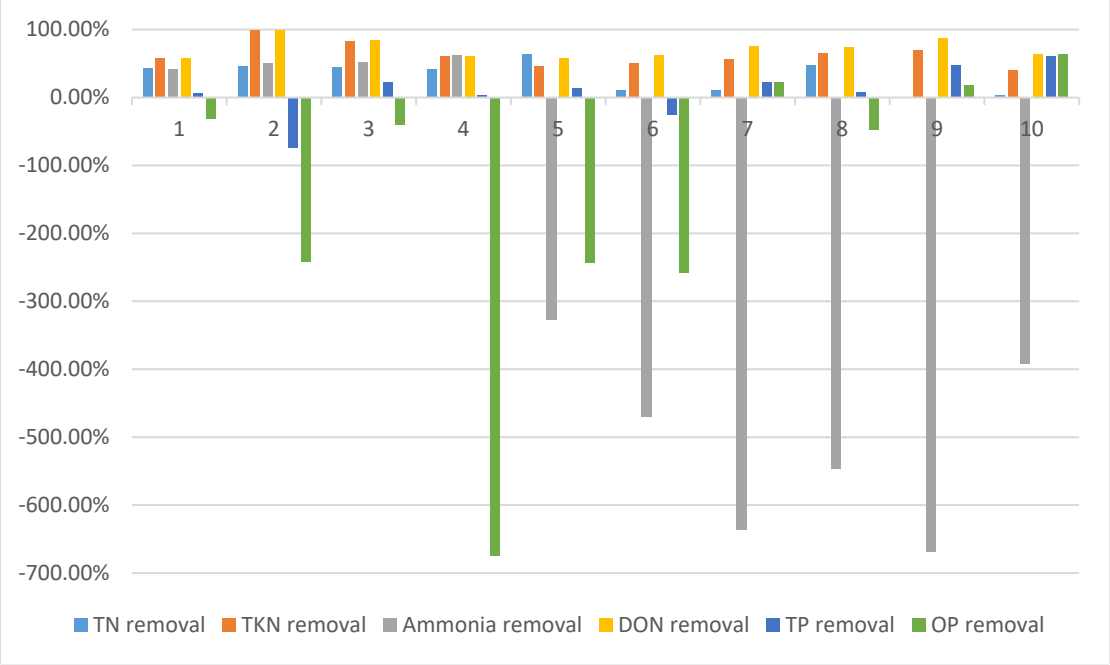

Figure 4-11: The removal rate of nutrients by CPS in cell 4.

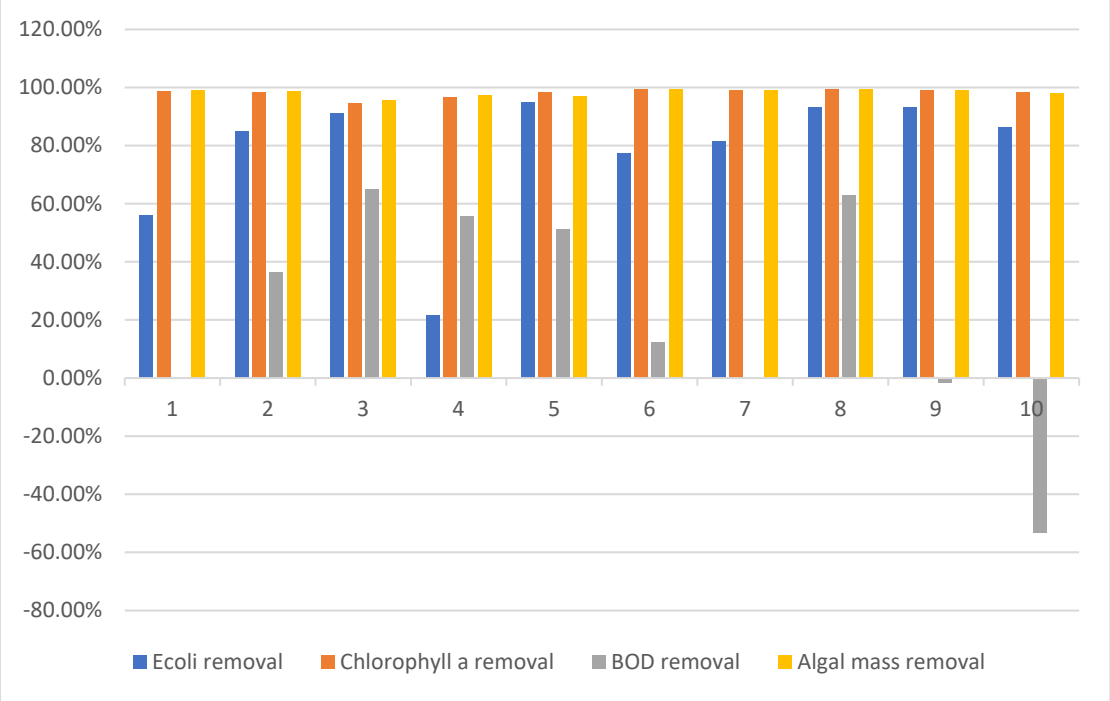

Figure 4-12: The removal rate of biological pollutants by ZIPGEM in cell 1.

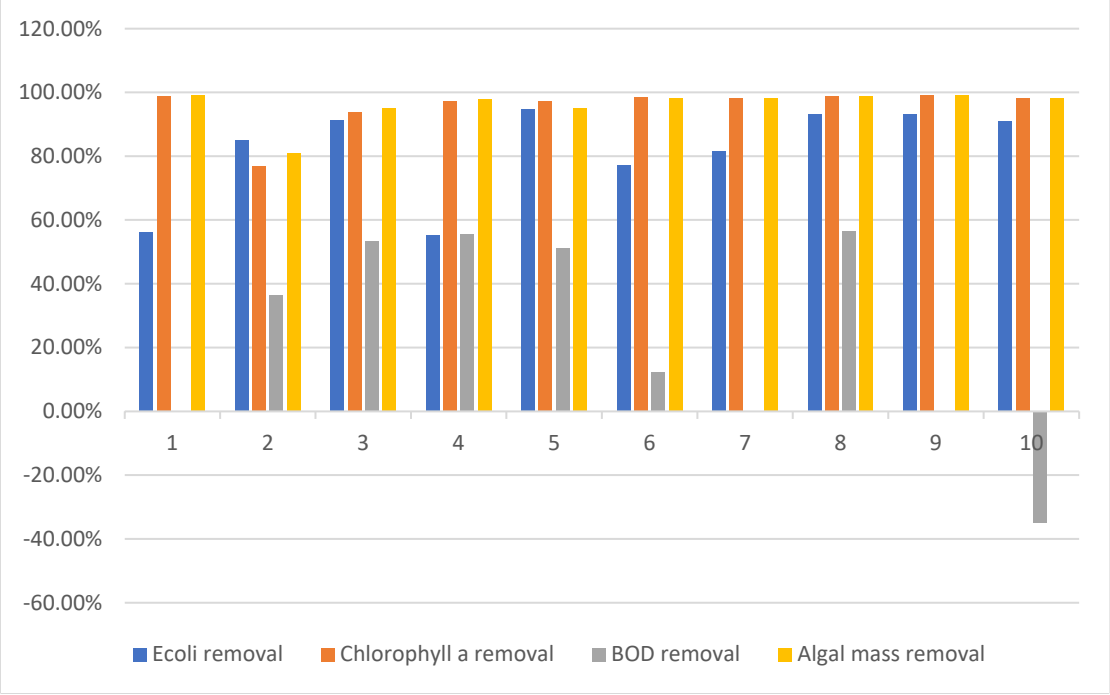

Figure 4-13: The removal rate of biological pollutants by ZIPGEM in cell 2.

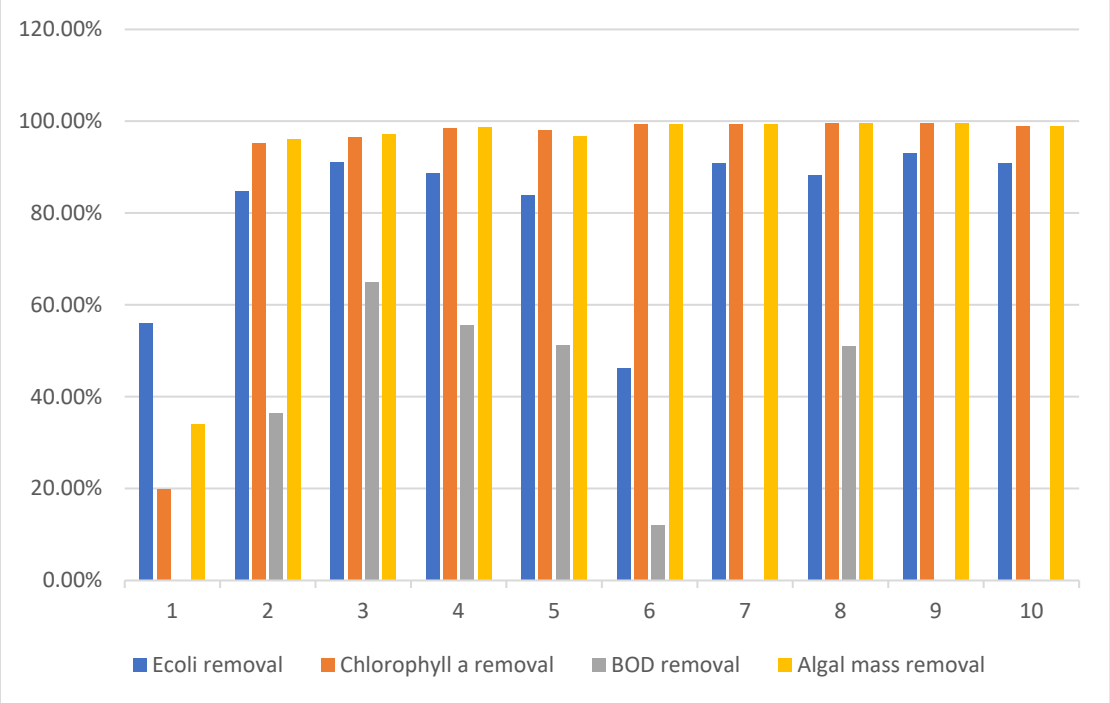

Figure 4-14: The removal rate of biological pollutants by CPS in cell 3.

Figure 4-15: The removal rate of biological pollutants by CPS in cell 4.

4.4.3 PFAS Removal

Table 4-7 shows the removal efficiencies of long-chain PFAS, calculated based on the average concentrations in cell 1 and cell 2 for ZIPGEM and cell 3 and cell 4 for CPS. Based on the ten field campaign results, ZIPGEM and CPS media appear to be highly effective in removing PFOS with removal efficiencies ranging from 87.1% to 95.6% in cell #1 and cell #2, respectively. When considering PFOA removal, ZIPGEM media was found to be more effective than CPS media as shown in Table 4-7. However, the media adsorption capacity appeared to diminish during the later events. Negative removals of PFOA by ZIPGEM were observed during Events 5, 7, 9, and 10 and by CPS during Events 5, 9, and 10. Negative removals of PFOS by ZIPGEM were observed during events 5 and 8 and by CPS during events 5, 8, 9, and 10. This could be due to the competition of other constituents for the media adsorption sites as well as the generation of ammonia from photo-ammonification and bacterial ammonification.

Table 4-7: Average removal efficiencies (%) of PFAS in ZIPGEM and CPS (gray section represents dry season and yellow section represents wet season)

the	ZIPGEM (%)										CPS (%)									
	Ev1	Ev2	Ev3	Ev4	Ev5	Ev6	Ev7	Ev8	Ev9	Ev10	Ev1	Ev2	Ev3	Ev4	Ev5	Ev6	Ev7	Ev8	Ev9	Ev10
PFOA	9.3	11.1	4.6	0.0	-9.1	11.1	-3.6	16.2	-1.0	-27.7	0.0	7.9	-11.9	10.1	-12.5	3.0	0.0	21.9	-31.0	-48.5
PFOS	95.6	4.9	-43.3	34.9	-4.0	4.4	6.7	-4.8	2.5	9.1	87.1	26.0	-88.3	20.0	-2.7	9.2	5.1	-5.2	-12.1	-10.9

Bar charts in Figure 4-16 depict the removal efficiencies of individual PFAS species whereas the line plots show the removal efficiency of total PFAS. It is noticeable from Figure 4-16 that both long- and short-chain PFAS removal efficiencies had an irregular pattern and the influent PFAS concentration seemed to have no effect on the removal efficiencies. Therefore, it is likely that other water quality parameters might influence PFAS removal efficiencies. For instance,

ammonia concentration in the influent and effluent showed a negative effect on the removal efficiency of both short-chain and long-chain PFAS, which will be discussed further in Chapter 5.

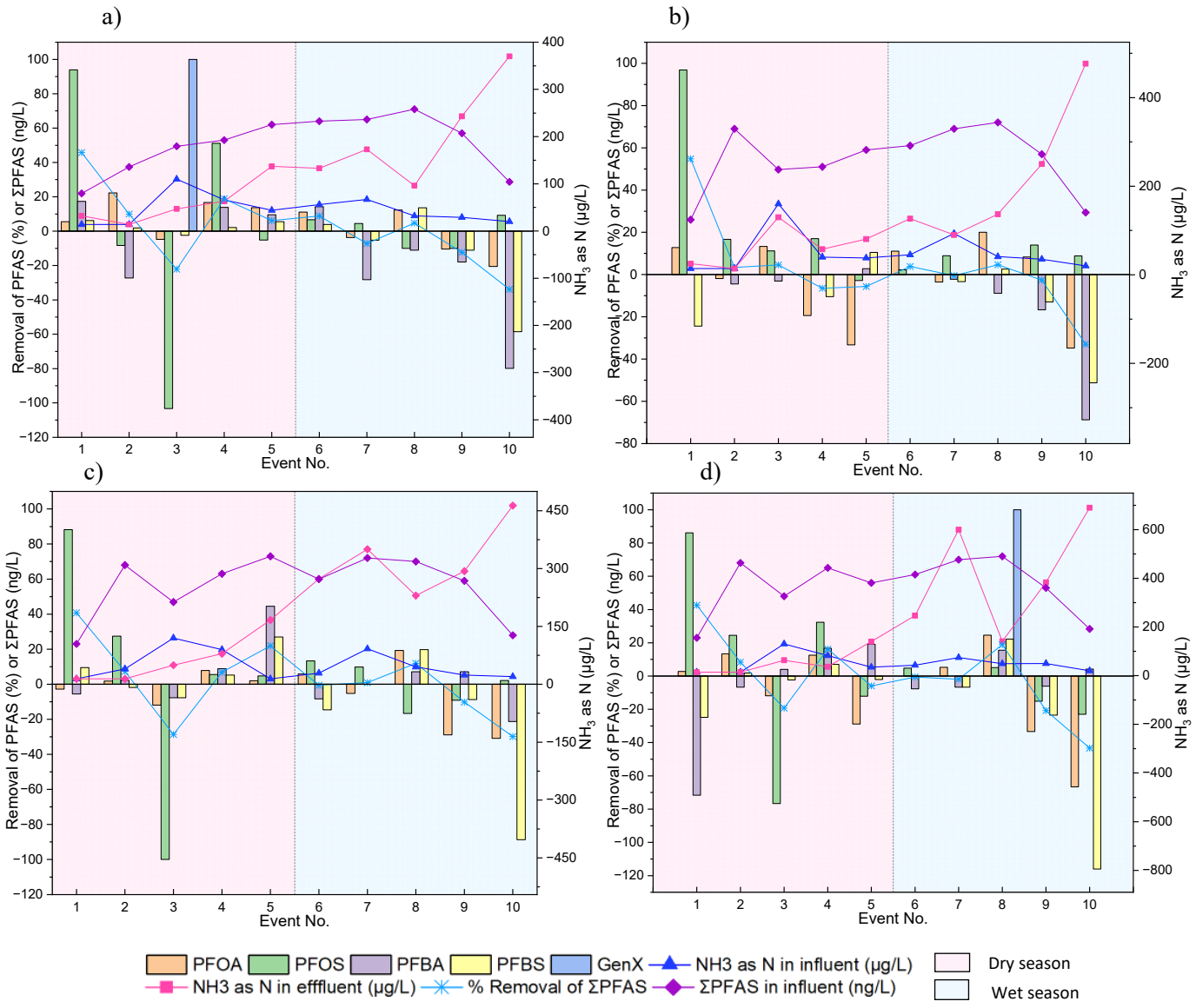

Figure 4-16: Removal efficiency of PFAS in different cell for all event cases. Subfigure a, b, c and d illustrates the removal efficiency in cell 1, 2, 3 and 4, respectively. Removal efficiencies were calculated based on the single influent and averaged triplicate effluent concentration.

The events with a spike in influent or effluent concentrations of ammonia are associated with low removals of either short-chain or long-chain PFAS. Total PFAS concentrations in the influent as well as the ammonia concentration in the influent and effluent are presented in Figure 4-16. Influent and effluent concentrations of ammonia shown in the figure may influence PFAS removal efficiency of PFAS. A high concentration of ammonia may increase pH (Scott et al., 2005), resulting in reduced PFAS adsorption due to the deprotonation of the sorbent functional groups (Hale et al., 2017; Kah et al., 2021) Besides, the richness and structure of microbial communities in biofilms were drastically changed following PFAS exposure (Ji and Zhao, 2023). For example, Ji et al. (2021) reported that the relative abundance of Acinetobacter, Anaerolineae, and Chloroflexia decreased substantially under PFOS stress.

Event 1 in cell of both ZIPGEM and CPS shows good removal of long-chain PFAS including PFOA and PFOS. The removal of short chain-PFAS is usually poor by these adsorbent media which can be due to the competition of long-chain and short-chain PFAS for adsorption sites or the higher solubility of short-chain PFAS. The influent ammonia concentration in cell 1 event 3 rose to 0.11 mg•L^{-1} from 0.014 mg•L^{-1} in event 1 and 2. This is associated with a significant drop in removal efficiency of total PFAS from approximately 46% in event 1 to -22% in event 3. Cell 2 showed a similar trend where ammonia concentration increases to 0.13 mg•L^{-1} in event 3 compared to event 1 and 2 of only 0.014 mg•L^{-1}. Cell 2 exhibited a low removal (4.56%) of total PFAS during event 3 compared to that (54.74%) in event 1. Total PFAS removal efficiency in cell 1 increased up to 18.8% in event 4 when both short-chain and long-chain PFAS removals were observed. This may be attributed to the decrease in the concentration of influent ammonia (0.063mg/L) from event 3 (0.11 mg/L). Note that the influent samples from each cell were collected from the influent pipes close to bubblers inside and the small differences in influent

concentrations among cells can be attributed to the sampling depth inside pipes and time lapse during individual sample collection.

However, event 4 of the cell 2 of ZIPGEM media does not exhibit similar improvement in the total PFAS removal efficiency despite the decrease in the influent ammonia concentration. This may be due to that ammonia concentration was still high (0.082 mg•L^{-1}) in event 4 of cell 2 compared to that (0.063 mg•L^{-1}) of cell 1. Besides, there might be other parameters affecting the removal efficiency which needs further analysis. PFAS removal in cell 1 was quite stable during events 5 and 6 given a steady influent ammonia concentration for event 5 (0.11 mg•L^{-1}) and event 6 (0.13 mg•L^{-1}). Similarly, PFAS removal in cell 2 improves in event 5 and 6 as influent ammonia concentration remains stable. A spike in influent ammonia concentration in both cell 1 and cell 2 (0.067 mg•L^{-1} and 0.074 mg•L^{-1}, respectively) from event 6 might have resulted in the poor removal efficiency of total PFAS (-7.18% and -0.48% respectively). The ammonia concentration decreases again in event 8 (0.032 mg•L^{-1} and 0.049 mg•L^{-1} for cell 1 and cell 2, respectively) and removal efficiency of total PFAS increases accordingly (4.69% and 4.63% respectively). The ammonia concentration consistently decreased throughout the subsequent events (9 and 10) in both cell 1 and 2. However, it is noteworthy that the total PFAS removal efficiency exhibited a decrease, which appears contradictory to the hypothesis. Yet, as illustrated in Figure 4, the effluent ammonia concentration experienced a significant increase from event 8 to event 10 (from 0.096 mg•L^{-1} to 0.37 mg•L^{-1} in cell 1 and from 0.141 mg•L^{-1} to 0.69 mg•L^{-1} in cell 2). Consequently, the removal efficiency demonstrated a negative correlation with effluent ammonia concentration.

This interaction was similarly observed in in CPS cells 3 and 4. The surge in influent ammonia concentration during event 3 led to a decline in removal efficiency, which subsequently

recovered in event 4 for both cells due to the decrease in ammonia concentration in the influent. PFAS removal increased during event 5 in cell 3 but decreased in cell 4. This contrast in results can be attributed to other water quality parameters that may be affecting PFAS removal mechanisms inside the cells. Besides, the influent concentration of total PFAS in cell 3 for event 5 was recorded at 62 ng•L^{-1} compared to 56 ng•L^{-1} in cell 4. A higher influent concentration was typically associated with an increased probability of micelle formation within the media, consequently leading to higher removal efficiency (Chen et al., 2020). Events 6 and 7 in cell 3 exhibited poor removal of PFAS (-0.55% and 0.93%, respectively), attributed to the increasing ammonia concentration (0.043 mg•L^{-1} and 0.074 mg•L^{-1}, respectively, from 0.035 mg•L^{-1} in event 3). The PFAS removal efficiencies in events 6 and 7 for cell 4 are analogous to that of cell 3. Event 8 of both CPS cells demonstrated commendable removal efficiency (approximately 12% and 5%, respectively). Hence, events associated with higher concentrations of PFAS and lower concentrations of ammonia in the influent exhibited better removal of both short- and long-chain PFAS, as evidenced by Events 4, 5, and 8 in all cells. Conversely, higher concentrations of ammonia and lower concentrations of PFAS in the influent resulted in reduced removal efficiency, as observed in events 3, 9, and 10 across all cells. This implies that high concentration of ammonia may lead to some desorption of the PFAS within the media, likely due to competition with DON (Eschauzier et al., Kah et al., 2021; 2012; McCleaf et al., 2017), possible pore blockage, and complexations (Jeon et al., 2011).

This page intentionally left blank.

Chapter 5: Removal Mechanisms of Pollutants in the Filtration Process

5.1 Removal Mechanisms of Nutrients

ZIPGEM and CPS employ a combination of absorption, adsorption, reduction–oxidation, ion exchange, and precipitation to remove nutrients. Each of the media's individual elements fulfills a unique functionality in the physiological and chemical mechanisms responsible for nutrient removal. Sand can provide not only an appropriate void space for the distribution of the influent (Valencia et al., 2019) but also Ca^{2+} in that negatively charged phosphorus and nitrate are attracted to positively charged Ca^{2+} (Eqs. 5.1–5.2) (Ghasemi & Sillanpää, 2015, Deng et al., 2018, Lei et al., 2018). The percentage of Ca^{2+} was 1.1% and 1.0% in CPS and ZIPGEM, respectively, suggesting that only minor nutrient removal can be associated with the electrochemical interaction between Ca^{2+} and nutrients (Figure 5-1).

$$2Ca^{2+} + PO_4^{2-} + OH^- \leftrightarrow Ca_2PO_4(OH)\cdot 2H_2O(s) \quad \text{Eq.5.1}$$

$$Ca^{2+} + 2NO_3^- \rightarrow Ca(NO_3)_2 \quad \text{Eq.5.2}$$

Furthermore, photoammonification, induced by photochemical reactions in surface waters (Funkey et al., 2005; Liu et al., 2023), may convert DON into NH_4^+, which could be a direct (Eq. 5.3) or an (Eq. 5.4) (Zhang et al., 2021). Especially in the case of indirect photoammonification, dissolved organic matter in natural water can be converted into highly reactive species like ^{3}CDOM [triplet excited state of chromophoric dissolved organic matter (CDOM)], which can react with O_2 to form reactive oxygen species (ROSs), such as singlet oxygen ($^1O_2$) and hydroxyl radicals (•OH), playing an important role in the photochemical transformation of small DON molecules (Kitidis et al., 2008; Yang et al., 2021; Zhang et al., 2021).

With kaolinite as the principal component, clay can not only facilitate ion exchange for ammonia and nitrate removal because of its physical characteristics (Lee et al., 2009), but also can serve as a flocculation aid to promote the formation of large, rapidly settling flocs with phosphate adsorbed (Özacar & Şengil, 2003). As a catalyst, kaolinite ($Al_2O_3 \cdot 2SiO_2 \cdot 2H_2O$) can further contribute to the reaction between ammonia and orthophosphoric chemicals to aid in the formation of ammonium dihydrogen phosphate (ADP; $NH_4H_2PO_4$) and diammonium hydrogen phosphate [DHP; $(NH_4)_2H_2PO_4$] (Eqs. 5.5 and 5.6, Figure 5-1), which are commonly used as phosphate fertilizers (Jiao et al., 2012; McGowen et al., 2001; Saueia & Mazzilli, 2006).

DON (under solar irradiation) → photolabile DON precursor →

→ Small molecules DON (amino acids) → $NH_4^+ \leftrightarrow NH_3$ Eq. 5.3

Under solar irradiation, DON → photolabile DON precursor →

→ Small molecules DON (amino acids) $\xrightarrow{3CDOM*,\cdot OH,etc.}$ $NH_4^+ \leftrightarrow NH_3$ Eq. 5.4

$Al_2O_3 \cdot 2SiO_2 \cdot 2H_2O + NH_3 + H_3PO_4 \rightarrow NH_4H_2PO_4(ADP) + Al_2O_3 \cdot 2SiO_2 \cdot 2H_2O$ Eq. 5.5

$Al_2O_3 \cdot 2SiO_2 \cdot 2H_2O + 2NH_3 + H_3PO_4 \rightarrow (NH_4)_2H_2PO_4(DHP) + Al_2O_3 \cdot 2SiO_2 \cdot 2H_2O$ Eq. 5.6

Previous studies have reported inconsistent nutrient removal efficiency of perlite. Baei et al. (2016) demonstrated that acid-activated perlite could remove 91% of nitrate from aqueous solutions in batch systems with a contact time of 120 min at pH of 5 using 0.7 g adsorbent while achieving a maximum sorption capacity of 32.63 $mg \cdot g^{-1}$. However, Ma et al. (2011) reported that the removal of OP using perlite, with an adsorption capacity of only 0.01 $mg \cdot g^{-1}$, was negligible. Williams et al., (2000) studied a peat–perlite medium and found no phosphate adsorption onto

perlite. Pradhan et al. (2020) treated greywater with perlite via a column study and demonstrated phosphate removals of up to only 15%.

Including ZVI filings in ZIPGEM assists in reducing nitrate to ammonia following Eq. 5.7. The precipitation of phosphate via Fe^{2+} results in the formation of vivianite precipitate [$Fe_3(PO_4)_2 \cdot 8H_2O$], following Eqs. 5.8–5.11 (Fredrickson et al., 1998; Haynes, 2014), whereas the particle interaction of iron filings and phosphate can result in the precipitation of $Fe_3(PO_4)_2$ and $FePO_4$ (Eqs. 5.12-5.16). Also, the content percentage of K^+ is 2.9% of CPS and 2.8% of ZIPGEM in terms of element composition; therefore, following Eq. 5.20 (de Barros, 2023), KH_2PO_4 can be precipitated.

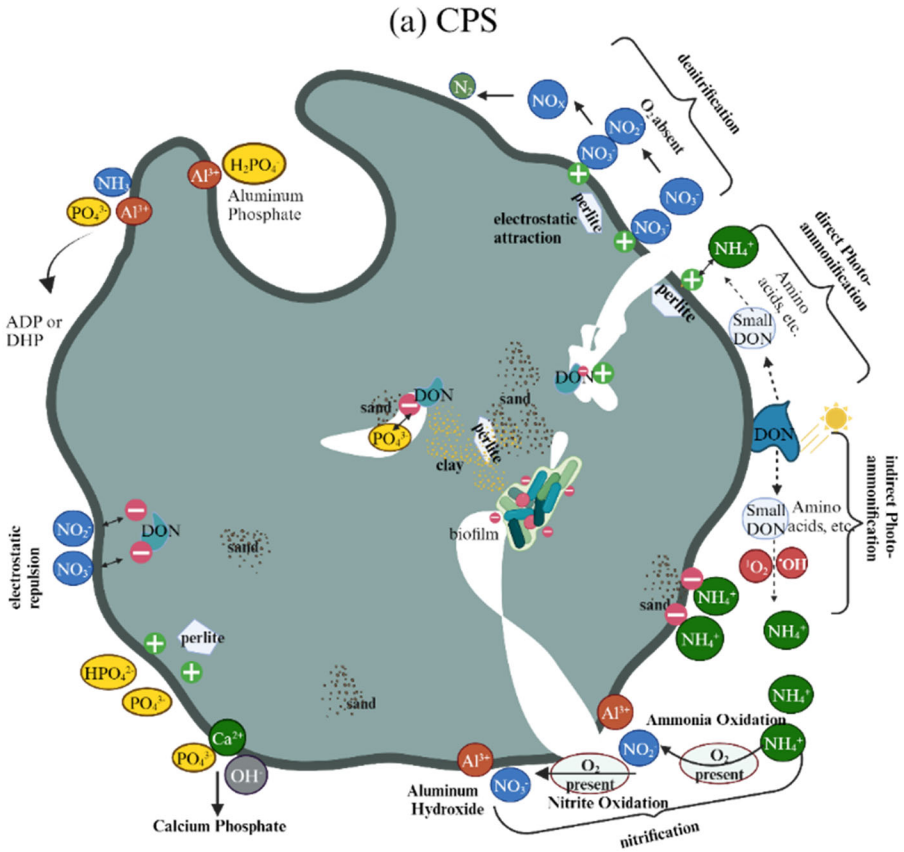

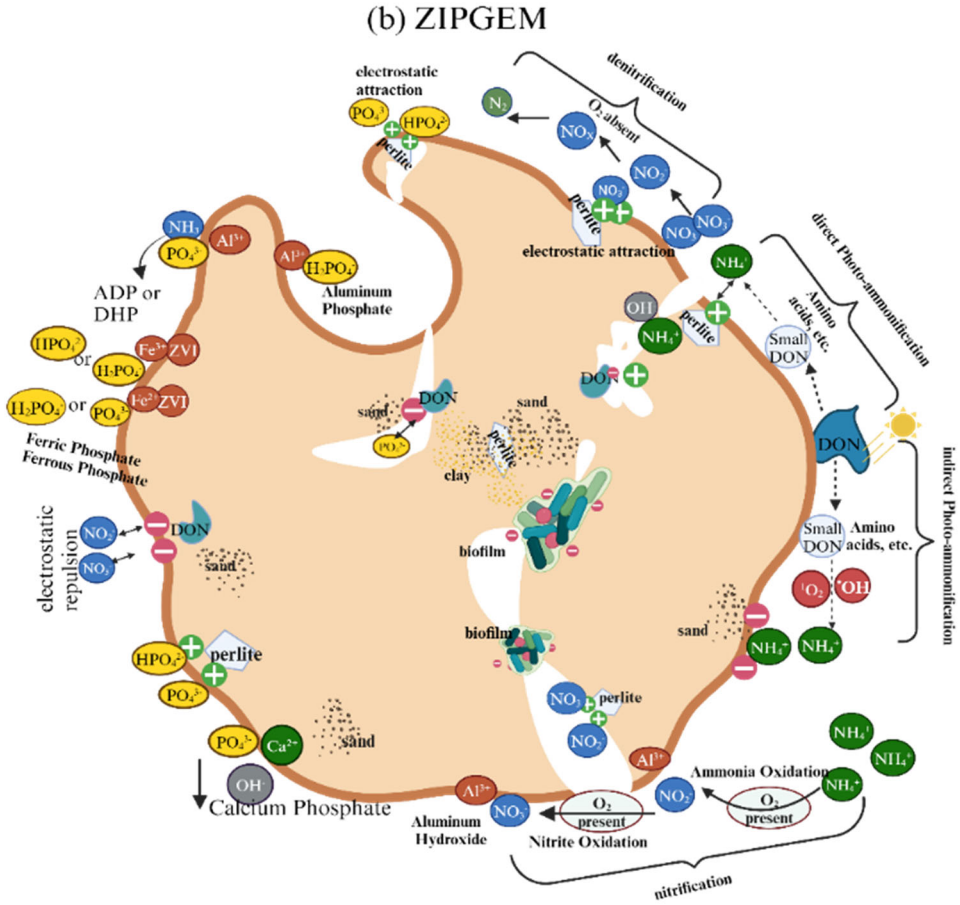

Figure 5-1: Illustration of nutrients removal mechanism in (a) CPS and (b) ZIPGEM and its influence by pH and dissolved oxygen (DO).

$$NO_3^- + 10H^- + 4Fe^0 \rightarrow NH_4^+ + 3H_20 + 4Fe^{2+} \quad \text{Eq. 5.7}$$

$$H_3PO_4 \leftrightarrow H_2PO_4^- + H^+ \quad \text{Eq. 5.8}$$

$$H_2PO_4^- \leftrightarrow HPO_4^{2-} + 2H^+ \quad \text{Eq. 5.9}$$

$$HPO_4^- \leftrightarrow PO_4^{3-} + H^+ \quad \text{Eq. 5.10}$$

$$3Fe^{2+} + 2H_2PO_4^- + 8H_2O \rightarrow Fe_3(PO_4)_2 \cdot 8H_2O + 2H^+ \quad \text{Eq. 5.11}$$

$$2\,Fe^0 + O_2 + 2H_2O \rightarrow 2Fe^{2+} + 4OH^- \quad \text{Eq. 5.12}$$

$$Fe^{2+} + O_2 \rightarrow Fe^{3+} + O^{2-} \quad \text{Eq.5.13}$$

$$Fe^{2+} + H_2PO_4^- \rightarrow Fe_3(PO_4)_{2(s)} + H^+ \quad \text{Eq. 5.14}$$

$$Fe^{3+} + PO_4^{3-} \rightarrow FePO_{4(s)} \quad \text{Eq. 5.15}$$

$$K^+ + H_2PO_4^- \leftrightarrow KH_2PO_{4(s)} \quad \text{Eq. 5.16}$$

The presence of Al^{3+} in CPS and ZIPGEM (10.5% and 8.4%, respectively) can further contribute to the nutrient removal by the media (Ordonez et al., 2023). Phosphate can be precipitated in the presence of aluminum, forming an insoluble salt, aluminum phosphate ($AlPO_4$), following Eq. 5.17 (Martin, 1986). Additionally, aluminum can aid in reducing nitrate to ammonia (Eqs. 5.18–5.19) or nitrogen gas (Eqs. 5.20) (Murphy, 1991; Luk & Au-Yeung, 2002). Aluminum hydroxide dehydration forms Al_2O_3 (Eq. 5.21) (Du et al., 2009), which is also a reactant in the formation of ADP and diammonium hydrogen phosphate (DAP) (Eq. 5.5–5.6).

$$Al^{3+} + H_2PO_4^- \rightarrow AlPO_4 + 2H^+ \quad \text{Eq. 5.17}$$

$$3NO_3^- + 2Al + 3H_2O \rightarrow 3NO_2^- + 2\,Al(OH)_{3(s)} \quad \text{Eq. 5.18}$$

$$NO_2^- + 2Al + 5H_2O \rightarrow NH_3 + 2Al(OH)_{3(s)} + OH^- \quad \text{Eq. 5.19}$$

$$2NO_2^- + 2Al + 4H_2O \rightarrow N_{2(g)} + 2Al(OH)_{3(s)} + 2OH^- \quad \text{Eq. 5.20}$$

$$Al(OH)_3 \rightarrow Al_2O_3 + 5H_2O \quad \text{Eq. 5.21}$$

Overall, as Figure 5-1 shows, calcium phosphate, ferric phosphate, ferrous phosphate, and aluminum phosphate could be amorphous solid or crystalline, such as $Ca_2PO_4(OH)\cdot 2H_2O$, $CaHPO_4\cdot 2H_2O$, $Ca_8(HPO_4)_2(PO_4)_4\cdot 5H_2O$, $Fe_3(PO_4)_2$, $FePO_4$, $Fe_3(PO_4)_2\cdot 8H_2O$, $AlPO_4$, and

$AlPO_4 \cdot nH_2O$ (n=1.1-2). Both pH and dissolved oxygen (DO) can affect these reactions in above directly or indirectly.

5.2 Removal Mechanisms of Biological Pollutants

Sand has long been used to remove microbiological contamination (Hijnen et al., 2007), which can be attributed to filtration processes in the sand filters (e.g., predation and bio-oxidation) (Haig et al., 2015). Given that C-23 canal water is nutrient-polluted, HABs have become a severe issue (Lapointe et al., 2017). During the wet season, a considerable amount of algae can be observed on the filtration cell surfaces. These algal concentrations are enough to increase oxygen concentrations inside the media to levels that may harm fecal bacteria (Ansa et al., 2022). Algal presence also leads to high pH levels that tend to be bactericidal even without high oxygen concentrations (Maynard et al., 1999). Similarly, *E. coli* removal was achieved by both direct (i.e., protozoan grazing and viral lysis) and indirect (i.e., lysis induced by algal ROSs production and fungal degradation of released biomass) mechanisms (Haig et al., 2015). Wang et al. (2022) demonstrated that ZVI, added as a permeable layer in a sand column, could significantly enhance *E. coli* capture and inactivate the captured *E. coli* through membrane damage and ROS-induced oxidative stress.

Both ZIPGEM and CPS contain 5% clay, which can play a vital role in removing algae via flocculation and sedimentation, including charge neutralization, bridging, and enmeshment (Liu et al., 2016, Shammas, 2005). With significant amount of pores inside the media, clay acts to ballast algae and promote cell sinking despite the organisms' motility and buoyancy (Sengco et al., 2004) in those pores. In addition to direct flocculation, Yu et al. (2017) demonstrated physio–biochemical and transcriptional mechanisms. The collision between the clay and HAB cells stimulates the HAB cells to produce large amounts of ROSs, resulting in significant increases in

cell superoxide dismutase and catalase activity (Apel & Hirt, 2004; Mittler, 2002), which can inhibit HAB cell growth.

The application of perlite alone to remove algae is yet to be studied. Most studies have mainly utilized the properties of perlite in combination with some metals to generate floating photocatalysts. Wang et al. (2017) demonstrated that solar-light–driven F-Ce-TiO_2/expanded perlite floating photocatalysts can achieve removal rates ranging from approximately 89% to 98% through photocatalytic oxidation. However, Zhao et al. (2023) demonstrated that the removal rates of three types of microalgae (*C. vulgaris*, *M. aeruginosa*, and *A. flos-aquae*) through closed-cell perlite (CCP) were only 30–40%. By using a magnetic bead prepared using Fe_3O_4, CCP, and cationic polyacrylamide, the microalgae removal could be further improved to more than 70% (Zhao et al., 2023). The above microalgae removal process does not involve chemical reactions. In the field work, although media components were mixed well, some floating perlites were still present on the surface of the filtration cells due to their light weight. Therefore, one may speculate that microalgal cells would adhere to some floatable perlites to form microalgae and floatable perlite aggregates through such mechanisms as settling, inertia, interception, and diffusion (Zhao et al., 2023).

Liu et al. (2019) demonstrated that adsorption on the ZVI surface may account for only a small amount of immobilized phycocyanin. The main removal pathway was coagulation by iron ions (Fe^{2+} or Fe^{3+}) (Eqs.5.12-5.13 and Eqs. 5.22-5.25, Figure 5-1). Wang et al. (2022) also demonstrated that a ZVI amended sand column system could not only effectively remove algae but also inactivate algae retained within the columns with the accumulation of ROS.

$$4Fe^{2+} + O_2 + 2H_2O \rightarrow 4Fe^{4+} + 4OH^- \qquad \text{Eq. 5.22}$$

$$Fe^{2+} + 2H_2O \rightarrow Fe(OH)_{2(s)} + 2H^+ \quad \text{Eq. 5.23}$$

$$4Fe^{2+} + O_2 + 10H_2O \rightarrow 4Fe(OH)_{3(s)} + 8H^+ \quad \text{Eq. 5.24}$$

$$4Fe^{2+} + O_2 + 6H_2O \rightarrow 4FeOOH_{(s)} + 8H^+ \quad \text{Eq. 5.25}$$

5.3 Microbial Population and Seasonality Effect in the Nitrogen Cycle

Microorganisms play an important role in the nitrogen cycle and can provide continual treatment in a nitrogen polluted water system. As such, the adsorption capacity of TN in the pilot study using CPS and ZIPGEM may not be estimated using an isotherm that primarily focuses on physicochemical adsorption in the beginning stage. It is anticipated that the continuous nitrogen removal via biofilms after physicochemical adsorption process can provide additional and sustained TN removal, including nitrate, nitrite, ammonia, and organic nitrogen for a much longer period. This is the reason why the life expectancy of the filtration system for TN removal is almost infinite, unlike TP and other pollutants.

The common microbial species involved in the nitrogen-cycle include anaerobic ammonium oxidation (anammox) bacteria (Snoeyenbos-West et al., 2000; Tsushima et al., 2007), ammonia oxidizing bacteria (AOB) (Rotthauwe et al., 1997), nitrite oxidizing bacteria (NOB) (Dionisi et al., 2002), dissimilatory nitrate reducing bacteria (nrfa) (Yin et al., 2017), denitrifiers (Azziz et al., 2017), and complete ammonia oxidation bacteria (Comammox) (Xia et al., 2018) (Figure 5-2). For example, *nirS*-type and nirK-type *denitrifier* communities mediate the conversion of nitrite to nitric oxide, which is the key step in *denitrification within the nitrogen cycle*. Higher diversity and abundance of denitrifying microorganisms in filter cells implies the denitrification is in a good order. This can be supported by the abundance of both ammonia oxidizers and *nirS*-type denitrifiers that dominate the nitrifying and denitrifying populations.

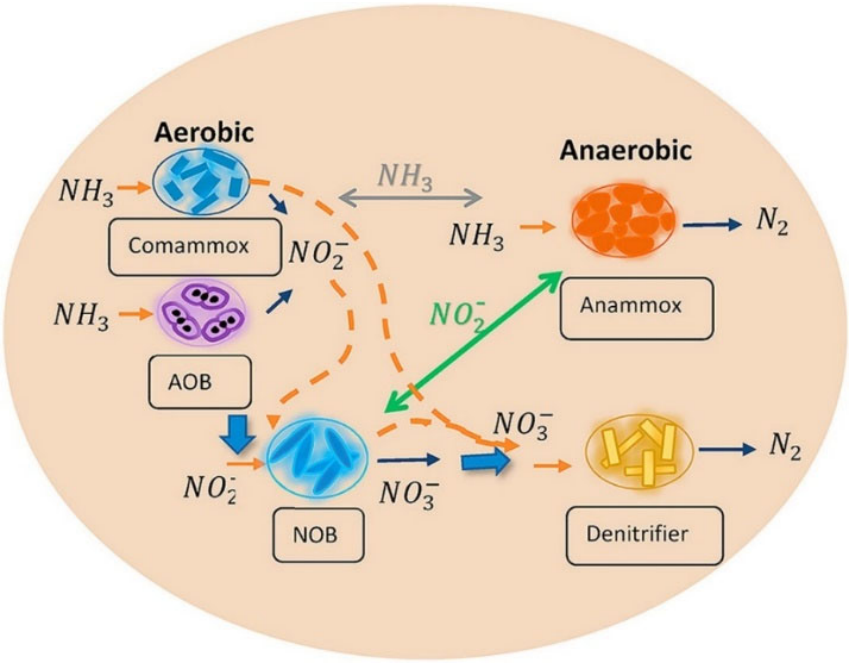

Figure 5-2: Common microbial species in nitrogen cycle contributing to nitrification and denitrification (Valencia et al., 2020).

A real-time polymerase chain reaction (RT-PCR) analysis can give us a lucid view of the population dynamics of these microorganisms in both CPS and ZIPGEM. Deoxyribonucleic acid (abbreviated DNA) extraction is required to identify microorganisms present for final gene expression determination from real-time polymerase chain reaction (qPCR). By using qPCR to analyze the collected media samples from the four media beds (cells), the aim is to determine the concentration of the bacteria present in CPS and ZIPGEM in this study. The initial step consists of sample collection, followed by DNA extraction, denaturation, annealing, extension, and DNA amplification [Figure 5-3(a)]. Figure 5-3(b) shows the population dynamics of the microbial species including nitrifiers and denitrifiers. The microbiological species target gene, primer information, and running methods are listed in Table 5-1.

(a) qPCR instrument and accessories used at UCF Lab. which include 1). DNeasy PowerSoil kit, 2). Applied Biosystem StepOne qPCR System, 3). PCR 48-well plate, 4). Centrifuge, and 5. Vortex mixer

(b) qPCR analysis procedure

Figure 5-3: qPCR instrument, accessories, and analysis procedure (Chang et al., 2018a, b).

Table 5-1: Summary of microbiological species target gene, primer, and running methods

Microbiological Specie (target gene)	Prime Name	Oligonucleotide Sequence	Running method/ Thermocycling conditions	Reference
Ammonia Oxidizing Bacteria (AOB) (amoA)	amoA1F	GGGGTTTCTACTGGTGGT	2 min 50 ° C and 2 min 95° C; 45 cycles [15 s at 95° C and 1 min at 62° C]	Rotthauwe et al. (1997
	amoA2R	CCCCTKGSAAAGCCTTCTTC		
Nitrite Oxidizing Bacteria (NOB) (nxrAB)	NSR113F	CCTGCTTTCAGTTGCTACCG	2 min 50 ° C and 2 min 95° C; 45 cycles [15 s at 95° C and 1 min at 62° C]	Dionisi et al. (2002
	NSR1264R	GTTTGCAGCGCTTTGTACCG		
Denitrifying bacteria (nirS)	Cd3AF	GTSAACGTSAAGGARACSGG	2 min 50 °C and 10 min for 95 °C; 40 cycles [60 s at 95 °C; 60 s at 51 °C; and 60 s at 60°C]	Azziz et al. (2017
	R3Cd	GASTTCGGRTGSGTCTTGA		

Anaerobic ammonium oxidation (Anammox) (amx)	**amx809-F**	**GCCGTAAACGATGGGCACT**	**2 min 50 ° C and 2 min 95º C; 45 cycles [15 s at 95º C and 1 min at 62º C]**	**Snoeyenbos-West et al. (2000; Tsushima et al. (2007**
	amx1066-R	**AACGTCTCACGACACGAGCTG**		
Dissimilatory nitrate reducing bacteria (DNRA) (nrfA)	**nrfA2F**	**CACGACAGCAAGACTGCCG**	**2 min 50 °C and 10 min for 95 °C;40 cycles [30 s at 95 °C; 60 s at 60 °C; 60 s at 72 °C]**	**Yin et al. (2017**
	nrfA2R	**CCGGCACTTTCGAGCCC**		
Complete Ammonia Oxidation (amoA)	**A378f**	**TGGTGGTGGTGGTCNAAYTAT**	**2 min 50 °C and 5 min for 95 °C;40 cycles [30 s at 95 °C; 30 s at 58 °C; 30 s at 72 °C]**	**Xia et al. (2018**

We selected two events, including event 3 for the dry season and event 9 for the wet season, for a comparative study. Population dynamics of typical microbial species in nitrification and denitrification including ammonia-oxidizing bacteria *(*AOB), nitrite oxidizing bacteria (NOB), and denitrifying bacterial (nirS), were selected as representative indices for a deepened understanding of the removal efficiency and seasonality effect. The final summary statistics could be helpful for illustrating the application potential of this emerging technology – GSM. More details of the event- or cell-based analysis can be found from Figures C1~C4 in Appendix C.

5.3.1 Nitrification process

Figure 5-4 shows the key microbial species in the nitrification and denitrification processes. The population density of the microbial ecology contributing to the nitrogen cycle was evaluated via qPCR for ZIPGEM and CPS at each sampling event. TEvent 3 (dry season) and event 9 (wet season) were selected for a comparative analysis. The population of AOB was significantly lower in event 3 (dry season) and increased in event 9 (wet season) (Figure 5-4(a)). This phenomenon was discovered and quantified by qPCR at the top of all of the cells. The population

of NOB in ZIPGEM increased more significantly than CPS from event 3 to event 9, with the highest quantities found at the top surface [Figure 5-4(b)].

5.3.2 Denitrification Process

The nirS population increased from event 3 to event 9 at all media locations. In contrast, during the wet season, the accumulation of nitrate in the nitrification reaction and the relatively high content of organic matter (carbon-to-nitrogen ratio) (Merbt et al., 2019) contribute to the high population of nirS (Figure 5-4(c)). Furthermore, the population of NOB in ZIPGEM increased more significantly than CPS from event 3 to event 9. These observations echo the findings shown in Figure 4-6(a). TN removal rate was generally higher in dry season than wet season and in ZIPGEM than CPS due to the abundance microbial species in the media mixes.

(a)

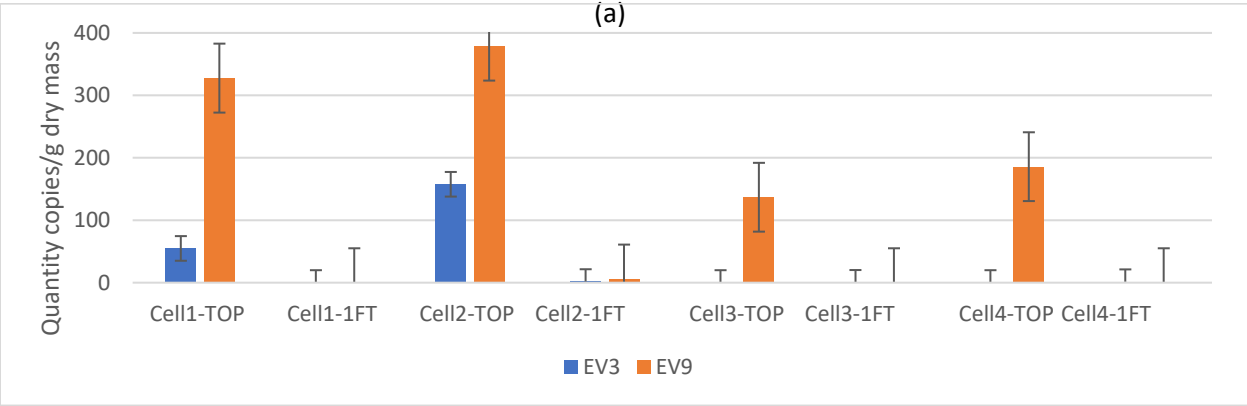

(b)

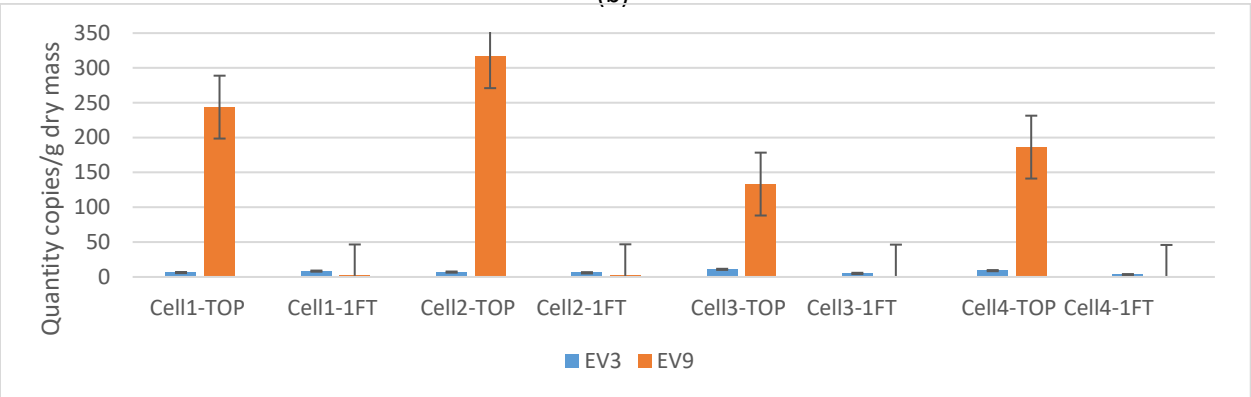

(c)

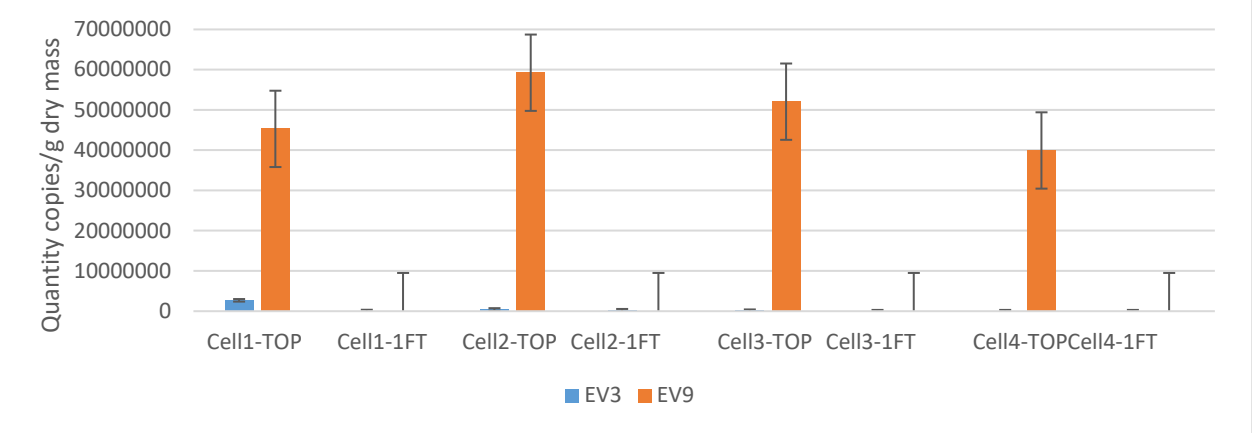

Figure 5-4 Microbial population density for (a) AOB, (b) NOB, (c) nirS in copy/gram for samples collected at event 3 and event 9 of cultivation.

5.3.3 Seasonality Effect on Microbial Population

The microbial nitrogen cycle is driven by nitrifying and denitrifying microorganisms collectively (Kim et al., 2016). The initial stage of the nitrification process entails the conversion of ammonium into nitrite by AOB, succeeded by the subsequent conversion of nitrite into nitrate by NOB ($NH_4^+ \rightarrow NO_2^- \rightarrow NO_3^-$) (Kim et al., 2016). This constitutes the rate-limiting step in nitrogen transformation. Conversely, the denitrification process reduces nitrate to nitrogen gas ($NO_3^- \rightarrow NO_2^- \rightarrow N_2$) (Arredondo et al., 2015). Nitrogen cycling in aquatic systems is influenced not only by shifts in climatic conditions but also by anthropogenic activities. For instance, alterations in climatic conditions not only impact the duration and intensity of dry and wet seasons (Fill et al., 2019), but anthropogenic activities, particularly those associated with agricultural production, affect both the nitrogen content of water bodies and the organic matter content (Xenopoulos et al., 2021). Additionally, habitat factors such as oxygen levels and pH undergo changes with the fluctuation between wet and dry seasons (Chen et al., 2022). Our study site is situated in the South Florida region, where the nitrogen cycle in surface waters is closely linked to climate, hydrology, and human activities. For example, in the St. Lucie Estuary, in

addition to discharges from Lake Okeechobee, the N and P enrichment arising from septic systems through shallow groundwaters also contribute to nutrient pollution and harmful algal blooms (Lapointe et al., 2017).

Elevated temperatures and nutrient-rich runoff during the wet season can lead to algal blooms. Algal blooms can deplete DO levels, which can favor denitrification. Conversely, in the dry season, cooler temperatures result in higher concentrations of DO, thus promoting nitrification, given that temperatures are slightly lower than in the wet season. However, during the dry season, the availability of ammonia is constrained. This corroborates the observation that ZIPGEM and CPS, in the initial four sampling events, exhibited some positive ammonia removal rates. Consequently, the augmentation of the AOB bacterial population was not pronounced. As NOB are heavily reliant on the product of AOB, namely nitrite, the population of NOB was even less substantial than that of AOB. Conversely, with the onset of the wet season, the reduction in DO levels and the accumulation of more nitrate led to a notable increase in the populations of nirS during this period.

In summary, seasonal effects were evident in the media of ZIPGEM and CPS, mainly in inhibiting the denitrification process in the dry season because the denitrification process required an anaerobic environment. In contrast, in the dry season, the DO content in the water was higher due to fewer aquatic algae and photosynthesis intensity resulting in higher content of DO (Cheung-Wong et al., 2022). The exuberant aquatic algae and higher organic matter content in the wet season depleted the DO, resulting in an anaerobic environment within the media (ZIPGEM and CPS), thereby stimulating the proliferation of nirS bacteria. As far as the nitrification process is concerned, oxygen is a prerequisite; thus, during the dry season, fewer nutrient inputs led to elevated levels of DO in the water, consequently engendering a certain

degree of nitrification reactions in both ZIPGEM and CPS. Nevertheless, in the wet season, despite an increase in rainfall frequency compared to the dry season, which augmented the DO concentration in the water, the profuse algal species consumed a significant portion of the DO, resulting in an insubstantial upsurge in the intensity of nitrification reactions. This is directly manifested by the negligible growth of both AOB and NOB populations during the wet season.

5.3.4 Effect of pH on Nutrient Removal Efficiency

Figure 5-5(a) and (b) demonstrate the correlations between pH and the removal efficiency of nutrients for ZIPGEM and CPS, respectively. This indicates that almost every nutrient species is negatively correlated with pH. This observation implies that TKN, DON, TP, and OP removal decreases when pH increases except for TN and ammonia. For OP, our results show a similar outcome with Ordonez et al. (2023). As pH increases, the media surface becomes less positively charged because of more OH^- in the influent. This leads to a decrease in OP adsorption as the negatively charged PO_4^{3-} competes with OH^- for the positively charged surface while increasing the electron repulsion between the increasingly negative surface sites and PO_4^{3-} (Figure 5-5). Thus, the removal of OP is negatively related to pH.

Figure 5-5 also shows that TP is negatively correlated with pH, likely because OP is part of the TP, which tends to present a negative valence (Xu et al., 2017). Therefore, as pH increases, the media surface also becomes more strongly negative, which in turn leads to decreased adsorption of TP and a consequent reduction in TP removal efficiency (Figure 5-5). When considering DON, the effect of pH is also evident because DON has a pH-dependent net negative charge because of the deprotonation of carboxylic and phenolic moieties in the DON structure (Ritchie et al., 2003). Consequently, DON strongly adsorbs onto positively charged sorbent surfaces. As pH increases, the surface of ZIPGEM is negatively charged. Thus, the efficiency of

DON removal is negatively correlated with increasing pH. When comparing across the two specialty adsorbents, the correlation coefficient between DON and CPS (-0.83) is smaller than that of ZIPGEM (-0.70) because its PZC (5.6) is significantly lower than that of ZIPGEM (9.2).

The same reasoning applies to TKN because DON is also a component of TKN. The removal efficiencies of TN and ammonia seem positively correlated with pH. Still, this relationship is weak, mainly because TN has diversified components, some of which may be negatively correlated with pH, such as DON, whereas others may be positively correlated with pH, such as ammonia, mainly for several reasons such as a pH increase, the liberation of the ionized NH_4^+ into gaseous phase NH_3, and the presence of more OH, which$^-$ favors conversion of ammonia into NO_3^-.

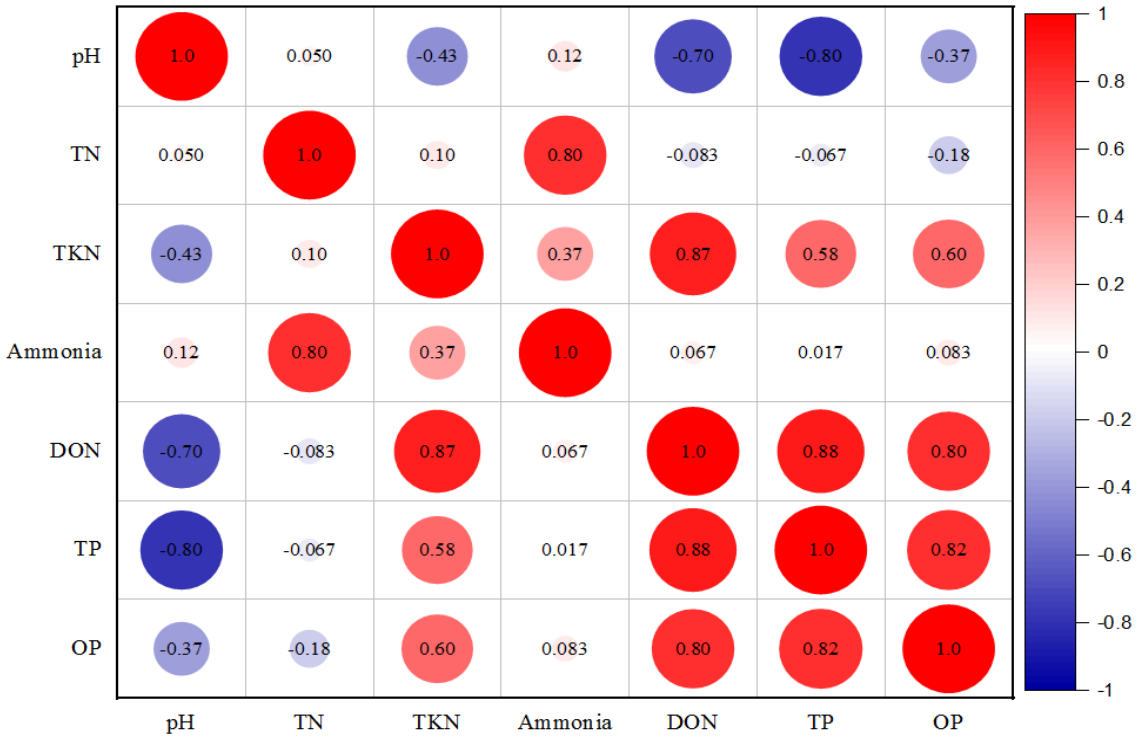

(a) Correlation between nutrients removal efficiencies and pH in ZIPGEM cells

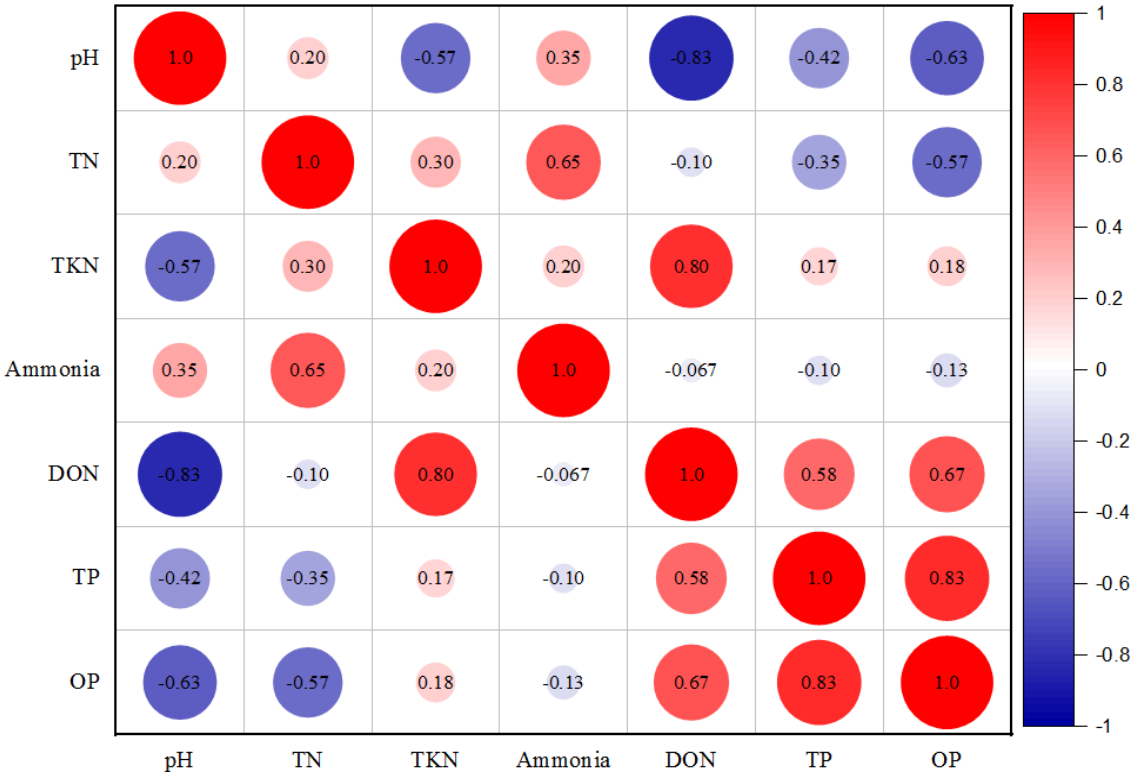

(b) Correlation between nutrients removal efficiencies and pH in CPS cells.

Figure 5-5: Correlation between nutrients removal efficiencies and pH.

Overall, at pH levels below the PZC, the surface of the media is positively charged. At pH levels above the PZC, the surface of the media is negatively charged. Therefore, pH can affect the adsorption of nutrients by changing the forms of nutrients and the charge on the reacting particle. In this way, electrostatic attraction and repulsion can happen at different sites of the media. Nutrients can be removed by electrostatic interactions, flocculation, and sedimentation in the form of amorphous solids or crystalline.

5.3.5 Effect of DO on Nutrient Removal Efficiency

Figure 5-6(a) and (b) demonstrate the correlation between nutrient removal efficiencies and DO. The positive relationship between DO and the ammonia removal rate may be explained by the fact that the higher content of DO supports the nitrification process whereas denitrification occurs in a low-DO environment. The correlation coefficient between DO and the removal rate of ammonia nitrogen is 0.40 for ZIPGEM and 0.35 for CPS, indicating that removing ammonia nitrogen involves a few complex microbiological metabolic reactions. Also, the removal rate of DON showed a positive relationship with DO, and this finding is consistent with Liao et al. (2022). Liao et al. (2022) showed that higher DO conditions would speed up the microbial oxidation process, leading to the decomposition of reduced DON molecules such as sugar-like compounds (proteins/amino), therefore resulting in a higher DON removal rate. The same reasoning applies to TKN because DON is an essential part of TKN. The value of DO was inversely related to TN's removal efficiency. Still, the correlation coefficient was only -0.13 for ZIPGEM, because high DO would inhibit the denitrification process, leading to somewhat of a decrease in TN removal efficiency. As for TP and OP, the removal efficiency also showed a positive relationship with DO. This finding is consistent with Zhang et al. (2020), who found that an increase in DO would contribute to phosphorus uptake and storage in biofilm with higher removal rate of TP and OP. In the case of CPS, Figure 5-6(b) showed some inverse relationship between DO and the removal rate of TP and OP, which may be due to the high phosphorus content of CPS itself.

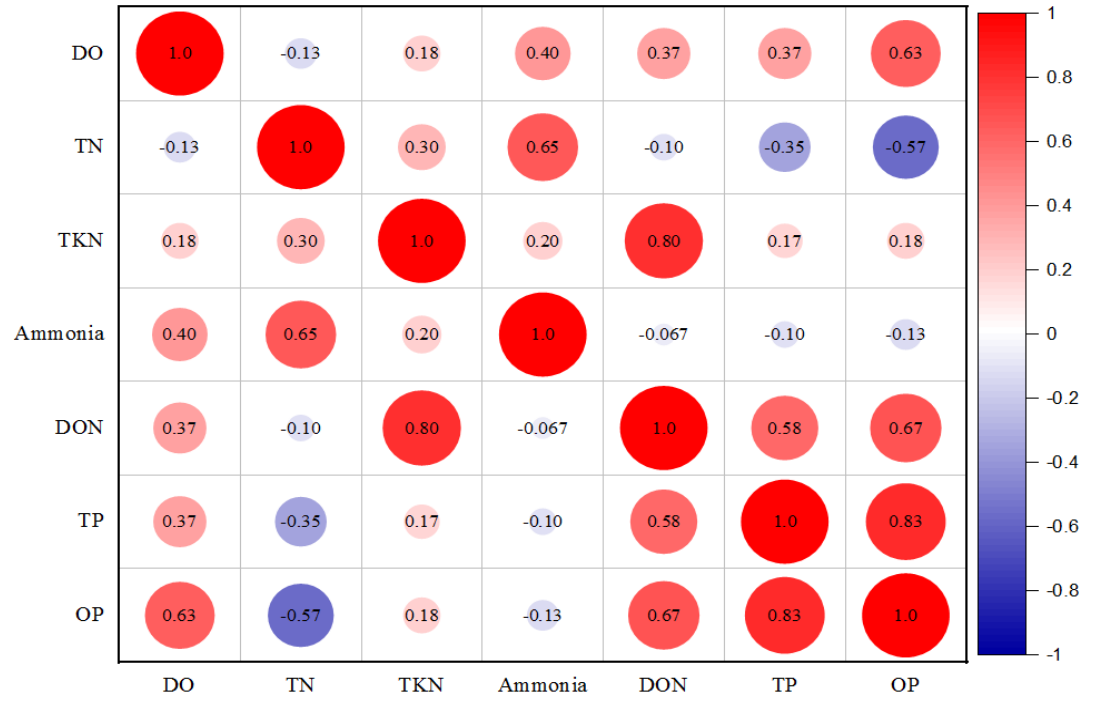

(a) Correlation between nutrients removal efficiencies and DO in ZIPGEM cells.

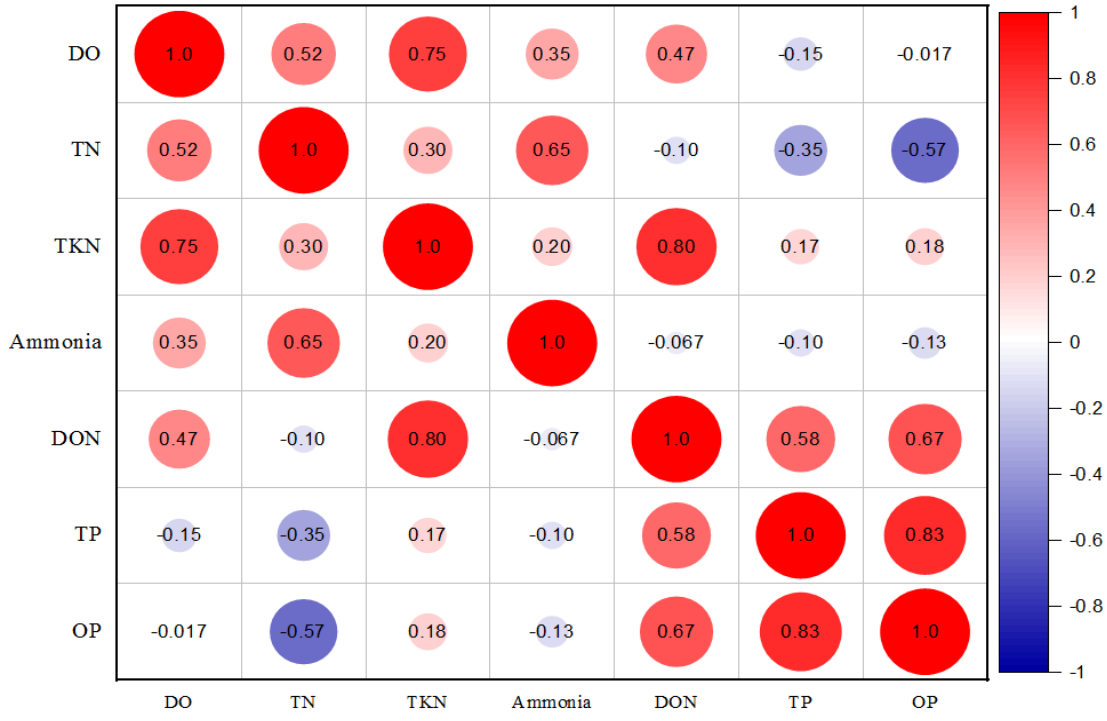

(b) Correlation between nutrients removal efficiencies and DO in CPS cells.

Figure 5-6: Correlation between nutrients removal efficiencies and DO.

5.4 Removal Mechanisms of PFAS

The first five sampling events were conducted during the dry season, and the remaining five events were conducted during the wet season (Table 5-2). Notably, no significant fluctuation in temperature was observed over the course of these events. Dissolved oxygen (DO) levels displayed an irregular pattern closely correlating with temperature changes. In the influent, turbidity was notably lower during the wet season in comparison with the dry season. Moreover, pH and conductivity demonstrated a gradual decrease during the wet season, while oxidation-reduction potential (ORP) exhibited a rather erratic trend.

Table 5-3 lists the physicochemical properties of the selected short- and long-chain PFAS, including pKa, Log D (or K_{ow}), and molecular weight based on the US EPA's 2022 lifetime health advisory levels. It is noteworthy that both the short-chain and long-chain PFAS exhibit very low pKa values, suggesting that they are likely to remain deprotonated in water at pH values. Additionally, the negative Log D value for PFBA indicates its low hydrophobicity compared with that of the other PFAS.

Table 5-2: Seasonal variation of the influent water characteristics

Event	Climate	Date	Rainfall* (mm)	Turbidity (NTU)	ORP (mv)	DO (mg/L)	pH	Temp (°C)	Conductivity (µs/cm)
1	Dry	3/1/23	0.00	11.7	65.8	9.00	8.62	23.4	952
2	Dry	3/14/23	0.01	11.7	65.8	9.00	8.62	23.4	952
3	Dry	3/28/23	0.00	5.39	182.9	8.37	8.38	32.5	958
4	Dry	4/11/23	0.09	11.3	97.1	10.29	9.00	21.9	953
5	Dry	4/25/23	0.46	37.1	145.3	9.61	8.82	30.1	885
6	Wet	5/9/23	0.28	3.96	67.2	9.08	8.70	29.6	907
7	Wet	5/23/23	0.09	3.32	41.8	5.83	8.29	27.5	959
8	Wet	6/6/23	1.13	3.26	168.3	7.74	8.16	26.1	968
9	Wet	6/20/23	0.64	2.43	187.3	8.38	8.10	28.5	641
10	Wet	7/3/23	0.99	9.01	150.3	3.51	8.00	29.0	536

* Data were collected from the weather station on site and City of Stuart, FL.

Table 5-3: Physicochemical properties of selected short-chain (upper section below in light gray) and long-chain PFAS (lower section below in light blue)

PFAS	CAS#	Chemical Formula	MW ($g \cdot mol^{-1}$)	pK_a	Log D[a]
Perfluorobutanoic acid (PFBA) [b]	375-22-4	C_3F_7COOH	214	0.40	-1.22
Perfluorobutanesulfonic acid (PFBS) [b]	375-73-5	$C_4F_9SO_3H$	300	0.14	0.25
Hexafluoropropylene oxide dimer acid (HFPODA, commonly known as GenX Chemicals) [b]	13252-13-6		330.05	2.84	0.47
Perfluorooctanoic acid (PFOA) [c]	335-67-1	$C_7F_{15}COOH$	414	- 0.20	1.58
Perfluorooctanesulfonic acid (PFOS) [c]	1763-23-1	$C_8F_{17}SO_3H$	500	0.14	3.05

[a] Log D (or K_{ow}): Octanol-water partition coefficient at pH 7 accounted for acid dissociation reactions (Ka) determined using software MarvinSketch (2023).

[b] Short-chain PFAS; [c] Long-chain PFAS

PFAS analyses were carried out by Eurofins Lancaster Laboratories, which followed the EPA method 533 (Zhang et al., 2020) (Table 5-4). The samples were collected in 250 mL plastic bottles, stored in a cooler filled with ice bags to keep the temperature below 4 °C, and then delivered to Eurofins Lancaster Laboratories for further processing and analysis. The method detection limits (MDLs) for PFOS, PFOA, GenX, PFBS and PFBA were 0.8, 1.2, 2, 0.4, and 1.5 $ng \cdot L^{-1}$, respectively.

Table 5-4: PFAS sampling and analysis protocols, methods, and MDLs

PFAS		Sample volume (mL)	On-site preservation chemical	Holding time (h)	Container type	Method	MDLs ($ng \cdot L^{-1}$)
Long-chain	PFOS	250	Trizma	14 days	Plastic	EPA 533	0.8
	PFOA	250			Plastic	EPA 533	1.2
Short-chain	PFBS	250			Plastic	EPA 533	0.4
	PFBA	250			Plastic	EPA 533	1.5
	HFPODA/GenX	250			Plastic	EPA 533	2

PFAS removal efficiencies of ZIPGEM and CPS were calculated according to Eq. 5.26 based on PFAS concentrations in the influent and effluent collected in triplicate.

$$\%\text{Removal} = (C_0 - C_e)/C_e \times 100\% \quad \text{Eq. 5.26}$$

where C_0 is the average concentration of PFAS in the influent in ng•L^{-1}; Ce is the average concentration of PFAS in the effluent in ng•L^{-1}.

The influent and effluent concentrations of PFAS for ZIPGEM and CPS media cells were found by averaging the respective values from the two cells containing the same type of specialty adsorbents. The average PFAS concentrations in influent and effluents for ZIPGEM and CPS media cells are presented in Tables 5-5 and 5-6, respectively. HFPODA was detected at concentrations above detection limits on only a few occasions. PFAS removal efficiencies calculated employing Eq. 5.26 are summarized in Table 5-7. Negative removal efficiency indicates that effluent concentrations were greater than influent concentrations.

The removal efficiencies of PFAS for each cell in all 10 events are displayed in Table 5-7 along with the average removal efficiencies of both media presented in Table 5-7 to capture both the temporal and spatial variations. The bars show the removal efficiency of individual PFAS, whereas the line plots show the total PFAS removal efficiency. Figure 4-16 presents the total PFAS concentrations in the influent as well as the ammonia concentration in the influent and effluent. Influent and effluent concentrations of ammonia may influence PFAS removal efficiency that will be discussed in a later section. The left y-axis shows the removal efficiencies (%) of individual and total PFAS as well as total influent PFAS concentrations (ng•L^{-1}), whereas the right y-axis shows ammonia concentrations (μg•L^{-1}). The dry season includes events one (1) through five, whereas the remaining events constitute the wet season.

Both long- and short-chain PFAS removal efficiencies varied throughout the sampling events. Further, the effect of the influent concentration of PFAS on removal appeared negligible. Therefore, it is possible that the water matrix constituents, under field conditions, might influence the two specialty absorbents' PFAS removal efficiency. Ammonia concentrations in the influent and effluent exhibit a strong negative correlation with the removal of both short- and long-chain PFAS, which will be further discussed in Section 5-4. Note that the influent ammonia concentrations were different from those in filtration cells because of photoammonification and mineralization effects via microbial species. Interestingly, all the events with a spike (e.g., a sharp increase) in either influent or effluent ammonia concentrations or both are associated with low removal of either short-chain or long-chain PFAS.

Table 5-5: Average influent and effluent concentrations of PFAS when using ZIPGEM

	Ev1		Ev2		Ev3		Ev4		Ev5		Ev6		Ev7		Ev8		Ev9		Ev10	
	Inf	Effl	Inf	Effl	Inf.	Effl	Inf.	Effl	Inf	Effl	Inf.	Effl	Inf	Effl.	Inf	Effl	Inf.	Effl	Inf	Effl.
PFBA	2.7	2.4	13.0	14.8	10.4	10.5	12.5	11.7	13.0	12.2	13.0	12.0	14.0	16.0	15.0	16.5	12.5	14.7	7.8	13.5
	(0.2)	(0.5)	(2.8)	(1.2)	(0.9)	(0.7)	(0.7)	(1.9)	(1.4)	(0.7)	(1.4)	(0.0)	(1.4)	(0.9)	(0.0)	(0.2)	(0.7)	(0.9)	(0.2)	(0.2)
PFBS	12.1	12.9	18.0	17.8	14.0	14.2	16.0	16.7	18.5	17.0	16.5	16.2	19.5	20.3	26.5	24.3	18.0	20.2	5.4	8.3
	(2.8)	(0.5)	(0.0)	(0.2)	(0.0)	(0.2)	(0.0)	(1.4)	(0.7)	(0.0)	(0.7)	(0.2)	(0.7)	(0.5)	(0.7)	(1.4)	(0.0)	(0.2)	(0.1)	(0.2)
PFOA	12.5	11.3	19.5	17.3	14.5	13.8	13.0	13.0	16.5	18	18	16	18.5	19.2	19.5	16.3	16	16.2	6.8	8.6
	(0.7)	(0.0)	(2.1)	(1.4)	(0.7)	(1.2)	(1.4)	(1.9)	(0.7)	(4.7)	(0.0)	(0.0)	(0.7)	(0.7)	(0.7)	(0.5)	(0.0)	(2.1)	(0.1)	(0.6)
PFOS	11.5	0.5	17.0	16.2	10.5	15.1	10.5	6.8	12.5	13.0	15.0	14.3	15.0	14.0	10.5	11.0	10.5	10.2	9.2	8.4
	(2.1)	(0.1)	(1.4)	(1.6)	(0.7)	(7.5)	(0.7)	(2.1)	(0.7)	(0.9)	(0.0)	(0.5)	(0.0)	(0.5)	(0.7)	(0.0)	(0.7)	(1.1)	(0.3)	(0.3)
HFPODA	NA	NA	NA	NA	0.39	NA	NA	NA	NA	0.17	NA	0.34	NA	NA	NA	NA	NA	NA	NA	NA

* Concentrations from Cell 1 and Cell 2 were averaged for both influent and effluent and standard deviations were provided in brackets. NA = Either not present or below detection limit

Table 5-6: Average influent and effluent concentrations of PFAS when using CPS

	Ev1		Ev2		Ev3		Ev4		Ev5		Ev6		Ev7		Ev8		Ev9		Ev10	
	Inf	Effl	Inf	Effl	Inf.	Effl	Inf.	Effl	Inf	Effl	Inf.	Effl	Inf	Effl.	Inf	Effl	Inf.	Effl	Inf	Effl.
PFBA	2.2	3.0	15.0	15.3	10.0	10.1	15.5	13.5	17.5	11.5	12.5	13.5	15.0	15.5	14.5	12.8	12.5	12.3	8.0	8.6
	(0.3)	(0.6)	(0.0)	(0.9)	(0.1)	(0.8)	(0.7)	(0.2)	(4.9)	(0.2)	(0.7)	(0.7)	(0.0)	(0.7)	(0.7)	(0.2)	(2.1)	(0.9)	(0.1)	(1.5)
PFBS	10.7	11.1	18.0	18.0	13.5	14.2	19.0	17.8	18.5	15.8	17.0	18.2	20.5	21.2	27.0	21.3	18.0	20.8	10.0	10.8
	(3.3)	(0.9)	(0.0)	(0.5)	(0.7)	(0.2)	(0.0)	(0.2)	(3.5)	(0.7)	(1.4)	(0.2)	(0.7)	(0.2)	(0.0)	(0.5)	(1.4)	(0.2)	(0.1)	(1.2)
PFOA	12.0	12.0	19.0	17.5	14.0	15.7	16.5	14.8	16.0	18.0	16.5	16.0	19.0	19.0	19.0	14.8	14.5	19.0	6.7	10.0
	(0.0)	(0.5)	(1.4)	(0.2)	(0.0)	(0.0)	(0.7)	(1.2)	(1.4)	(1.9)	(0.7)	(0.0)	(0.0)	(1.4)	(0.0)	(0.7)	(0.7)	(0.5)	(0.1)	(1.5)
PFOS	11.0	1.4	16.0	11.8	10.0	18.8	13.0	10.4	12.5	12.8	14.5	13.2	16.5	15.7	10.5	11.1	11.0	12.3	8.1	9.0
	(0.0)	(0.2)	(1.4)	(0.7)	(0.0)	(1.6)	(1.4)	(1.3)	(2.1)	(0.7)	(0.7)	(0.2)	(0.7)	(0.5)	(0.7)	(0.9)	(0.0)	(0.5)	(0.4)	(1.9)
HFPODA	NA	NA	NA	NA	NA	NA	NA	NA	NA	NA	NA	NA	NA	NA	0.35	NA	NA	NA	NA	NA

* Concentrations from Cell 1 and Cell 2 were averaged for both influent and effluent and standard deviations were provided in first brackets.
NA = Either not present or below detection limit

Table 5-7: Average removal efficiencies of PFAS using ZIPGEM and CPS

	ZIPGEM (%)										CPS (%)									
	Ev1	Ev2	Ev3	Ev4	Ev5	Ev6	Ev7	Ev8	Ev9	Ev10	Ev1	Ev2	Ev3	Ev4	Ev5	Ev6	Ev7	Ev8	Ev9	Ev10
PFBA	8.2	-14.1	-1.4	6.7	6.4	7.7	-14.3	-10.0	-17.3	-74.2	-35.6	-2.2	-1.8	12.9	34.3	-8.0	-3.3	11.5	1.3	-8.6
PFBS	-6.6	0.9	-1.2	-4.2	8.1	2.0	-4.3	8.2	-12.0	-54.8	-3.9	0.0	-4.9	6.1	14.4	-6.9	-3.3	21.0	-15.7	-102.5
PFOA	9.3	11.1	4.6	0.0	-9.1	11.1	-3.6	16.2	-1.0	-27.7	0.0	7.9	-11.9	10.1	-12.5	3.0	0.0	21.9	-31.0	-48.5
PFOS	95.6	4.9	-43.3	34.9	-4.0	4.4	6.7	-4.8	2.5	9.1	87.1	26.0	-88.3	20.0	-2.7	9.2	5.1	-5.2	-12.1	-10.9
HFPODA	NA	NA	100	NA	0.0	0.0	NA	NA	NA	NA	NA	0	NA	NA	0.0	0.0	NA	100	NA	NA

* Removal efficiencies were calculated from the average concentrations in Cell 1 and Cell 2 for ZIPGEM and Cell 3 and Cell 4 for CPS. Negative removal efficiencies in ZIPGEM were set to zero for HFPODA in Event 5 and 6 as the effluent concentrations were too low.

5.4.1 Influence of Ammonia on PFAS Removal Efficiency

Spearman's correlation was run to assess the effect of ammonia in the influent and effluent on the removal of PFAS by ZIPGEM and CPS in the filtration cells during both dry and wet seasons. Although the effluent ammonia concentration may not be directly equivalent to that in the pore water within the media, it provides a more representative measure than the influent ammonia concentration. Figure 5-7 illustrates the correlation between PFAS removal efficiency

and influent and effluent ammonium concentrations using the Spearman's correlation coefficient. Red circles denote a positive correlation, while blue circles indicate a negative correlation. The influent water goes through the media and equilibrates inside the media through the exchange (adsorption, desorption, cation exchange, etc.) of its constituents with the media. Thus, the correlation with the effluent water may reveal the interactions with the media mix.

As depicted in Figure 5-7, long-chain PFAS such as PFOS display a slight negative correlation (Spearman correlation coefficient = -0.18), whereas PFOA displays a modest negative correlation (Spearman correlation coefficient = -0.52) with effluent ammonia concentration. Short-chain PFAS such as PFBA and PFBS demonstrate higher negative correlations with effluent ammonia concentration when compared to their long-chain counterparts. Notably, total PFAS removal efficiency also exhibits a significant negative correlation (-0.60) with effluent ammonia concentration. In contrast, the correlation pattern with influent ammonia concentration differs. Specifically, PFOS demonstrates a notable negative correlation (-0.5), whereas other shorter-chain PFAS show a slight positive correlation. This discrepancy may occur because PFOS removal efficiencies are typically affected by desorption through elevated ammonia concentrations. However, as the shorter-chain PFAS are not adsorbed to the same degree, their desorption through high ammonium concentrations is comparatively lower. Moreover, desorption of long-chain PFAS such as PFOS frees up some adsorption sites and facilitates the removal of short-chain PFAS.

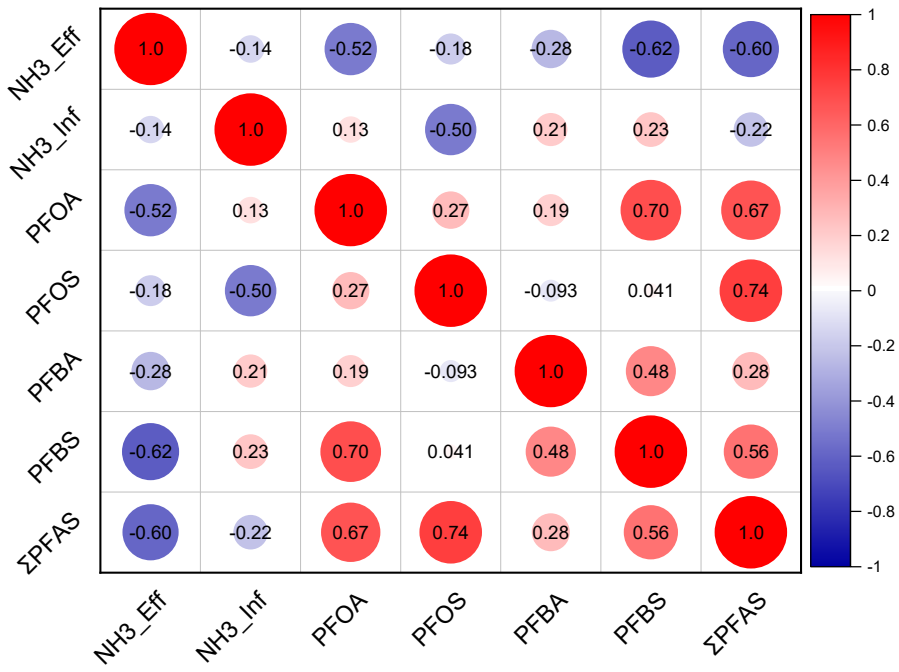

Figure 5-7: Correlation between short- and long-chain PFAS removal efficiencies and influent and effluent ammonia concentrations.

Nevertheless, total PFAS removal still demonstrates a slight negative correlation (-0.22) with influent ammonia concentration. Furthermore, it is evident that effluent ammonia concentration exhibits a more pronounced correlation with the removal efficiency of both long- and short-chain PFAS than does influent ammonia concentration. Notably, the ammonia concentration in the influent displays a negative correlation (-0.14) with that in the effluent. This phenomenon arises because higher influent ammonia concentrations typically enhance adsorption, resulting in lower effluent concentration. This analysis leads us to conclude that ammonia acts as an inhibiting factor for PFAS removal efficiency when using the GSM. However, it is not yet confirmed whether this negative effect on PFAS removal is attributed to competition between ammonia and PFAS for adsorption sites or to the desorption of PFAS facilitated by ammonia. Moreover, it is

likely that there are other water quality parameters, as discussed below, that may alter PFAS removal efficiency.

5.4.2 Effect of pH on PFAS Removal Efficiency

The discussion in the previous section suggests that other water quality parameters can affect PFAS removal efficiencies in a similar fashion as ammonia. Accordingly, Spearman's correlation was run to assess the effect of pH on the removal of PFAS by ZIPGEM and CPS in the filtration cells during both dry and wet seasons. The removal efficiencies of both CPS and ZIPGEM media were considered in the same analysis here as no significant differences were found between the media. As shown in Figure 5-8, both short- and long-chain PFAS removal efficiencies are negatively correlated with proton (H^+) concentration (i.e., PFAS removal decreases when pH decreases). However, the long-chain PFAS exhibit weaker negative correlation than the short-chain PFAS, likely because the long-chain PFAS are removed via hydrophobic interactions and may not be affected by positive charge adsorption or charge neutralization of media. On the contrary, short-chain PFAS are usually removed via electrostatic interaction. Thus, the screening or shielding of media functional groups with proton (as pH decreases) would retard the association of the short-chain PFAS with the media surface (Figure 5-9). This can also hinder the adsorption of polyvalent cations complexed with dissolved organic matter (DOM) and short-chain PFAS. Moreover, a decrease in pH (increased proton concentration) resulted in charge neutralization, which, in turn, led to less complexation with the polyvalent cations and DOM. The total PFAS removal efficiencies also exhibit negative correlation (Figure 5-8), confirming the role of pH in conjunction with ammonia in PFAS removal efficiency.

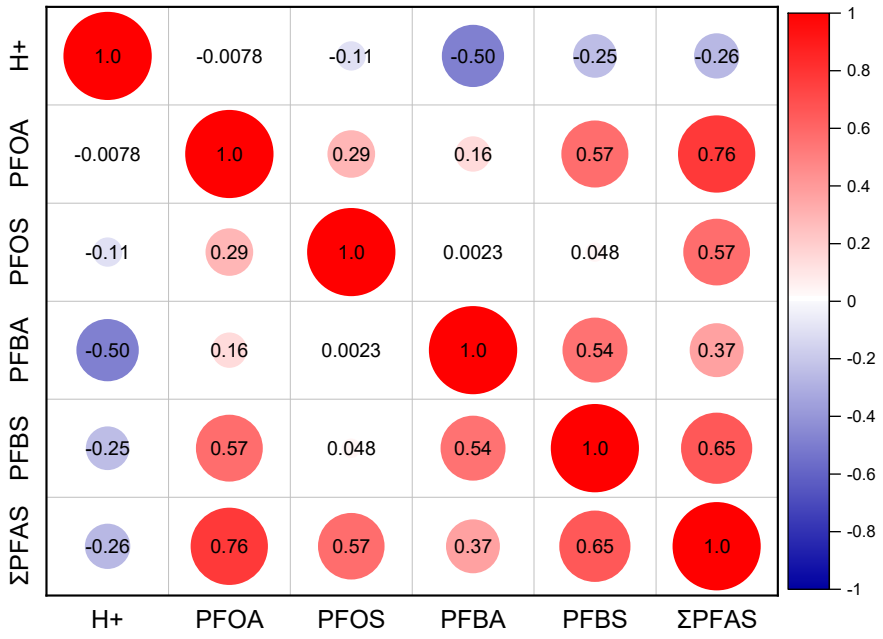

Figure 5-8: Correlation between short- and long-chain PFAS removal efficiencies and pH.

The discernible trends in PFAS removal efficiency can be elucidated by scrutinizing the event-wise data presented in Figure 4-16. A notable decline in removal efficiency was observed during event 3 (-22%) compared with event 1 (46%), concurrent with a drop in influent water pH from 8.62 (event 1) to 8.38 (event 3). Subsequently, removal efficiency exhibited an upward trajectory during event 4 (19%), correlating with an increase in pH to 9. The pH continued to decline to 8.29 in event 7, with a corresponding decrease in removal efficiency to -7% in the same event. Events 9 and 10 registered even lower pH levels (8.1 and 8.0, respectively), resulting in even lower removal of PFAS (-12% and -34% respectively). A similar trend was observed in cell 2 (ZIPGEM) and cells 3 and 4 (CPS). It is noteworthy that pH decreased from 8.62 to 8 in cell 1, 8.7 to 7.82 in cell 2, 8.66 to 8.2 in cell 3, and 8.63 to 8.2 in cell 4 (i.e., consequently, proton concentrations increased 4, 7.6, 2.88, and 2.7 times in cells 1, 2, 3, and 4, respectively).

5.4.3 Combined Effect of Ammonia and pH on the Adsorption Behavior of ZIPGEM and CPS

In light of the discussion in previous two Subsections, it is evident that influent and effluent ammonia concentration exhibit a negative correlation with PFAS removal efficiency. However, a more comprehensive analysis is warranted to elucidate the combined influence of pH and ammonia on removal efficiency. Ammonia is a weak base with a pKa of 9.25. It accepts a proton while in water and forms ammonium ions (NH_4^+), which can be represented by Eq. 5.27. Low pH indicates a high concentration of proton, which makes it favorable for ammonia to accept H^+ ions and form ammonium. The pH of the canal water investigated herein is around 8, which favors the forward reaction and facilitates the formation of ammonium ions (NH_4^+). Then ammonium ions join the nitrification process as illustrated in Eq. 5.28 (i.e., refer to subsections 5.3.1). As illustrated in Figure 5-9, the presence of a significantly elevated level of positively charged ammonium ion in the pore water within the media may lead to competition with PFAS for adsorption sites. This elucidates the initial high PFAS adsorption observed in Event 1, followed by a notable drop in subsequent events. Both CPS and ZIPGEM contain clay, perlite, and sand, with the exception of ZVI in ZIPGEM. CPS possesses a PZC of 5.5± 0.22, whereas ZIPGEM exhibits a PZC of 9.2± 0.33 (see Figure 4-4). The inclusion of ZVI (PZC = 7.7) raises the PZC of ZIPGEM. However, PFAS removal by these media occurs mostly through hydrophobic interactions. Consequently, despite ZVI's positive charge, it does not significantly enhance removal efficiency. Additionally, unlike other media components, ZVI lacks the porosity necessary for PFAS removal via entrapment. Clay, perlite, and sand maintain negative charges at a pH around 8, rendering ammonium adsorption more favorable than PFAS.

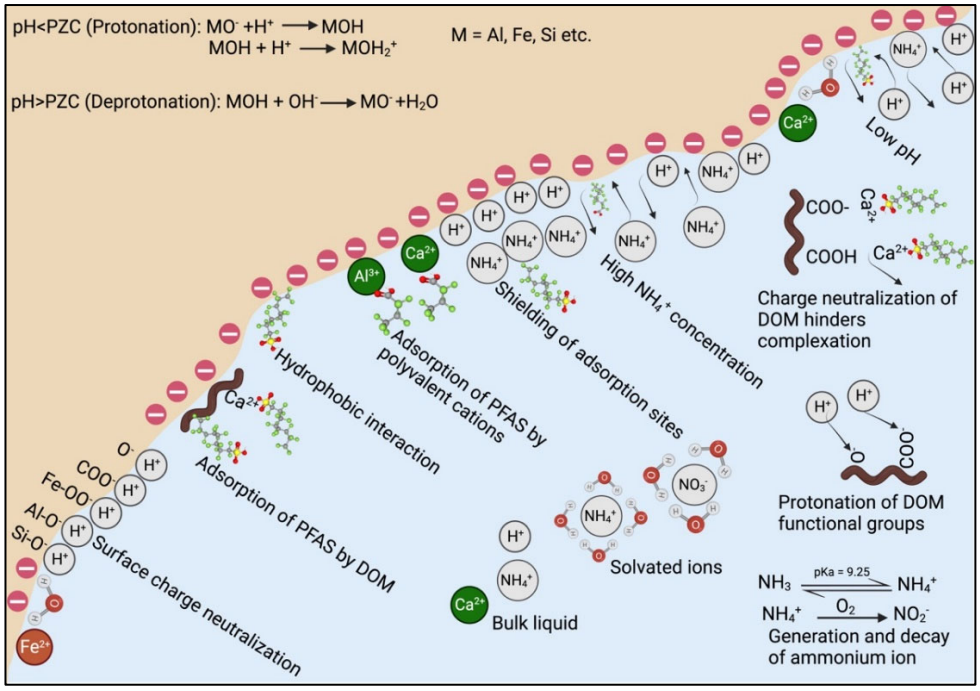

Figure 5-9: Illustration of PFAS interactions with water matrix constituents as influenced by ammonia and pH.

Apart from the competition for the adsorption sites, ammonium can also charge neutralize PFAS by binding to their carboxylic and sulfonic functional groups. Consequently, ammonia can neutralize the negative charges of counterions in the water, as well as those of the media components. Neutralization renders the media less amenable to adsorbing negatively charged PFAS, particularly when the functional groups of PFAS are neutralized by NH_4^+. Furthermore, this charge neutralization mechanism contributes to PFAS desorption from the media, as observed in events exhibiting negative removal efficiencies (events 3, 9, and 10). The continuous formation of ammonium in all events, coupled with the persistently favorable pH (around 8) during both dry and wet seasons, substantiated the process. However, event 4, characterized by a higher pH (approximately 9), offers valuable insights into the impact of ammonia disassociation. Notably, event 4 manifests an enhancement in PFAS removal efficiency across all cells except cell 2. In this event, influent and effluent ammonia concentrations were equal, implying the

absence of NH_4^+ formation based on the high pH (around 9), precluding ammonia adsorption. Consequently, PFAS removal efficiency might not have been negatively impacted by the above-mentioned occurrences of competition, charge neutralization, or desorption.

As ammonia concentration in the canal water was significantly higher (up to 0.16 mg•L^{-1}) compared with PFAS concentration (up to 69 ng•L^{-1}), and pH remained favorable for NH_4^+ formation, PFAS removal efficiency did not improve after the decline observed in Event 2. It is noteworthy that influent and effluent ammonia concentration do not accurately represent the NH_4^+ concentration within the media. As time progresses, the NH_4^+ concentration within the overhead water significantly increases, as evidenced by the rise in effluent ammonia concentration over time. This analysis reveals that the media does not reach exhaustion, as the observed enhancement in removal efficiency in certain events demonstrates. Therefore, the removal efficiency is primarily governed by the influent water quality parameters. The concentration of ammonia or an increase in the pH of influent water above its pK_a can improve the tested media's removal efficiency. The integration of a pretreatment media capable of ammonia removal in series could prevent spikes in ammonia concentration in the receiving water. Furthermore, to counter the effect of low pH, the addition of a new media component capable of elevating the pH of interfacial water may be considered.

$$NH_3 + H_2O \rightleftharpoons NH_4^+ + OH^- \quad \text{Eq. 5.27}$$

$$NH_4^+ \xrightarrow{\text{Oxygen}} NO_2^- \quad \text{Eq. 5.28}$$

$$pH<PZC \text{ (Protonation): } MO^- + H^+ \rightarrow MOH \quad \text{Eq. 5.29}$$

$$MOH + H^+ \rightarrow MOH_2^+ \quad \text{Eq. 5.30}$$

$$-COO^- = H^+ \rightarrow -COOH \quad \text{Eq. 5.31}$$

$$pH>PZC \text{ (Deprotonation): } MOH + OH^- \rightarrow MO^- + H_2O \quad \text{Eq. 5.32}$$

$$-COOH + OH^- \rightarrow -COO^- + H_2O \quad \text{Eq. 5.33}$$

$$\text{Polyvalent cation complexation: } -COO^- + Ca^{2+} + PFAS^- \rightarrow -COO\text{-}Ca\text{-}PFAS \quad \text{Eq. 5.34}$$

Figure 5-10 illustrates the removal efficiency of NH_4^+ along with the respective pH and PFAS removal during each event. As previously noted, The media of ZIPGEM and CPS exhibit PZC values of approximately 9.3 and 5.5, respectively. Consequently, they respond differently to influent water pH levels. In this study, the water pH consistently hovered around the PZC of ZIPGEM. Below the PZC of ZIPGEM (pH < PZC), the medium is expected to attract positive ions (Eqs. 5.29–5.31), whereas above the PZC (pH > PZC), it should attract negative ions (Eqs. 5.32–5.33). Conversely, CPS media, which consistently experienced pH levels above its PZC, should attract negative ions. During the dry season, the pH closely approximated the PZC of ZIPGEM, whereas in the wet season, a significant decrease was observed. Hence, during the wet season ZIPGEM media should exhibit an enhanced affinity for cations. As shown in Figure 5-10(a), ZIPGEM media adsorbed fewer protons during the dry season, which markedly improved the PFAS removal rate while it deteriorates in the wet season. This shift can be attributed to the fact that, beginning in event 6, the pH dropped well below the PZC of ZIPGEM. As a result, the medium underwent a charge reversal, causing proton adsorption in subsequent events. This phenomenon also elucidates the observed decline in ammonia removal efficiency during the wet season. Factors such as competition from high proton concentrations (low pH) for adsorption sites and the conversion of ammonia to more mobile ammonium ions collectively resulted in low ammonia removal during the wet season (Figure 5-9). Figure 5-10 further demonstrates that proton adsorption by the media is inversely associated with low removal of ammonia and PFAS. Certain events, such as event 3, exhibited elevated ammonia concentrations, wherein ammonia

could outcompete protons, resulting in satisfactory removal. However, this leads to the desorption of PFAS from the media.

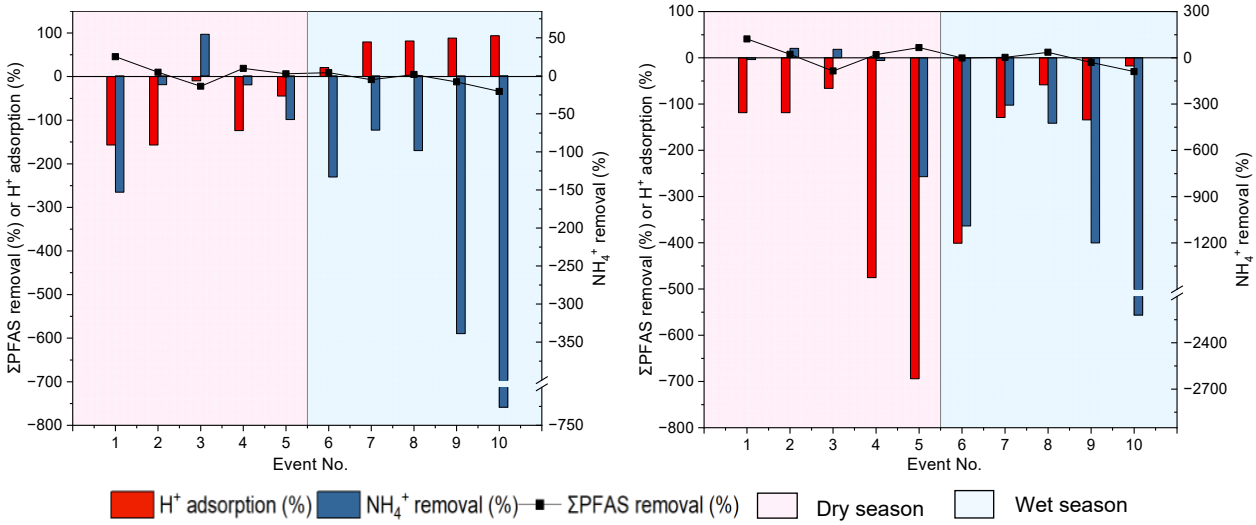

Figure 5-10: Combined effect of pH and ammonium (NH_4^+) on total PFAS removal by a) ZIPGEM and b) CPS media.

In line with the findings of our prior lab-scale study (Islam et al., 2023), the two primary mechanisms of PFAS removal—hydrophobic and electrostatic interactions—are validated by the field-scale results. However, unlike the lab-scale study, this investigation allowed for an exploration of the impact of competitive adsorption of co-ions or counterions on the PFAS removal rate, given the varying influent water quality parameters across different events. Additionally, environmental factors such as rainfall, temperature variations, and changes in turbidity, which were absent in the lab-scale study, were present in the field-scale scenario. Therefore, it can be concluded that 1) the fundamental removal mechanisms—electrostatic and hydrophobic interactions—remain applicable at the field scale; 2) CPS and ZIPGEM show variation in terms of PFAS removal efficiency; 3) CPS and ZIPGEM respond differently (though not significantly) to seasonal variations; and 4) higher concentration of counterions in the

influent water, such as ammonium and protons, can hinder PFAS removal through competitive adsorption.

This page intentionally left blank.

Chapter 6: Lab-scale Testing and Life Expectancy Estimation for the Filtration System

6.1 Implication of Life Expectancy

The estimation of life expectancy for downflow filtration cells containing CPS and ZIPGEM at C-23 canal is discussed in this chapter. The efficiencies of removal of target pollutants were calculated based the data obtained from manual sampling and the water quality probes. It should be noted that the canal water used in the pilot study contains multiple pollutants, whereas the laboratory water was spiked with each pollutant individually. Hence, the life expectancy estimated based on the laboratory results for each target pollutant provides a guidance as to how long the relevant cells can sustain at the field-scale for the known amount of GSM after extrapolation before saturation. Furthermore, based on the parameters listed in Tables 6-1 and 6-2, this estimate only considers physicochemical adsorption and not microbiological removal facilitated by microbial species, specifically for nitrogen removal. Such findings at the laboratory scale provides design guidelines for the pilot study located at C-23 canal in the St. Lucie River Basin in the future.

Table 6-6: Filter design parameters used for life expectancy analysis

Parameter	Value (English Unit)	Value (Metric Unit)
Width of reactor	14 ft	4.27 m
Free board (water head)	0.50 ± 0.16 ft	15.25 cm ± 4.88 cm
Filter depth	2.00 ft	60.96 cm
Filter length	43.5 ft	13.26 m
Filter width	22 ft	6.71 m
Sidle slope ratio 1:1	2.00	2.00
Volume design filter	994.00 ft^3	28.15 m^3

ZIPGEM mass of media	17.23×10^4 lb	7.83×10^4 kg
CPS mass of media	16.17×10^4 lb	7.35×10^4 kg

Table 6-7: Media characteristics used for life expectancy analysis

Media Parameter	ZIPGEM	CPS
Density ($kg \cdot m^{-3}$)	2,780	2,610
Porosity (%)	0.33	0.26
Hydraulic Conductivity, k ($cm \cdot s^{-1}$)	0.028	0.017

Each cell was equipped with an underdrain covered by a 6-inch layer of gravel and a permeable geomembrane liner. This arrangement was succeeded by a 2-feet deep media layer, either consisting of CPS or ZIPGEM material. The effluent originating from each cell was conveyed through the underdrain system, comprising PVC pipes, and subsequently passes through an individual drainage control box, as illustrated in Figure 2b. This configuration serves the dual purpose of facilitating drainage control for each cell and regulating the water head on the cell. Water is sourced from the C-23 canal, managed through a check-valve mechanism, and distributed to each cell utilizing rip rap bubbler pads. These pads not only dissipate energy but also sustain a water head of 0.5 feet above the media layer to ensure optimal functionality (Figure 6-1).

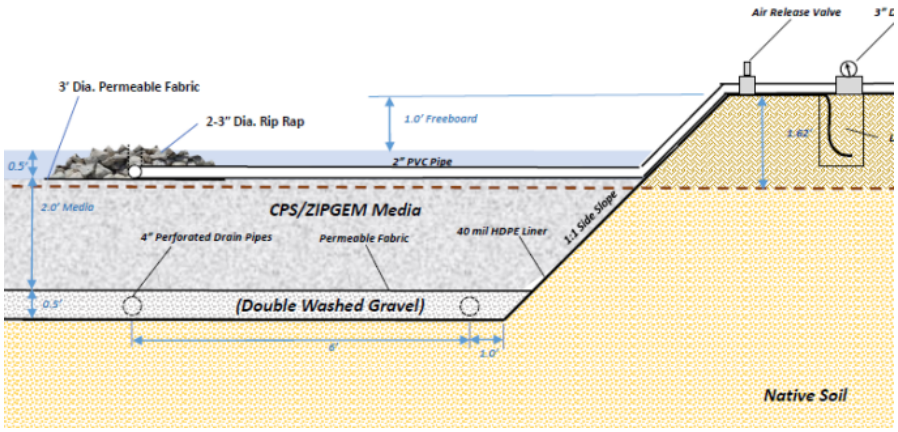

Figure 6-1: Filter profile view used for life expectancy analysis.

6.1.1 Discharge Flow Rate for Life Expectancy Analysis

The flow rate or discharge velocity of each reactor cell was calculated based on the discharge from the orifice of each drainage box. Considering the continuity equation, the Bernoulli equation (Eq. 6.1) was modified to Eq. 6.2 to first determine the velocity of the water. Considering the area of the orifice and the height of the water head from the center of the orifice to the top of the weir, the discharge was determined according to Eq. 6.3.

$$\frac{P_1}{\rho g} + \frac{v_1^2}{2g} + h_1 = \frac{P_2}{\rho g} + \frac{v_2^2}{2g} + h_2 \qquad \text{Eq. 6.1}$$

$$v_2 = \sqrt{2gh} \qquad \text{Eq. 6.2}$$

$$Q = \mathrm{A}\sqrt{2gh} \qquad \text{Eq. 6.3}$$

Where P_1, P_2 is the pressure of water at point 1 and 2 (psi), ρ is density of water (kg•m^{-3}), g is the gravity constant (m•s^{-2}), v_1, v_2 are the velocities at points 1 and 2 (m•s^{-1}), respectively, h_1, h_2 are the water heads at points 1 and 2 (m), respectively, h is the water height (m) where $h = h_1 - h_2$, Q is the discharge rate (m^3•s^{-1}), and A is the orifice area (cm^2).

6.1.2 Media Characterization

The media compositions (percentage by volume for each component) and characteristics are listed in Table 6-3. The physical characteristics including density and BET surface area were performed at the EMSL Analytical, Inc laboratories, while the saturated hydraulic conductivity and porosity were measured at the UCF Geotechnical laboratories. The Zero-Valent Iron (ZVI) utilized for the production of the filtration media was obtained from Connelly-GPM, Inc, and the perlite utilized was obtained from Miracle-Gro®. The components and media matrix in

percentage by volume as well as the physical characteristics of each sorption media are presented in Table 6-3. The density and surface area of ZIPGEM are higher than those of CPS; the former being attributed to the presence of iron, and the latter to a higher percentage of perlite (5% > 3%). In terms of porosity, ZIPGEM is also slightly higher than CPS, which is also attributed to the higher percentage of perlite.

Table 6-3: Media composition and media characteristics

Name	Media Composition	Density ($g \cdot cm^3$)	BET Surface Area ($m^2 \cdot g^{-1}$)	Saturated Hydraulic Conductivity ($m \cdot sec^{-1}$)	Porosity (%)
CPS	92% sand, 5% clay, 3 % perlite	2.61	1.08	$1.7(10^{-4})$	26
ZIPGEM	85% sand, 5% clay, 5% perlite and 5% ZVI	2.80	1.50	$2.8(10^{-4})$	33

6.1.3 Water Quality Parameters

The influent water utilized for the fixed-bed columns studies was collected from C-23 at Location 3 as this location was near a boat ramp with convenient accessibility. The methodology for analyzing water samples collected for the lab-scale experiments (both isotherms and column studies) is provided in Table 6-4. The removal rates and adsorption capacity obtained from the isotherms and column studies were used in the life expectancy analysis.

Table 6-4: Water quality parameters in the isotherm and column study

Parameter	Analysis/ Method	Laboratory
PFOS	EPA method 537 (Isotope Dilution)	Eurofins Lancaster

PFOA	EPA 537 (Isotope Dilution)	Eurofins Lancaster
Total Phosphorus	HACH TNT 843 HACH TNT 844 HACH TNT 845	University of Central Florida
MC-LR	Liquid chromatography mass spectrometry/mass spectrometry (LC-MS/MS)	Greenwater Laboratories

6.2 Isotherm Studies

The lab-scale adsorption isotherm studies focused on investigating the filtration media removal efficiency for four individual contaminants (i.e., PFAS, nitrogen, phosphorus, and microcystin). Distilled water spiked with a known concentration of the pollutants to mimic the actual surface water composition was used in the study (Figure 6-2). The isotherm studies conducted and overall setup per pollutant are summarized in Table 6-5.

Figure 6-2: Isotherm Schematic for Lab-Scale Studies.

Table 6-5: Summary of isotherm studies conducted for determining adsorption capacity of ZIPGEM and CPS

PFAS	Total Nitrogen	Total Phosphorus	Microcystin
• Kinetic isotherm • 50 g of media were aggregated to 400 mL distilled water spiked at initial PFAS concentration of 10 µg·L-1 (5 µg·L^{-1} of PFOS and 5 µg·L^{-1} of PFOA)	• Kinetic isotherm • 50 g of media and 200 mL of distilled water spiked to a concentration of 2 mg·L^{-1} N	• Equilibrium isotherm • 5 grams of media and 40 mL of distilled water spiked to different concentrations (i.e., 0, 0.7, 2, 3, 4, 5, 15, 30, 60, 120, and 240 mg·L^{-1} PO_4^{3-})	• Equilibrium isotherm • 10 g of media and 250 ml of DI water spiked with MC-LR to different initial concentrations ranging from 5–350 µg·L-1 (5, 35, 50, 100, and 350 µg·L^{-1}

6.2.1 PFAS Isotherm Study Method

Adsorption kinetic studies or adsorption batch studies were performed for PFOS and PFOA to determine the adsorption capacity of ZIPGEM and CPS. A sequence of kinetic isotherm studies was performed in duplicate using 500-mL polypropylene flasks. Each flask was initially washed with methanol and 50 g of media were added to 400 mL of distilled water spiked at initial PFAS concentration of 10 µg·L^{-1} (i.e., 5 µg·L^{-1} of PFOS and 5 µg·L^{-1} of PFOA). The beakers were then placed on a benchtop orbital shaker and agitated at 160 rpm; samples were collected at seven time intervals including 2, 5, 10, 20, and 30 hrs following media addition for ZIPGEM with additional sampling at 36 hrs and 42 hrs for CPS to capture the adsorption breakthrough because of its lower adsorption capacity for PFAS. Samples were allowed to settle for 60 minutes before filtration using a 0.8-µm pore size polypropene membrane filter. The filtered water samples were stored at 4 °C and delivered within 24 hrs to the external laboratory Eurofins Lancaster Laboratory for analysis of PFOS and PFOA.

6.2.2 Phosphate Isotherm Study

Several isotherm tests were carried out to determine phosphate adsorption capacity of CPS and ZIPGEM. Before starting the isotherm study, the media were washed with distilled water [3 Bed Volumes (BV)] and subsequently dried for 24 hrs at a temperature of 78 °C to remove any possible contaminants that could affect the experiment. In glass Erlenmeyer flasks, 5 grams of media were placed in 40 ml of DI water spiked at various concentrations (i.e., 0, 0.7, 2, 3, 4, 5, 15, 30, 60, 120, and 240 $mg \cdot L^{-1}$ PO_4^{3-}). The flasks were then shaken for 6 hours on an orbital shaker at 180 rpm at room temperature. Samples were then left for 30 minutes to settle before filtration with 0.45-µm pore size membrane filters and analyzed for phosphate in triplicate in-house.

6.2.3 Microcystin Isotherm Study

Equilibrium isotherm studies were performed to determine microcystin removal capacity of CPS and ZIPGEM. The sorption media were first washed with distilled water (3 BV) and subsequently dried for 24 hours at a temperature of 78 °C to remove any possible contaminants that could affect the experiment. The equilibrium isotherm consisted of five Erlenmeyer Flasks that were filled with 10 g of media and 250 ml of DI water spiked with MC-LR at initial concentrations ranging from 5–350 $\mu g \cdot L^{-1}$ (5, 35, 50, 100, and 350 $\mu g \cdot L^{-1}$). The flasks were placed on a benchtop orbital shaker and agitated at 160 rpm for 24 hours. At the end of the shaking time, samples were collected and left for 1 hr to settle before filtration using 0.45-µm pore size membrane filters; duplicate water samples (100 mL) were collected in plastic bottles to be delivered to the external laboratory Green Water laboratories for MC-LR analysis.

6.2.4 Nitrate Isotherm Study Method

Equilibrium isotherms were performed to determine nitrate adsorption capacity of CPS, and ZIPGEM. CPS and ZIPGEM were first washed with distilled water [3 Bed Volumes (BV)] and

subsequently dried for 24 hours at a temperature of 78 °C to remove any possible contaminants that could affect the experiment. Erlenmeyer flasks with 50 grams of media and 200 ml of DI water spiked at 0.9, 1.5, 2, 5, and 7 mg•L^{-1} N were shaken for 48 hours on an orbital shaker at 180 rpm at room temperature. Samples were then left for 0.5 hr to settle before filtration with 0.45-µm pore size membrane filters and analyzed for nitrate concentrations in triplicate in-house.

6.2.5 Results of Isotherm Studies

The results from the PFAS isotherm experiments were fitted to the isotherm models to obtain the adsorption capacity, q_e. The isotherm models for the PFAS isotherm studies included the pseudo-first order model (Lagergren, 1898) and the pseudo-second order model (Ho et al., 1996). A summary of the kinetic model parameters, variables, and correlation coefficients for the kinetic models is presented in Table 6-6. Considering the adsorption capacity of each media, q_e of 8.7×10^{-7} mg·g^{-1} (0.87 ng·g^{-1}) and $2.12\text{x}10^{-7}$ mg·g^{-1} (2.12 ng·g^{-1}) for PFOS can be estimated for CPS and ZIPGEM, respectively. Only ZIPGEM obtained a q_e. of 5.72 ng·g^{-1} for PFOA removal.

Table 6-6: Summary of kinetic models for green sorption media investigated for PFAS removal

Kinetic Parameters and Variables	CPS		ZIPGEM	
	Pseudo-First Order	**Pseudo-Second Order**	**Pseudo-First Order**	**Pseudo-Second Order**
PFOS				
q_e (ng·g^{-1})	**0.87**	-1.28	--	**2.12**
k_1(·min^{-1})	$2.30(10)^{-4}$	--	--	--
k_2 (g·ng^{-1}·min^{-1})		$9.06(10)^{-4}$	--	-0.004
C	--	--	--	--
k_{id} (g·ng^{-1}·min^{-1})	--	--	--	--
R^2	0.425--	0.426	--	0.904

PFOA				
q_e ($ng \cdot g^{-1}$)	--	-4.623	**5.72**	0.447
k_1($\cdot min^{-1}$)	--	--	-0.0005	--
k_2 ($g \cdot ng^{-1} \cdot min^{-1}$)	--	$-1.87(10)^{-4}$	--	-0.004
C	--	--	--	--
k_{id} ($g \cdot ng^{-1} \cdot min^{-1}$)	--	--	--	--
R^2	--	0.161	0.900	0.480

* Ordonez et al. (2022c): influent spiked with 0.7 $\mu g \cdot L^{-1}$ of PFOS and 1.62 $\mu g \cdot L^{-1}$ of PFOA

Based on Langmuir model, the phosphate and microcystin adsorption capacities (q_m) of CPS and ZIPGEM were evaluated following the Langmuir (Langmuir, 1918) and Freundlich (Freundlich, 1907) isotherm models (Table 6-7). The phosphate q_m for ZIPGEM was 1.796 $mg \cdot g^{-1}$ and the q_m obtained for CPS was 0.140 $mg \cdot g^{-1}$. Microcystin adsorption capacity of CPS and ZIPGEM was 0.00074 $mg \cdot g^{-1}$ and 0.001 $mg \cdot g^{-1}$, respectively.

Table 8: CPS and ZIPGEM Langmuir and Freundlich isotherm parameters for phosphate and microcystin removal

Parameters and Variables	CPS		ZIPGEM	
Phosphate Removal				
Langmuir	R^2	0.838	R^2	0.942
	K_L($L \cdot mg^{-1}$)	0.042	K_L($L \cdot mg^{-1}$)	0.165
	q_m ($mg \cdot g^{-1}$)	**0.140**	q_m ($mg \cdot g^{-1}$)	**1.796**
Freundlich	R^2	0.928	R^2	0.952
	K_f	0.008	K_f	0.171
	n	1.696	n	1.504
Microcystin Removal				
Langmuir	R^2	0.841	R^2	0.239
	K_L($L \cdot mg^{-1}$)	0.009	K_L($L \cdot mg^{-1}$)	0.005
	q_m ($mg \cdot g^{-1}$)	**0.00074**	q_m ($mg \cdot g^{-1}$)	**0.001**
Freundlich	R^2	0.893	R^2	0.771
	K_f	0.009	K_f	0.023
	n	1.258	n	1.709
Nitrate Removal				

Langmuir	R^2	0.9	R^2	0.8929
	K_L(L·mg^{-1})	0.606	K_L(L·mg^{-1})	2.129
	q_m (mg·g^{-1})	0.00036	q_m (mg·g^{-1})	0.00958
Freundlich	R^2	0.9714	R^2	0.8787
	K_f	0.0014	K_f	0.00584
	n	2.35	n	2.69

6.3 Fixed-Bed Column Studies

While isotherms only indicate static adsorption capacity, dynamic adsorption capacity has to be tested by fixed bed down flow columns. Fixed-bed column studies were conducted in triplicate to determine the efficiency of ZIPGEM and CPS in removing PFAS, phosphate, and microcystin from the canal water. The general column setup is depicted in Figure 6-3. The methodology employed to determine the adsorption capacity of the media relied on fitting the experimental data to selected dynamic models and assessing the goodness of fit between the experimental and the models' theoretical results via the correlation coefficient (R^2). The linear regression performed enabled the determination of the model parameters such as the maximum adsorption capacity (q_0).

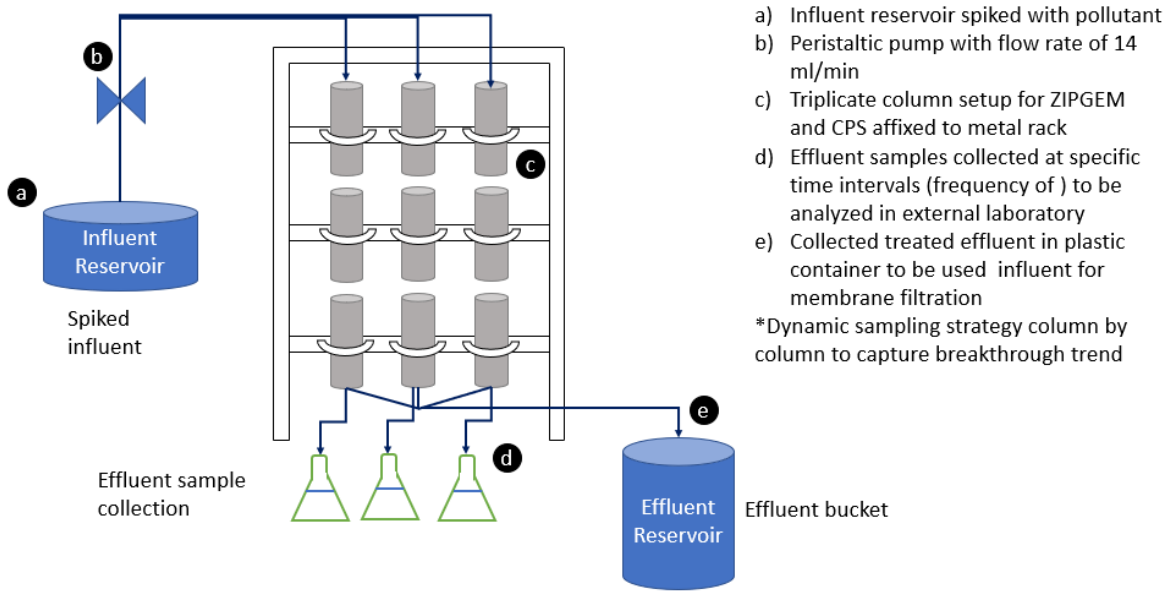

Figure 4-3: Fixed-bed column study setup in triplicate (column depths may vary among the column studies).

6.3.1 PFAS Column Study

A column study, in triplicate, was conducted to evaluate PFAS (PFOS and PFOS) removal efficiency and adsorption capacity of CPS and ZIPGEM, for a total run time of 32 hours and 48 hours, respectively. The columns consisted of polyvinyl chloride (PVC) pipe with a length of 91 cm (3 ft) and 10-cm (4-in) diameter with three equal length sections. The three column sections were sealed with parafilm and water-resistant tape creating a single column and to prevent outside disturbances caused by air intrusion. Each column section contained a bottom filter followed by a layer of pebbles and approximately 2,600 mL of filtration media. An additional layer of pebbles was placed at the top of each section to facilitate water distribution. The columns were first flushed with DI water for approximately two bed volumes and left to drain for approximately 8–10 hours to remove any impurities present in the media. The influent canal water was spiked with 70 $ng \cdot L^{-1}$ of PFOA and PFOS, each, for a total PFAS concentration of

140 ng·L^{-1}. The influent was delivered at a constant downflow of 14 mL·min^{-1}. The experimental data were then applied to three dynamic adsorption models, Thomas (Thomas, 1944), Modified Dose Response (MDR) (Yan et al., 2001), and Yoon-Nelson (Yoon and Nelson, 1984) to estimate the adsorption capacity of the filtration media (Ordonez et al., 2022b; 2022c).

6.3.2 Phosphate Column Study

To understand the dynamic phosphate removal and characterize the adsorption capacity, two column studies were performed using ZIPGEM and CPS. A triplicate set of columns filled with 7.8 L of CPS with a weight of 20.36 kg of CPS media, was set up to determine the dynamic removal of phosphate by CPS. Each column consisted of a PVC pipe with a diameter of 10 cm (4 in) divided into 3 sections of 30 cm (1 ft). The column length for ZIPGEM was shortened to accelerate the breakthrough in ZIPGEM column since ZIPGEM mix has an extremely large adsorption capacity, according to the isotherm study. Therefore, a triplicate set of PVC columns of 12.7 cm (5 in) length and 10 cm (4 in) diameter filled with 700 mL of ZIPGEM with a weight of 1,000 grams of ZIPGEM media was constructed to determine the dynamic removal of phosphate. Each column was first flushed with DI water for 3 BV and left to drain for about eight hours. The columns consisted of a filter and layer of pebbles at the bottom of each media to prevent clogging, and a layer of pebbles at the top of each column to aid in water distribution. DI water spiked with phosphate standard solution at a concentration of 4 mg·L^{-1} PO_4^{3-} was supplied to each column at a flow rate of 8 mL·min^{-1}. Water samples were collected from the effluent at different time intervals after 23 hrs until the ZIPGEM and CPS media reached exhaustion. Water samples were analyzed for TP using the Hach TNT 843. Data obtained from the dynamic phosphate column study were applied to dynamic models including Thomas (Thomas, 1944) and Yoon-Nelson models (Yoon and Nelson, 1984).

6.3.3 Microcystin Column Study

A fixed-bed column study for CPS and ZIPGEM was conducted to determine the removal efficiency and adsorption capacity for MC-LR treatment in a dynamic environment. The experimental setup (in triplicate) for both CPS and ZIPGEM consisted of a PVC column of 5 in. Length and 4 in. diameter. Each column contained a bottom filter and layer of pebbles at the top to prevent clogging, followed by 1,000 g of media (i.e., CPS, and ZIPGEM) which were covered with a layer of pebbles to aid in water distribution at the surface of the column.

A peristaltic pump was used to deliver a constant flowrate of 14 $mL \cdot min^{-1}$ in a downflow manner to the columns. The influent was prepared by spiking surface water from C-23 canal at a concentration of 70 $\mu g \cdot L^{-1}$ of MC-LR which approximates the high range of MC-LR concentrations in natural environments. The column experimental data were fitted to selected dynamic models including the Thomas model (Thomas, 1944) and the Modified Dose-Response (MDR) model (Yan et al., 2001).

6.3.4 Nitrate Column Study

To determine the dynamic nitrate removal of ZIPGEM and characterize the adsorption capacity, two dynamic column studies were performed using ZIPGEM and CPS. A triplicate set of columns filled with 7.8 L of CPS media (an equivalent weight of 20.36 kg), was constructed to determine the dynamic removal of CPS. Each column consisted of a PVC pipe with a diameter of 10 cm (4 in) divided into three sections of 30 cm (12 in). The column length for ZIPGEM analysis was shortened to accelerate the breakthrough in ZIPGEM column since the ZIPGEM mix has an extremely large adsorption capacity according to the isotherm study. Therefore, a triplicate set of PVC columns of 30 cm (1 ft) depth and 10-cm (4 in) diameter filled with 2,600 mL of ZIPGEM media (7,228 g) was constructed to determine the dynamic removal by ZIPGEM.

Each column was first flushed with DI water for three BV and left to drain for about eight hours. The columns consisted of a filter and layer of pebbles at the below each media to prevent clogging and a layer of pebbles at the top of each column to aid in water distribution. DI water spiked with nitrate standard solution to a concentration of 2 $mg \cdot L^{-1}$ NO_3^- as nitrogen was delivered to each column at a flow rate of 8 $mL \cdot min^{-1}$. Water samples were collected from the effluent at different time intervals after one hour until the ZIPGEM and CPS media reached exhaustion. Water samples were analyzed for nitrate using the Hach TNT 835. Data obtained from the dynamic nitrate column study was applied to dynamic models such as Thomas (Thomas, 1944) and Yoon-Nelson models (Yoon and Nelson, 1984).

As previously described, a triplicate column study was conducted to evaluate biological nitrate removal efficiency and adsorption capacity of CPS and ZIPGEM. A separate set of columns were prepared to explore the microbial effects only. Similar to the previous column settings, the columns for nitrate removal during incubation period consisted of polyvinyl chloride (PVC) pipe with a length of 91 cm (3 ft) and 10-cm (4-in) diameter with three equal sections. The three column sections were sealed with parafilm and water-resistant tape creating a single column to prevent outside disturbances such as air intrusion. Each column section contained a bottom filter followed by a layer of pebbles and approximately 2,600 mL of filtration media. An additional layer of pebbles was placed at the top of each section to enhance water distribution. The nitrate column study procedure began with an incubation period of four weeks, during which stormwater from a stormwater wet detention pond by the Student Union at the University of Central Florida was collected and utilized to continuously feed each column. At the culmination of the incubation period, stormwater spiked with nitrate (1,000 $mg \bullet L^{-1}$ standard solution) and phosphate (50 $mg \bullet L^{-1}$) standard solution) at a concentration of 0.9 $mg \bullet L^{-1}$ NO_3^- and 0.3 $mg \bullet L^{-1}$

PO_4^{3-} for condition 1 was fed to each column for 3 h. Subsequently, water samples were collected from the influent and effluent ports of each column. The columns were then flushed with stormwater alone for more than 24 h to counteract any possible media changes due to the influent conditions. The same process (after incubation) was repeated for two more influent conditions: 1.3 mg•L^{-1} NO_3^-, 0.5 mg•L^{-1} PO_4^{3-} (condition 2), and 1.7 mg•L^{-1} NO_3^-, 0.7 mg•L^{-1} PO_4^{3-} (condition 3). The downward influent flow rate of 8 ml•min^{-1} was maintained with peristaltic pumps.

Water samples from the influent and effluent ports of each column were collected at the culmination of the 3-hour run time for conditions 1, 2, and 3. Collected samples were analyzed in-house for pH, ORP, and DO immediately after collection. The Waterproof Double Junction pH Testr® 30 was used to measure pH, while DO and ORP were measured using the HACH HQ40D IntelliCAL/MTC101.The water samples were analyzed in triplicates for TN (TNT826), NOx (TNT835 and TNT839), ammonia (TNT830), TP (TNT843), alkalinity (TNT870), iron (TNT858), and aluminum (TNT848) within 24 hour of collection using Hach kits. DON was calculated as the difference between TN, NOx, and ammonia.

For quantification of the microbial species in both ZIPGEM and CPS, quantitative polymerase chain reaction (qPCR) was employed (Chang et al., 2018 a, b). Media samples were collected from the locations at the top of three sections of each column, two and four weeks after the beginning of the experiment (before the addition of spiked stormwater) to assess biofilm growth. After the addition of spiked stormwater, for each influent condition, media samples were collected at the end of run time (3hrs) from the top of three sections of each column. All media samples were stored at -80 °C after collection until conducting the qPCR analyses. The qPCR analyses were thus employed to help visualize the microbial population dynamics and microbial

ecology. DNA extraction was performed via the Dneasy PowerSoil Kit (Qiagen) by following the steps recommended by the vendor. The primer and standards utilized were acquired from ThermoFisher Scientifc and GenScript. A 48-well plate was used to process the samples via the Step-One-Plus qPCR instrument. Each well was composed of 10 µL of SybrGreen, 1.6 µL of primer (0.8 µL forward and 0.8 µL reverse), 5 µL of sample, and 3.4 µL of qPCR water.

6.3.5 Results of the Column Study

A. PFAS Column Study

In general, the efficiency of PFOS removal by CPS and ZIPGEM was the highest, with concentrations consistently falling below the method detection limits (MDL) of 0.90 $ng \cdot L^{-1}$ for the majority of samples analyzed in this column study. The PFOS removal rates in ZIPGEM columns at 32, 36, and 42 hours exhibited variations within the range of 98% to 94%. CPS demonstrated a higher initial removal efficiency for PFOA, reaching 91%, while ZIPGEM achieved an initial removal efficiency of 84%. Despite CPS exhibiting superior PFOA removal, ZIPGEM media experienced breakthrough slightly later than CPS, attributable to its increased adsorption capacity for PFAS. Moreover, the maximum PFOA adsorption capacities, determined through the Thomas model (Thomas, 1944) with correlation coefficients (R^2) > 0.84, were 0.07 $ng \cdot g^{-1}$ for ZIPGEM and 0.08 $ng \cdot g^{-1}$ for CPS, as presented in Table 6-8.

Table 6-8: Results from the dynamic modeling of the PFOA adsorption in a fixed bed column study

Media	*Dynamic Model*	R^2	*Parameters*
CPS	Thomas	0.85	$q_o = 0.08\ ng \cdot g^{-1}$ $K_T = 5.9\ E^{-5}\ L \cdot ng^{-1} \cdot min^{-1}$
	MDR	0.74	$a_{mdr} = 2.67$ $q_o = 0.06\ \mu g \cdot g^{-1}$

ZIPGEM	Thomas	0.84	q_o = 0.07 ng·g^{-1} K_T = 3.7 E^{-5} L·ng^{-1}·min^{-1}
	MDR	0.85	a_{mdr} = 2.23 q_o = 0.05 ng·g^{-1}

B. Phosphate Column Study

The phosphate removal efficiency of ZIPGEM in the dynamic column study ranged from 73% to 92% across three columns. In contrast, CPS demonstrated a removal efficiency ranging from an initial 92% to a final 4.8%. The dynamic column study outcomes pertaining to phosphate adsorption by ZIPGEM and CPS were subjected to fitting with two dynamic models, as detailed Table 6-9. As shown in Table 6-9, the R^2 values obtained from the linear regression curves of the Thomas (Thomas, 1944) and Yoon-Nelson (Yoon and Nelson, 1984) models for ZIPGEM were both 0.721.

Table 6-9: Results from the dynamic modeling of the Phosphate adsorption in a fixed bed column study

Media	Dynamic Model	R^2	Parameters
ZIPGEM	Thomas	0.721	q_o = 7.65 mg·g^{-1} K_T = 2.5 E^{-6} L·µg^{-1}·min^{-1}
	Yoon-Nelson	0.721	τ = 166 d K_{YN} = 1 E^{-5} L·min^{-1}
CPS	Thomas	0.6732	qo = 3.73 mg·g^{-1} K_T = 5.00E^{-5} L·µg^{-1}·min^{-1}
	Yoon-Nelson	0.6732	τ =40h K_{YN} = 2.00E^{-4} min^{-1}

C. Microcystin Column Study

ZIPGEM media exhibited ~38% microcystin removal within the first hour, reaching its exhaustion point of adsorption capacity (i.e., zero removal rate) after 32 hours, whereas CPS media achieved 20% microcystin removal in the first hour, reaching exhaustion after only 2 hours. The dynamic column results were used for the Thomas (Thomas, 1944) and MDR (Yan et al., 2001) models to determine the adsorption capacity (q_o). As presented in Table 6-10, q_o for CPS predicted by the Thomas model (Thomas, 1944) was 0.15 ug·g^{-1} and that for ZIPGEM was 0.97 ug·g^{-1}. Yet, despite the fact that the Thomas model (Thomas, 1944) is based on the Langmuir model (Langmuir, 1918), the R^2 obtained from the linear regression was low (R^2 = 0.35). Since CPS exhibited a quick removal time, the MDR dynamic model (Yan et al., 2001) was not applicable. For ZIPGEM, the MDR model (Yan et al., 2001) obtained a q_o 0.016 ug·g^{-1}. Moreover, the correlation coefficients for ZIPGEM when applying the Thomas (Thomas,1944) and MDR (Yan et al., 2001) models were 0.651 and 0.776, respectively.

Table 6-10: Results from the dynamic modeling of the MC-LR adsorption in a fixed bed column study (Ordonez et al. 2023)

Media	Dynamic Model	R^2	Parameters
CPS	Thomas	0.350	q_o = 0.15 µg·g^{-1} K_T = 7.9 E^{-6} L·µg^{-1}·min^{-1}
	MDR	---	---
ZIPGEM	Thomas	0.651	q_o = 0.97 µg·g^{-1} K_T = 3.16 E^{-6} L·µg^{-1}·min^{-1}
	MDR	0.776	a_{mdr} = 0.632 q_o = 0.016 µg·g^{-1}

D. Nitrate column study

The nitrate removal efficiency of ZIPGEM in the dynamic column study ranged from 18% to 88 %, when compared to the phosphate removal efficiency for CPS, which ranged from 3.22% to

95.1%. Hence, ZIPGEM can perform well for removing both nitrate and phosphate. The dynamic column study results obtained for nitrate adsorption by ZIPGEM and CPS were fitted to two dynamic models (Table 6-11). For CPS, the R^2 obtained from the nonlinear regression curve of the Thomas (Thomas, 1944) and Yoon-Nelson (Yoon and Nelson, 1984) models was 0.967 and 0.914, respectively. The q_0 for CPS was calculated as 0.198 $mg \cdot g^{-1}$ with a K_T constant from the Thomas model (Thomas, 1944) calculated from the linear regression of 0.01185 $L \cdot \mu g^{-1} \cdot min^{-1}$. While the calculated K_{YN} obtained from the linear regression of the data is 0.0233 min^{-1} and the value of τ is ~3.4 hrs (204 min) for the CPS column. For ZIPGEM, the R^2 obtained from the linear regression curve of the Thomas (Thomas, 1944) and Yoon-Nelson models (Yoon and Nelson, 1984) is 0.4305 and 0.4305, respectively. The K_T constant from the Thomas models (Thomas, 1944) calculated from the linear regression is 9.66E-6 $L \cdot \mu g^{-1} \cdot min^{-1}$ and the calculated q_0 is 1.03 $mg \cdot g^{-1}$, while the calculated K_{YN} obtained from the linear regression is 2E-4 min^{-1} and the value of τ is 7.5 hrs (448 min) for the ZIPGEM column (Figure 6-4).

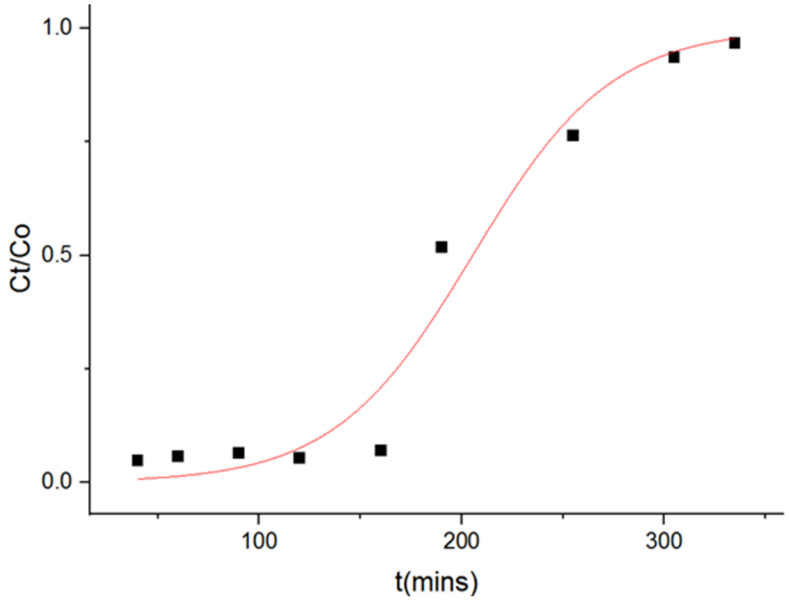

(a) The nonlinear Thomas modeling of the nitrate adsorption in a fixed bed CPS column study

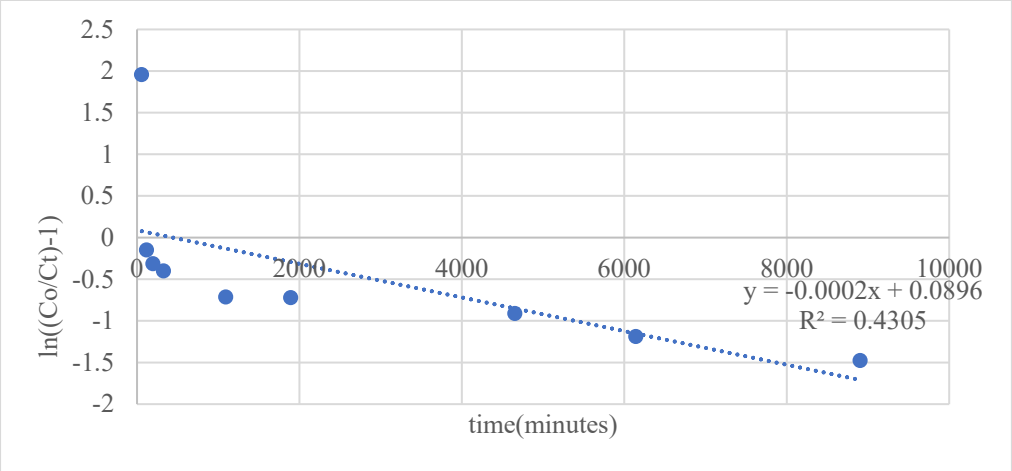

(b) The linearized Thomas model for the nitrate adsorption in a fixed bed ZIPGEM column study

Figure 6-4: Results of column study for nitrate removal.

Table 6-11: Results from the dynamic modeling of the nitrate adsorption in a fixed bed column study

Media	Dynamic Model	R^2	Parameters
CPS	Nonlinear Thomas	0.967	$q_o = 0.198\ mg \cdot g^{-1}$ $K_T = 0.01185 L \cdot \mu g^{-1} \cdot min^{-1}$
	Yoon-Nelson	0.914	$\tau = 3.4h$ $K_{YN} = 0.0233\ L \cdot min^{-1}$
ZIPGEM	linear Thomas	0.4305	$q_o = 1.03\ mg \cdot g^{-1}$ $K_T = 9.66E^{-5} L \cdot \mu g^{-1} \cdot min^{-1}$
	Yoon-Nelson	0.4305	$\tau = 7.5h$ $K_{YN} = 0.0002\ L \cdot min^{-1}$

E. Microorganisms for Nitrogen Removal in Column Study

The results of the PCR analysis were correlated with the changes in the concentrations of various species of nitrogen in the influent and effluent water samples, as well as with DO and ORP

values to obtain a holistic understanding of the nitrogen cycle and biological nitrogen removal (Figures 6-5 and 6-6). This was further investigated in the field study.

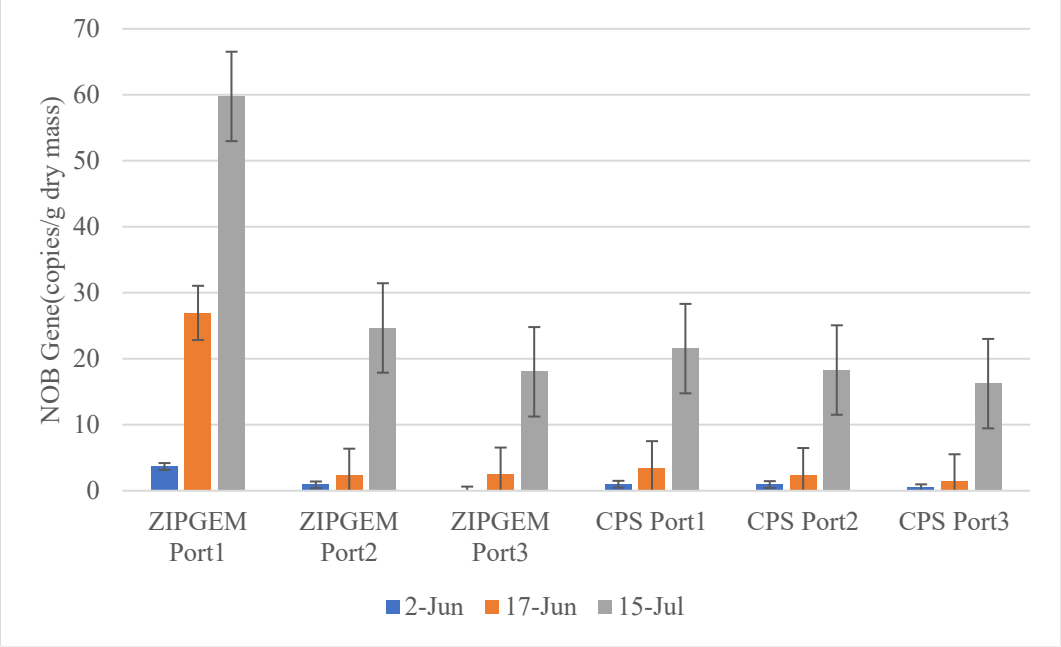

Figure 6-5: Population density for NOB (enzyme nxrAB) in copy/gram for samples collected at week 2, month 1 and month 2 of cultivation.

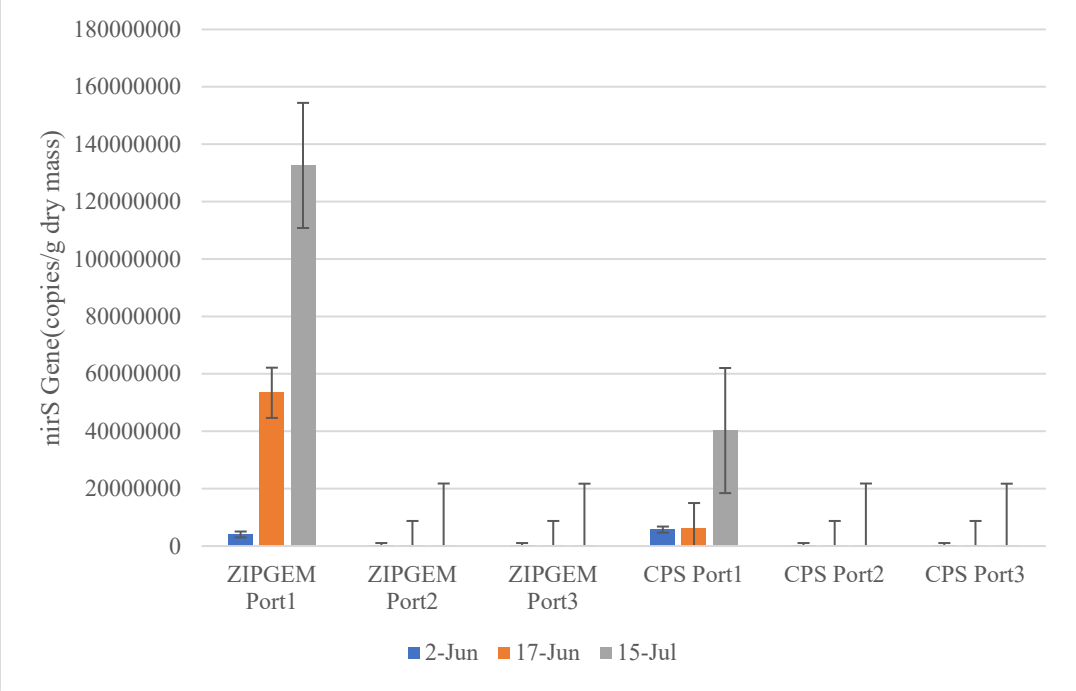

Figure 6-6: Population density for nirS in copy/gram for samples collected at week 2, month 1 and month 2 of cultivation in which Port 1 corresponds to the top section, port 2 corresponds to the middle section, and port 3 corresponds to the bottom section.

6.4 Life Expectancy or Service Life of Media

6.4.1 Methodology

The life expectancy of the sorption media used for filtration is an important engineering design parameter that ensures possible period of time to sustain the treatment for contaminated water by sorption media before replacement. The life expectancy or service life calculations were performed for CPS and ZIPGEM for each pollutant individually. The methodology is divided into two parts. One part involves the design of the treatment system and the other is related to the water quality improvement. The final step is to generate life expectancy curves as a function of removal efficiencies (e.g., 20-90%) when treating a specific contaminant which is displayed in a media mass versus volume of treated water graph used for engineering applications.

The life expectancy of CPS and ZIPGEM was evaluated according to the methodology provided in previous studies using Equations 6.4 ~ 6.14 (Ordonez et al. 2022a, b). To calculate the life expectancy of the media, the following parameters are required: 1) initial and final pollutant concentrations, 2) maximum adsorption capacity obtained from lab experiments (e.g., isotherm study based on the most fitting adsorption model), 3) design of reactor cell (i.e. dimensions), 4) media characteristics (i.e., porosity, density, and hydraulic retention time) and 5) pumping flow rate (derived according to filter cell surface area and media hydraulic conductivity via a constant head permeability test). The method to estimate such life expectancy follows the flow chart presented in Figure 6-7.

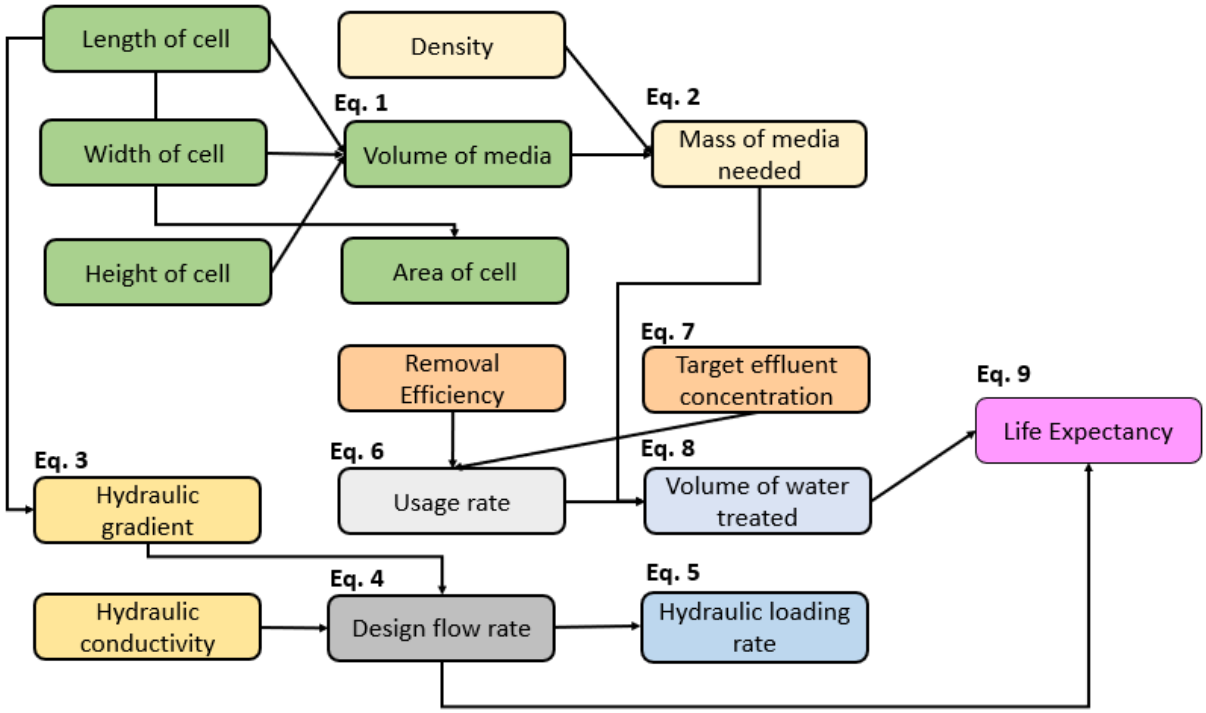

Figure 6-7: Life Expectancy Flow Diagram.

A. Design Parameters of Filter System

The mass of media ($Mass_{media\ in\ reactor}$) in kg is determined based on the volume of media ($V_{media\ in\ reacort}$) in ft^3 and the dry density of the sorption media (ρ_{media}). The volume of media

($V_{media\ in\ reactor}$) in ft^3 is calculated using Eq. 6.4. Consequently, the $Mass_{media}$ in kg specified by the desired cell design and the $V_{media\ in\ reactor}$, are determined where the dry density of the sorption media (ρ_{media}) in $kg \bullet m^{-3}$ is used (Eq. 6.5).

$$V_{media\ in\ reactor} = L * W * D \quad \text{Eq. 6.4}$$

$$Mass_{media\ in\ reactor} = V_{media} * \rho_{media} \quad \text{Eq. 6.5}$$

If the design pumping flow rate (Q_{design}) in $L \bullet hr^{-1}$ (Eq. 6.7) to be administered at each filter cell is unknown, it can be projected utilizing the experimental hydraulic conductivity (*k*), reactor surface area (*A*) and hydraulic gradient (*i*) (Eq. 6.6), where the hydraulic conductivity (*k)* is in $cm \bullet sec^{-1}$, reactor surface area (*A*) in m^2 and hydraulic gradient (*unitless*). However, the flow rate or discharge rate was collected during field campaign (see Chapter 4). Hence, the hydraulic loading rate (HLR) required to maintain the specified water head (e.g., 0.15 m ± 0.05 m) is determined based on Q and *A* (Eq. 6.7). Also, the hydraulic loading rate (*HLR*) in $gal \bullet day^{-1} \bullet ft^{-2}$ required to maintain the specified water head (e.g., 0.5 ft ± 0.17 ft) is determined based on *Q* and *A* (Equation 8). Additionally, the hydraulic retention time (*HRT*) in h can be calculated using Eq. 6.10 utilizing the void volume (V_{void}) in m^3. V_{void} represents the volume of water passing through the media, calculated based on the media mass ($Mass_{media\ in\ reactor}$), media porosity, and density (ρ_{media}) using Eq. 6.9.

$$i = \frac{\Delta H}{\Delta Z} = \frac{\Delta H}{L} \quad \text{Eq. 6.6}$$

$$Q_{design} = k * i * A \quad \text{Eq. 6.7}$$

$$HLR = \frac{Q}{A} \quad \text{Eq. 6.8}$$

$$V_{void} = \left(\frac{Mass}{\rho_{media}}\right) * \text{porosity} \quad \text{Eq. 6.9}$$

$$\text{HRT} = \frac{V_{void}}{Q} \quad \text{Eq. 6.10}$$

B. Water Treatment

To obtain the removal efficiency curves to be used for life expectancy calculations and produce the mass of media versus volume of treatment plot, the volume of water that can be treated at each specific removal efficiency needs to be determined. First, the usage rate in $g \cdot L^{-1}$ is calculated using Equation 6-11, where it defines the specific mass of media (*Mass*) in g that can treat 1 L of water to achieve a desired percent removal (i.e., pollutant removal efficiency (R)). Here, the units of influent concertation (C_o) are $ug \cdot L^{-1}$, $ng \cdot L^{-1}$, or $mg \cdot L^{-1}$, and the average target effluent concertation (C_1) are in $\mu g \cdot L^{-1}$, $ng \cdot L^{-1}$, or $mg \cdot L^{-1}$, as obtained from Equation 6.12. The equilibrium adsorption capacity (q_0) in $ng \cdot g^{-1}$ or $mg \cdot L^{-1}$are obtained from the model with the most appropriate fit utilizing a) an isotherm kinetic model or b) the dynamic model that best fits the experimental data. Hence, the volume of influent water (*V*) in L that can be treated by its corresponding mass of the media (*Mass*) is then determined following Equation 6.13 employing the *usage rate.* This process is repeated for a range of *Mass* to produce the removal efficiency curves.

$$\text{Usage Rate} = \frac{C_0 - C_1}{q_0} \quad \text{Eq. 6.11}$$

$$C_1 = C_0(1 - R) \quad \text{Eq. 6.12}$$

$$Mass = \text{V} * \text{Usage Rate} \quad \text{Eq. 6.13}$$

$$\text{Life Expectancy} = \text{V}\left(\frac{1}{\text{Q}}\right)(conversion\ factor) \quad \text{Eq. 6.14}$$

The life expectancy for target pollutant removal at a time in yr for the specific media inside the filter cell was projected following Equation 6.14. It is a function of the volume (V) of media, the volume of treated water, and the adsorption capacity from the mass of media.

C. Nutrient Loading Over Operational Period

The total quantity of nutrient/pollutant (L) fed to each reactor cell can be calculated based on the operation time ($time_{run}$) in hrs, the summation of the average concentration of feed ($C_{avg,f}$) in $mg \cdot L^{-1}$ throughout its operation time, and the flow rate (Q) (Eq. 6.15).

$$L = Q * time_{run} * \sum C_{avg,f} \quad \text{Eq. 6.15}$$

6.4.2 Results of Life Expectancy Estimation

According to our filter design in the field, the average discharge flow rate for the filtration cells at the drainage box was calculated as 4.08×10^3 $L \bullet hr^{-1}$ or 2.59×10^4 $gal \bullet d^{-1}$ using an orifice of diameter of 2.54 cm (1 in) with an adjustable overhead water.

For filtration applications such as sand filtration or other functional media filtration, the life expectancy of ZIPGEM and CPS designed for a downflow filter cell of 60.96 cm (2 ft) depth, 6.71 m (22 ft) width, and 13.26 m (43.5 ft) length was estimated for individual nutrients and contaminants considering physicochemical removal. Based on the reactor cell side slope ratio of 1:1 and height of media, the total volume of media was determined as 28.2 m^3 (994 ft^3), the mass of ZIPGEM occupying the cell was calculated as 7.83×10^4 kg, and the mass of CPS occupying the cell was calculated as 7.35×10^4 kg. A desired pollutant removal efficiency of 70% was utilized to evaluate the life expectancy for the filter cells. This removal efficiency was selected to be less than the observed highest average total phosphorus removal efficiency of 80%.

However, there are limitations to the estimation of life expectancy as only the removal of one pollutant in the water matrix at a time is considered. When simultaneous removal of multiple pollutants is considered, competitive effects among pollutants for the adsorption sites could reduce the estimated life expectancy herein. Additionally, the life expectancy for total nitrogen is assumed to be extended due to the presence of microbial ecology and its involvement in the natural nitrogen cycle.

A. Life Expectancy for PFAS Removal

The adsorption capacities of CPS and ZIPGEM derived from the PFAS isotherm study with the best fit to the experimental data were used for the calculations of life expectancy. The adsorption capacity of each media of 8.7×10^{-7} mg·g^{-1} (0.87 ng·g^{-1}) and 2.12×10^{-7} mg·g^{-1} (2.12 ng·g^{-1}) were selected for CPS and ZIPGEM, respectively based on the pseudo-first order adsorption model after the performance evaluation via a typical model selection procedure (Lagergren, 1898). The water quality parameters were selected for a filter cell that provides a desired PFOS removal efficiency of 70% of the polluted water based on influent concentration of 11.25 ng•L^{-1}. This value was adopted according to the average influent PFOS concentration obtained from the manual water samples collected from initial field events. The total volume of treated water ($V_{treated}$) over its operation period (life expectancy) was estimated as 2.11×10^{7} L for ZIPGEM cell and 8.12×10^{6} L for CPS cell based on the design pumping rate in the field. The volume of water treated ($V_{treated}$) over the service life of ZIPGEM, and CPS were obtained from the intercept of a graph of mass of filtration media versus volume of treated water for the given mass of ZIPGEM of 7.83×10^{4} kg and the mass of CPS of 7.35×10^{4} kg as shown by the red arrows in Figure 6-8. The life expectancy or service life for PFOS removal was then estimated as 0.56 yr (283.8 days) for ZIPGEM cell. The life expectancy or service life for PFOS removal was

estimated as 0.37 yr (133.5 days) for CPS cell. It should be noted that the average discharge rate determined in the field was 4.08×10^3 L•hr^{-1} or $2.59\text{x}10^4$ gal•d^{-1}, while the calculated design pumping flow rate (Q_{design}) of 4.31×10^3 L•hr^{-1} or 2.74×10^4 gal•d^{-1}was estimated as the design flow rate for ZIPGEM. The calculated pumping flow rate for CPS cell was 2.53×10^3 L•hr^{-1} or 1.61×10^4 gal•d^{-1}. Additionally, the HLR was estimated at 51.7 gal•day^{-1}•ft^{-2} for ZIPGEM and 32.4 gal•day^{-1}•ft^{-2} for CPS, respectively (Table 6-12).

Table 6-12: PFOS Life Expectancy Parameters and Results

Parameters	**CPS**	**ZIPGEM**
$Mass_{media\ in\ reactor}$ (kg)	7.35×10^4	7.83×10^4
Q_{design} (L•hr^{-1})	2.53×10^3 L•hr^{-1}	$4.31\text{x}10^3$ L•hr^{-1}
HLR (gal•day^{-1}•ft^{-2})	32.4	51.7
q_m (ng·g^{-1})	0.87	2.12
C_0 (ng•L^{-1})	11.25	11.25
C_1 (ng•L^{-1})	3.38	3.38
Usage rate (g•L^{-1})	9.05	3.71
$V_{treated}$ (L)	8.12×10^6	2.11×10^7
Life Expectancy (yr)	0.37	0.56

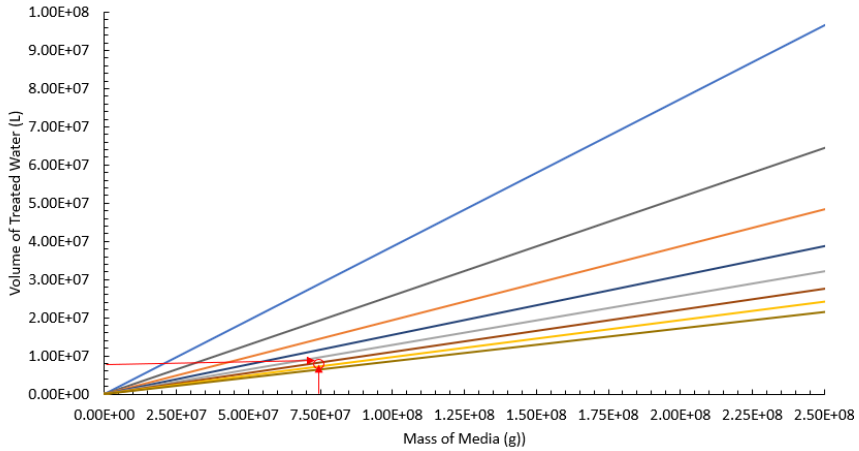

(a) CPS

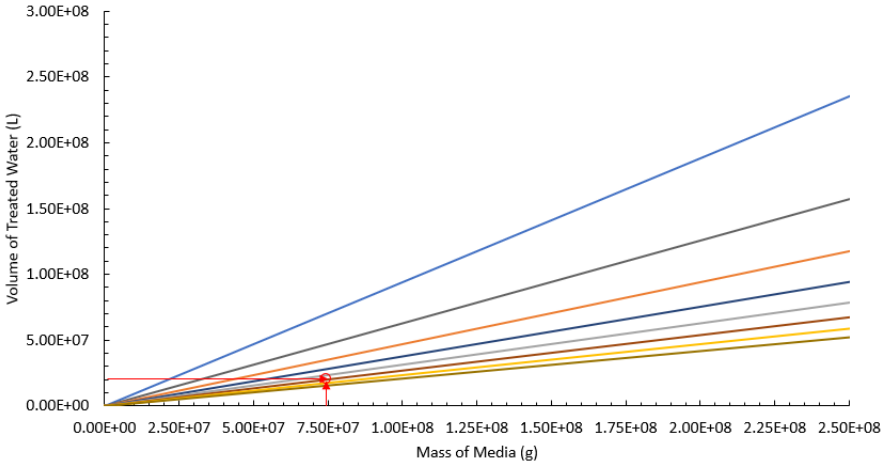

(b) ZIPGEM

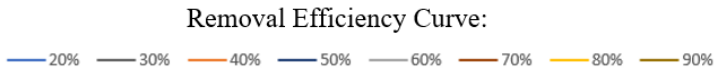

Figure 6-8: PFOS life expectancy graph demonstrating the relationship between mass of media versus volume of treated water for (a) CPS and (b) ZIPGEM.

B. Life Expectancy for Removing Phosphate

The life expectancy of ZIPGEM and CPS for phosphate removal was estimated by considering the same filter cell dimensions, volume of media in each cell, and media mass as discussed in Section 4.4.1. The Langmuir model (Langmuir, 1918) best fit the experimental isotherm results for CPS and ZIPGEM, and hence, the maximum adsorption capacity, q_m of 0.14 $mg \cdot g^{-1}$ and 1.80

$mg \cdot g^{-1}$ were selected for calculation of the media usage rate of CPS and ZIPGEM, respectively. This is based on the proposed filter cell design that provides a desired phosphate removal efficiency of 70% from the polluted canal water with field average phosphorus influent concentration of 0.06 $mg \bullet L^{-1}$. Conservatively, the media removal efficiency was selected to be less than the observed maximum removal from field Events 1-3 of 80% (i.e., samples collected in the rest of events have not yet been fully analyzed at this moment). $V_{treated}$ over the operational period (life expectancy) was estimated to be 3.35×10^9 L for ZIPGEM cell and 2.45×10^8 L for CPS cell. $V_{treated}$ over the service life of ZIPGEM, and CPS were obtained from the intercept of a graph of mass of filtration media versus volume of treated water for the given mass of ZIPGEM of 7.83×10^4 kg and the mass of CPS of 7.35×10^4 kg as shown by the red arrows in Figure 6-9. Utilizing the calculated Q_{design} of 4.31×10^3 $L \cdot hr^{-1}$ or 2.741×10^4 $gal \bullet d^{-1}$ for ZIPGEM and 2.53×10^3 $L \cdot hr^{-1}$ or 1.61×10^4 $gal \bullet d^{-1}$ for CPS, the life expectancy or service life for total phosphorus removal was estimated as 88.7 yr (32,375 days) for ZIPGEM cell and 11.0 yr (4,028 days) for CPS cell. Additionally, the HLR was estimated as 51.7 $gal \bullet day^{-1} \bullet ft^{-2}$ for ZIPGEM and 32.4 $gal \bullet day^{-1} \bullet ft^{-2}$ for CPS (Table 6-13).

Table 6-13: Phosphate Life Expectancy Parameters and Results

Parameters	**CPS**	**ZIPGEM**
q_m ($mg \cdot g^{-1}$)	0.14	1.80
C_0 ($mg \bullet L^{-1}$)	0.06	0.06
C_1 ($mg \bullet L^{-1}$)	0.018	0.018
Usage rate ($g \bullet L^{-1}$)	0.30	0.02
V_{trated} (L)	2.45×10^8	3.35×10^9
Life Expectancy (yr)	11.0	88.7

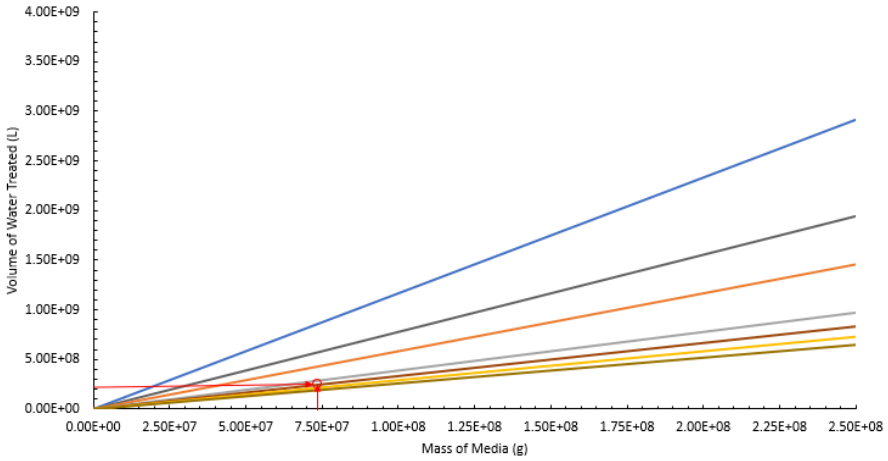

(a) CPS

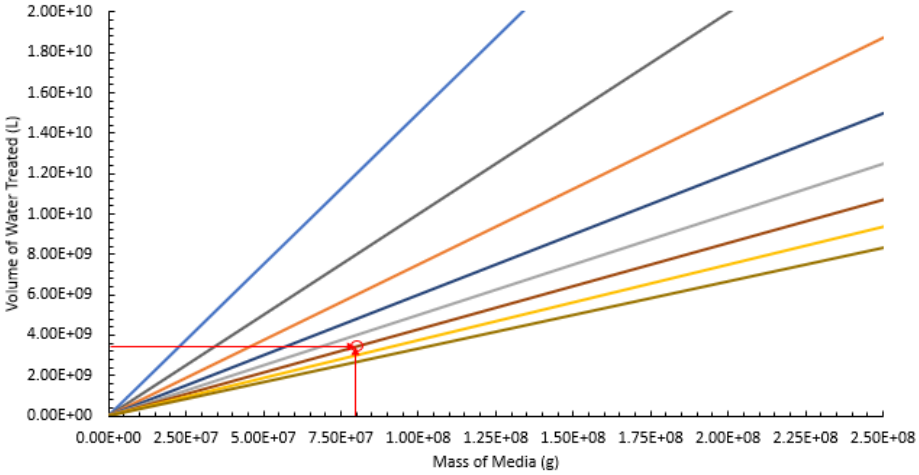

(b) ZIPGEM

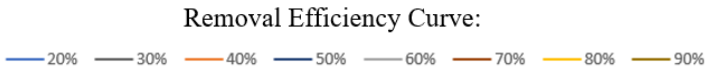

Figure 6-9: Phosphate life expectancy graph demonstrating the relationship between mass of media versus volume of treated water for (a) CPS and (b) ZIPGEM.

C. Life Expectancy for Removing MC-LR

Although microcystin was not found in the canal water, the life expectancy of ZIPGEM and CPS for microcystin removal was estimated following the previously discussed methodology to determine the pilot study service life in case microcystin concentrations increase in the C-23

canal water in the future. Employing the isotherm study experimental results, the Langmuir model (Langmuir, 1918) provided the best R^2 for CPS and ZIPGEM. The maximum adsorption capacity q_o selected for ZIPGEM and CPS where 0.001 mg·g^{-1} (1.0 μg·g^{-1}) and 0.00074 mg·g^{-1} (0.74 μg·g^{-1}), respectively. For the filter cell with 70% removal efficiency of microcystin based on theoretical influent concentration of 0.02 ng·L^{-1} (20 μg·L^{-1}), the total volume of treated water ($V_{treated}$) was estimated as 5.59×10^6 L for ZIPGEM cell and 3.88×10^6 L of CPS cell. $V_{treated}$ over its service life of ZIPGEM and CPS were obtained from the graph of the mass of filtration media versus volume of treated water as shown in Figure 6-10. The calculated Q_{design} of 4.31×10^3 L•hr^{-1} or 2.741×10^4 gal•d^{-1} for ZIPGEM and 2.53×10^3 L•hr^{-1} or 1.61×10^4 gal•d^{-1} for CPS were used, and the life expectancy or service life for microcystin removal was estimated as 54.1 days (0.15 y) for ZIPGEM cell and as 63.9 days (0.18 y) for CPS cell. Additionally, the HLR was estimated as 51.7 gal•day^{-1}•ft^{-2} for ZIPGEM and 32.4 gal•day^{-1}•ft^{-2} CPS (Table 6-14). Table 6-15 depicts the life expectancy estimated for PFOS, total nitrogen, total phosphorus and microcystin removal for the filter at the field site. The life expectancy CPS and ZIPGEM was estimated to be the highest when removing TP, followed by PFOS.

Table 6-14: Life Expectancy Parameters and Results

Parameters	**CPS**	**ZIPGEM**
q_m (mg·g^{-1})	0.00074	0.001
C_0 (mg•L^{-1})	0.02	0.02
C_1 (mg•L^{-1})	0.008	0.008
Usage rate (g•L^{-1})	0.016	0.014
$V_{treated}$ (L)	3.88x10^6	5.59x10^6
Life Expectancy (yr)	0.18	0.15

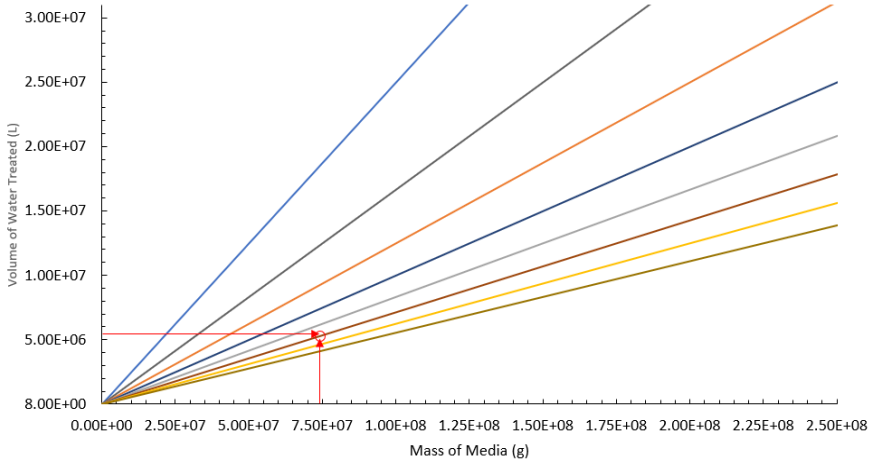

(a) CPS

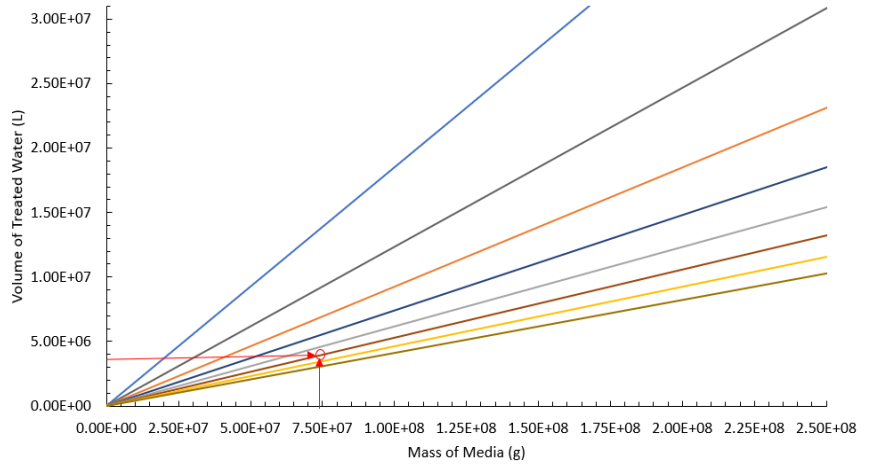

(b) ZIPGEM

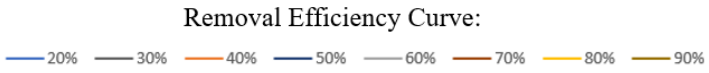

Figure 6-10: Microcystin (MC-LR) Life expectancy graph demonstrating the relationship between mass of media versus volume of treated water for (a) CPS and (b) ZIPGEM.

Table 6-15: Summary of life expectancy (years) for treating PFAS, Nitrate, Phosphate and MC-LR via CPS and ZIPGEM at 70% removal rate

Life Expectancy (yr)	PFOS	Total Nitrogen [b]	Total Phosphorus [c]	Microcystin [d]
CPS	0.37	0.001	11.0	0.18
ZIPGEM	0.56	0.014	88.7	0.15

[a] Influent concentration of 14 ng•L^{-1} PFOS [b] Influent concentration of 2.00 mg•L^{-1} Total Nitrogen with physicochemical adsorption capacity only. The media should have unlimited life expectancy if microbial species in the nitrogen cycle can be taken into account [c] Influent concentration of 0.06 mg•L^{-1} Total Phosphorus [D] Influent concentration of 20.0 ug•L^{-1} Microcystin

Chapter 7 Cost-benefit Analysis and TMDL Implications

7.1 Cost-benefit Analysis

A cost-benefit analysis was conducted based on the comparison of construction and maintenance costs of the filters relative to the benefits associated with nutrient removal throughout their anticipated service life. Table 21 provides a summary of the construction and operation costs incurred during the pilot study for CPS and ZIPGEM filter cells. Notably, as the two media cells shared common infrastructure elements such as pumping, piping, control, and other facilities, it is assumed that the construction and operation costs are equal for all cells. An interest rate of 5% was employed for the cost analysis. The cost-benefit analysis was performed over an *n* time interval of 11 years, representing as a conservative estimate for the service life of the reactors. This choice aligns with the determined life expectancy for total phosphorus (TP), which was estimated as 11.0 years for CPS. Concurrently, for ZIPGEM, the cost-benefit analysis spanned an *n* time interval of 84 years, reflecting a conservative estimate for the service life of the reactors. This duration corresponds to the TP life expectancy for ZIPGEM, estimated at 88.7 yrs.

Table 9: Construction and operating costs for CPS and ZIPGEM filter cells

Cell	Reactor Cell Area (SF)	Construction Cost per Cell ($/SF)[a]	Operating Cost/yr ($)[b]
CPS	529	212	12,500
ZIPGEM	529	232	12,500

[a] Includes media cost [b] Includes electricity cost

Conducting an individual cost-benefit analysis over the time interval aligned with the estimated life expectancy for CPS and ZIPGEM facilitates a more robust comparison of the annual cost of pollutant removal per unit mass of filtration media used (expressed as $ per lb). In this cost and benefit analysis, the influent water characteristics from events 1-3 (occurring during the dry season) were utilized to estimate the average pollutant load to the filtration cells over

their service life. Pollutant load means the amount of a particular pollutant delivered to a waterbody measured in units of mass per unit time (e.g., pounds per year). As anticipated, the annual cost per pound of nutrient removed is lower for ZIPGEM compared to CPS, attributable to its extended service life (84 years vs. 11 years), as detailed in Table 7-2. A higher cost is observed for total phosphorus removal, given the relatively small influent concentration introduced to the filtration system in comparison to total nitrogen. However, the cost-benefit analysis was not extended to PFOS, as the loading of PFOS to the filter cells was minimal.

Table 10: Annual loading and cost per pound of each pollutant removed by CPS or ZIPGEM over the medium's life expectancy

		PFOS[b]	**Total Nitrogen***	**Total Phosphorus***
CPS	**Loading (lb)[a]**	1.01×10^{-2}	2.46×10^{5}	1.63×10^{2}
	Cost per mass of pollutant removed for all media used ($/lb)	--	0.17	251.00
	Cost per mass of pollutant removed for each cell ($/lb)	--	0.08	125.50
ZIPGEM	**Loading (lb)**	$8.04\times x10^{-2}$	2.54×10^{4}	1.55×10^{3}
	Cost per mass of pollutant removed for all media used ($/lb)	--	0.96	15.82
	Cost per mass of pollutant removed for each cell ($/lb)	--	0.48	7.91

* Using loading from Event 1, Event 2 and Event 3 [a] Utilizing calculated Q_{design} of $4.31x10^{3}$ L•hr^{-1}

In Table 7-2, a comprehensive cost-benefit analysis was performed for CPS and ZIPGEM to aid in decision-making and evaluate the reactor cells' overall removal efficiency. The total removal of phosphate and nitrate were estimated over the anticipated operation period (e.g., life expectancy). The annual cost per unit of total nutrient removed ($ per lb) by the media during the pilot study's treatment phase was calculated (denoted as E). The cost for production includes the cost of the system construction as well as the production of the media, accounting for raw material acquisition (i.e., sand, clay, perlite,

ZVI). The annual operation and maintenance expenses for the downflow reactor cells include the electricity costs for pump operation. Assuming a 5% compound interest (i = 5%), the construction cost can be expressed as equivalent annual cashflow (AW) considering the operational life according to the life expectancy results (Eqs 7.1 and 7.2). n is the media service life (in years) for phosphate removal. Thus, the annual cost per unit nutrient loading ($ per lb) is estimated using the total quantity of nutrient/pollutant (L) removed in the reactor cells, based on the field campaign results and the AW value (Eq. 7-3).

$$\frac{A}{P} = P\left(\frac{(i(1+i)^n)}{(1+i)^n-1}\right) \quad \text{Eq. 7.1}$$

$$AW = A_{construction} + A_{O\&M} \quad \text{Eq. 7.2}$$

$$Cost\ per\ nutrientloading = \frac{AW}{L} \quad \text{Eq. 7.3}$$

7.2 Summary of the TMDL Implications in This Pilot Study

It is expected that the filtration cells will improve the quality of water entering the St. Lucie River and Estuary region by lowering the concentrations to or below the Total Maximum Daily Load (TMDL) for the St. Lucie River Basin established for TN, TP, and BOD (i.e., 0.72 mg•L^{-1} for TN, 0.081 mg•L^{-1} for TP, and 2.0 mg•L^{-1} for BOD). The average removal percentage and daily removal (in grams) for each of the three pollutants were estimated (Table 7-3). Most records meet the TMDL standards for effluent concentrations. The values reported in the table were calculated based on the average removal rates of ZIPGEM and CPS cells. Tables 7-4 – 7-6 further list the pollutant removal percentages for all events based on either concentration or mass. This is the first pilot study at the field scale that demonstrates the effectiveness of simultaneous removal of multiple regulated contaminants and emerging contaminants of concern from surface water.

It is notable that this is the first pilot study at field-scale that proves the effectiveness of simultaneous removal of multiple regulated contaminants and emerging contaminants of concern in environmental engineering. These two new specialty adsorbents with chemical, molecular, and even microbial insights trigger a new scientific initiative for developing a plethora of integrated sustainable technologies tailored for different field applications for watershed restoration across any landscape in the future.

Table 7-3: Average removal efficiencies (%) of TN, TP, and BOD in ZIPGEM and CPS cells

	TN				TP				BOD			
Event	Influent ($mg \cdot L^{-1}$)	Effluent ($mg \cdot L^{-1}$)	removal rate (%)	Daily Removal (g)	Influent ($mg \cdot L^{-1}$)	Effluent ($mg \cdot L^{-1}$)	Removal Rate (%)	Daily Removal (g)	Influent ($mg \cdot L^{-1}$)	Effluent ($mg \cdot L^{-1}$)	removal rate (%)	Daily Removal (g)
1	1.63	0.77	52.86	56.48	0.05	0.04	26.09	0.84	1.00	1.00	0.00	0.00
2	133.64	0.70	99.48	43.22	0.07	0.06	17.61	0.86	1.58	1.00	36.51	37.61
3	0.69	0.32	53.50	20.12	0.08	0.03	62.78	2.57	2.85	1.08	61.99	96.30
4	1.54	0.66	56.98	47.83	0.06	0.03	40.37	1.28	2.25	1.00	55.56	68.14
5	1.03	0.65	36.50	16.35	0.05	0.04	30.83	0.69	2.05	1.00	51.22	45.79
6	1.20	0.87	27.43	14.35	0.05	0.04	17.72	0.37	2.28	2.00	12.09	11.99
7	1.47	0.98	33.05	18.47	0.09	0.04	53.71	1.77	2.00	2.00	0.00	0.00
8	1.99	0.96	51.76	39.21	0.07	0.04	47.26	1.32	5.73	2.36	58.8	128.46
9	0.62	0.56	9.54	1.94	0.15	0.04	71.48	3.56	2.00	2.01	-0.42%	-0.27
10	1.66	1.23	25.80	14.01	0.21	0.04	78.63	5.34	2.00	3.48	-73.75	-48.24

Table 7-4: Average removal efficiencies (%) of nutrients and biological pollutants in ZIPGEM and CPS cells

	TN		TKN		ammonia		DON		TP	
	ZIPGEM	CPS	ZIPGEM	CPS	ZIPGEM	CPS	ZIPGEM	CPS	ZIPGEM	CPS
Event1	64.09%	41.64%	72.22%	55.63%	33.33%	50.33%	74.17%	55.90%	46.80%	5.39%
Event2	53.74%	43.55%	73.12%	67.77%	47.67%	53.83%	74.26%	68.39%	79.93%	-44.70%
Event3	57.49%	49.52%	86.51%	84.14%	31.92%	56.67%	89.98%	85.88%	94.67%	30.89%
Event4	61.58%	52.38%	61.48%	62.58%	13.43%	16.79%	63.77%	64.76%	74.71%	6.03%
Event5	30.74%	42.25%	30.74%	42.25%	-231.81%	-368.19%	39.38%	55.77%	71.04%	-9.39%
Event6	39.72%	15.14%	63.83%	51.25%	-200.58%	-501.16%	69.68%	63.46%	71.93%	-36.49%
Event7	50.28%	15.81%	75.31%	58.19%	-61.55%	-482.82%	79.20%	73.56%	85.68%	21.74%
Event8	58.77%	44.75%	72.49%	63.87%	-178.24%	-498.80%	76.06%	71.87%	81.66%	12.86%
Event9	15.59%	3.49%	73.83%	70.08%	-410.20%	-583.67%	85.99%	86.50%	93.11%	49.84%
Event10	38.96%	12.65%	61.76%	45.28%	-202.38%	-311.19%	76.49%	65.17%	96.22%	61.04%
	OP		BOD		Chlorophyll a		E. coli		Algal mass	
	ZIPGEM	CPS	ZIPGEM	CPS	ZIPGEM	CPS	ZIPGEM	CPS	ZIPGEM	CPS
Event1	90.43%	-36.42%	0.00%	0.00%	98.79%	46.41%	99.70%	97.71%	99.01%	55.87%
Event2	66.20%	-179.17%	36.51%	36.51%	87.60%	95.15%	84.85%	84.85%	89.79%	96.00%
Event3	95.88%	-13.84%	59.06%	64.91%	94.17%	96.75%	91.11%	91.11%	95.20%	97.33%
Event4	63.96%	-629.73%	55.56%	55.56%	97.04%	98.69%	88.80%	88.80%	97.56%	98.92%
Event5	55.61%	-241.84%	51.22%	51.22%	97.66%	98.38%	71.54%	94.83%	95.91%	97.17%
Event6	40.45%	-247.22%	12.09%	12.09%	98.73%	99.37%	90.34%	80.19%	98.73%	99.37%
Event7	84.36%	11.72%	0.00%	0.00%	98.67%	99.55%	78.53%	51.17%	98.67%	99.55%
Event8	45.72%	-64.66%	59.53%	58.08%	99.11%	99.48%	86.10%	93.16%	99.10%	99.47%
Event9	95.04%	15.29%	-0.83%	0.00%	99.15%	99.76%	92.50%	89.87%	99.16%	99.76%
Event10	93.90%	36.19%	-44.17%	-103.33%	98.25%	99.21%	92.86%	92.86%	98.18%	99.18%

Table 7-5: Average mass removal (mg/kg/day) of nutrients and biological pollutants in ZIPGEM and CPS cells

	TN		TKN		Ammonia		DON		TP	
	ZIPGEM	CPS	ZIPGEM	CPS	ZIPGEM	CPS	ZIPGEM	CPS	ZIPGEM	CPS
Event1	0.64	0.45	0.93	0.77	0.02	0.03	0.91	0.73	0.01	0.00
Event2	0.45	0.39	1.04	1.04	0.03	0.04	1.02	1.00	0.04	-0.02
Event3	0.20	0.19	0.96	1.00	0.02	0.04	0.94	0.96	0.04	0.01
Event4	0.48	0.44	0.48	0.52	0.00	0.01	0.47	0.52	0.02	0.00
Event5	0.13	0.19	0.13	0.19	-0.03	-0.05	0.16	0.24	0.01	0.00
Event6	0.19	0.08	0.52	0.45	-0.04	-0.09	0.56	0.54	0.01	-0.01
Event7	0.26	0.09	0.79	0.66	-0.02	-0.15	0.81	0.81	0.03	0.01
Event8	0.42	0.34	0.77	0.73	-0.03	-0.08	0.80	0.81	0.02	0.00
Event9	0.03	0.01	0.45	0.46	-0.06	-0.09	0.51	0.55	0.04	0.02
Event10	0.20	0.07	0.50	0.39	-0.09	-0.14	0.59	0.54	0.06	0.04
	BOD		Chlorophyll a		E. coli (MPN/kg/day)		OP		Algal mass	
	ZIPGEM	CPS	ZIPGEM	CPS	ZIPGEM	CPS	ZIPGEM	CPS	ZIPGEM	CPS
Event1	0.00	0.00	0.00	0.00	13861.87	14574.25	0.014922	-0.00645	0.06	0.03
Event2	0.35	0.00	0.01	0.01	34224.72	36716.18	0.014566	-0.04229	0.09	0.11
Event3	0.86	0.01	0.01	0.01	52202.89	56003.10	0.025881	-0.00401	0.05	0.06
Event4	0.64	0.01	0.02	0.02	40361.74	43299.96	0.001808	-0.0191	0.21	0.23
Event5	0.43	0.00	0.02	0.02	56328.19	80098.09	0.002441	-0.01139	0.15	0.17
Event6	0.11	0.00	0.02	0.02	38095.38	36279.08	0.001582	-0.01037	0.13	0.14
Event7	0.00	0.00	0.01	0.01	30867.61	21577.13	0.013684	0.00204	0.07	0.07
Event8	1.22	0.01	0.01	0.01	44890.24	52110.20	0.007457	-0.01131	0.08	0.09
Event9	-0.01	0.00	0.01	0.01	37662.47	39256.81	0.019313	0.003333	0.04	0.05
Event10	-0.27	0.00	0.00	0.00	39725.12	42616.99	0.018437	0.007622	0.02	0.02

Table 7-6: Average influent and effluent concentration ($mg \cdot L^{-1}$) of nutrients and biological pollutants in ZIPGEM and CPS cells

	TN			TKN			ammonia			DON			TP		
	Influent	Effluent		Influent	Effluent		Influent	Effluent		Influent	Effluent		Influent	Effluent	
		ZIPGEM	CPS		ZIPGEM	CPS		ZIPGEM	CPS		ZIPGEM	CPS		ZIPGEM	CPS
Event1	1.63	0.59	0.95	2.10	0.58	0.93	0.10	0.07	0.05	2.00	0.52	0.88	0.05	0.03	0.05
Event2	1.36	0.63	0.77	2.34	0.63	0.75	0.10	0.05	0.05	2.24	0.58	0.71	0.07	0.02	0.11
Event3	0.69	0.29	0.35	2.18	0.29	0.35	0.13	0.09	0.06	2.05	0.20	0.29	0.08	0.00	0.05
Event4	1.54	0.59	0.73	1.53	0.59	0.57	0.07	0.06	0.06	1.46	0.53	0.51	0.06	0.01	0.05
Event5	1.03	0.71	0.59	1.03	0.71	0.59	0.03	0.11	0.15	0.99	0.60	0.44	0.05	0.01	0.06
Event6	1.20	0.72	1.02	2.00	0.72	0.98	0.04	0.13	0.26	1.96	0.59	0.72	0.05	0.01	0.06
Event7	1.47	0.73	1.23	2.95	0.73	1.23	0.08	0.13	0.48	2.87	0.60	0.76	0.09	0.01	0.07
Event8	1.99	0.82	1.10	2.98	0.82	1.08	0.04	0.12	0.25	2.93	0.70	0.83	0.07	0.01	0.06
Event9	0.62	0.52	0.60	2.00	0.52	0.60	0.05	0.25	0.34	1.95	0.27	0.26	0.15	0.01	0.08
Event10	1.66	1.01	1.45	2.65	1.01	1.45	0.14	0.42	0.58	2.51	0.59	0.87	0.21	0.01	0.08
	OP			BOD			Chlorophyll a (μg/L)			E. coli (MPN/100mL)					
	Influent	Effluent		Influent	Effluent		Influent	Effluent		Influent	Effluent				
		ZIPGEM	CPS		ZIPGEM	CPS		ZIPGEM	CPS		ZIPGEM	CPS			
Event1	0.03	0.00	0.04	1.00	1.00	1.00	7.78	0.09	4.17	2.28	0.01	0.05			
Event2	0.04	0.01	0.10	1.58	1.00	1.00	14.43	1.79	0.70	6.60	1.00	1.00			
Event3	0.05	0.00	0.06	2.85	1.17	1.00	11.40	0.67	0.37	11.25	1.00	1.00			
Event4	0.01	0.00	0.04	2.25	1.00	1.00	42.00	1.25	0.55	8.93	1.00	1.00			
Event5	0.01	0.00	0.04	2.05	1.00	1.00	48.25	1.13	0.78	19.33	5.50	1.00			
Event6	0.01	0.01	0.03	2.28	2.00	2.00	39.25	0.50	0.25	10.35	1.00	2.05			
Event7	0.05	0.01	0.04	2.00	2.00	2.00	27.00	0.36	0.12	11.03	2.37	5.38			
Event8	0.05	0.02	0.08	5.73	2.32	2.40	34.25	0.30	0.18	14.63	2.03	1.00			
Event9	0.07	0.00	0.06	2.00	2.02	2.00	23.75	0.20	0.06	13.33	1.00	1.35			
Event10	0.06	0.00	0.04	2.00	2.88	4.07	9.80	0.17	0.08	14.00	1.00	1.00			

This page intentionally left blank.

Chapter 8 Conclusion

This study evaluated a field-scale filtration system capable of removing nutrients and biological pollutants from surface water in South Florida using two specialty absorbents, CPS and ZIPGEM. Based on ten sampling events (from March 1 to July 3, 2023), the average removal rate of TN, TKN, DON, TP, and OP by ZIPGEM was 49.3%, 67.1%, 72.9%, 79.6%, and 73.2%, respectively, which were significantly higher than the removal rate for CPS. More details can be seen in the supplementary file. Besides, all the influent and effluent samples contained low concentrations of aluminum (only 10% of the MCL for aluminum) supporting a lack of leaching from the media. Ammonification is the key process for removing nutrient-related pollutants in the nitrogen cycle.

ZIPGEM and CPS achieved similar removal efficiencies for biological pollutants, which were confirmed via statistical analysis. ZIPGEM and CPS showed positive removal rates during the initial four sampling events. It was indicative that the removal rates vary significantly during the dry and wet season. In terms of ammonia removal, both ZIPGEM and CPS exhibited negative efficiencies since the fifth sampling event. The negative values are attributed to strong photoammonification in the wet season resulting in higher ammonia nitrogen released from the media and treated water. In fact, even without photoammonification, ammonia is continuously released during organic nitrogen mineralization. In comparison, ZIPGEM and CPS demonstrated an excellent removal rate for biological pollutants such as *E. coli*.

Subsequent to the life expectancy estimation, a cost-benefit analysis was conducted for CPS and ZIPGEM, aiding in determining the cost associated with removing one pound of pollutant, thereby facilitating informed decision-making for CPS and ZIPGEM applications. The report concludes with a discussion on the long-term operation of ZIPGEM as a BMP for multi-pollutant removal, affirming its potential contribution to enhancing the water quality entering the St. Lucie River via C-23. These observations imply that the two engineered media have great application potential in the field depending on the target pollutants.

Overall, the introduction of two novel specialty adsorbents, encompassing chemical, molecular, and microbial insights, initiates a new scientific endeavor aimed at developing a diverse array of integrated sustainable technologies customized for various field applications, facilitating different types of watershed restoration across any landscape in the future. The calculation of the anticipated total amount of pollutants that can be removed during the life cycle of the filter helps understand the ultimate contribution of this filtration technology. A summary of the TMDL implications in this pilot study supports future applications. Finally, it is notable that this study is a synthesis of engineering practices, where a design–build–test–learn cycle is conducted through enhanced sustainable engineering to iteratively improve the performance of specialty absorbents for watershed remediation. Future work may be directed toward enhancing the understanding of the stability of a filed-scale filtration system adaptable to the variability of water quality conditions.

References

Apel, K. and Hirt, H. (2004). Reactive oxygen species: metabolism, oxidative stress, and signal transduction. Annu. *Rev. Plant Biol.*, 55, 373-399.

Ateia, M., Maroli, A., Tharayil, N., and Karanfil, T. (2019) The overlooked short-and ultrashort-chain poly-and perfluorinated substances: A review. *Chemosphere*, 220, 866-882.

Ansa, E. D. O., Lubberding, H. J., Ampofo, J. A., and Gijzen, H. J. (2011). The role of algae in the removal of Escherichia coli in a tropical eutrophic lake. *Ecological Engineering*, 37(2), 317-324.

Arredondo, M. R., Kuntke, P., Jeremiasse, A. W., Sleutels, T. H. J. A., Buisman, C. J. N., and Ter Heijne, A. (2015). Bioelectrochemical systems for nitrogen removal and recovery from wastewater. *Environmental Science: Water Research & Technology*, 1(1), 22-33.

Azziz, G., Monza, J., Etchebehere, C., and Irisarri, P. (2017) nirS-and nirK-type denitrifier communities are differentially affected by soil type, rice cultivar and water management. *European Journal of Soil Biology,* 78, 20-28.

Baei, M. S., Esfandian, H., and Nesheli, A. A. (2016). Removal of nitrate from aqueous solutions in batch systems using activated perlite: an application of response surface methodology. *Asia-Pacific Journal of Chemical Engineering*, 11(3), 437-447.

Chang, N. B., Wanielista, M., Xuan, Z., and Daranpob, A. (2010). Using a Subsurface Upflow Wetland for Nutrient and Pathogen Removal in an On-Site Sewage Treatment and Disposal System. In World Environmental and Water Resources Congress 2010: Challenges of Change (pp. 983-993).

Chang, N. B., Wanielista, M. P., and Henderson, D. (2011). Temperature effects on functionalized filter media for nutrient removal in stormwater treatment. *Environmental Progress & Sustainable Energy*, 30(3), 309-317.

Chang, N. B., Lin, K. S., Wanielista, M. P., Crawford, A. J., Hartshorn, N., and Clouet, B. (2016). An innovative solar energy-powered floating media bed reactor for nutrient removal (I): reactor design. *Journal of Cleaner Production*, 133, 495-503.

Chang, N. B., Wen, D., McKenna, A. M., and Wanielista, M. P. (2018a) The impact of carbon source as electron donor on composition and concentration of dissolved organic nitrogen

in biosorption-activated media for stormwater and groundwater co-treatment. *Environmental Science & Technology* 52(16), 9380-9390.

Chang, N. B., Wanielista, M., Singh, A., Duranceau, S. J., and Wang, D. (2018b). Bio-sorption Activated Media for Nitrogen Removal in a report of Rapid Infiltration Basin–Monitoring Project. Florida Department of Environmental Protection (FDEP).

Chang, N. B., Wen, D., Colona, W., and Wanielista, M. P. (2019). Comparison of biological nutrient removal via two biosorption-activated media between laboratory-scale and field-scale linear ditch for stormwater and groundwater co-treatment. *Water, Air, & Soil Pollution*, 230, 1-19.

Chen, Y., Chen, R., Liu, Z., Ren, B., Wu, Q., Zhang, J., ... and Wu, Q. (2022). Bioretention system mediated by different dry–wet alterations on nitrogen removal: Performance, fate, and microbial community. *Science of The Total Environment*, 827, 154295.

Chen, Z., et al. (2020). Efficient reductive destruction of perfluoroalkyl substances under self-assembled micelle confinement. *Environmental Science & Technology*, 54(8), 5178-5185.

Cheung-Wong, R. W., Kotta, J., Hemraj, D. A., and Russell, B. D. (2022). Persistence in a tropical transition zone? Sargassum forests alternate seasonal growth forms to maintain productivity in warming waters at the expense of annual biomass production. *Science of The Total Environment*, 851, 158154.

Davis, A. P., Shokouhian, M., Sharma, H., and Minami, C. (2006). Water quality improvement through bioretention media: Nitrogen and phosphorus removal. Water Environment Research, 78(3), 284-293.

de Barros, I. R., Benincá, C., and Zanoelo, E. F. (2023). Kinetics of the precipitation reaction between aluminium and contaminant orthophosphate ions. *Environmental Technology*, 16:1-18.

Deng, Y., Li, Y., Li, X., Sun, Y., Ma, J., Lei, M., and Weng, L. (2018). Influence of calcium and phosphate on pH dependency of arsenite and arsenate adsorption to goethite. *Chemosphere* 199, 617-624.

Dionisi, H. M., Layton, A. C., Harms, G., Gregory, I. R., Robinson, K. G., and Sayler, G. S. (2002) Quantification of Nitrosomonas oligotropha-like ammonia-oxidizing bacteria and Nitrospira spp. from full-scale wastewater treatment plants by competitive PCR. *Applied and Environmental Microbiology,* 68(1), 245-253.

Du, X., Wang, Y., Su, X., and Li, J. (2009). Influences of pH value on the microstructure and phase transformation of aluminum hydroxide. *Powder Technology*, *192*(1), 40-46.

Duan, S., Banger, K., and Toor, G. S. (2021). Evidence of phosphate mining and Agriculture influence on Concentrations, forms, and ratios of nitrogen and phosphorus in a Florida River. *Water*, 13(8), 1064.

Elhakiem, H. (2019). Adsorption Capacity Assessment of Advance Green Environmental Media to Remove Nutrients from Stormwater-Runoff. Master thesis, University of Central Florida.

Eschauzier, C., Beerendonk, E., Scholte-Veenendaal, P., and De Voogt, P. (2012). Impact of treatment processes on the removal of perfluoroalkyl acids from the drinking water production chain. *Environmental Science & Technology*, 46(3), 1708-1715.

EPA (2022) Drinking Water Health Adivisiories for PFAS Fact Sheet for Communities. Agency, U.E.P. (ed).

EPA (2023) PFAS National Primary Drinking Water Regulation Relemaking, EPA.

EPA (2015) Drinking Water Health Advisory for the Cyanobacterial Microcystin Toxins Agency. EPA (ed).

Fill, J. M., Davis, C. N., and Crandall, R. M. (2019). Climate change lengthens southeastern USA lightning-ignited fire seasons. *Global Change Biology*, 25(10), 3562-3569

Fredrickson, J. K., Zachara, J. M., Kennedy, D. W., Dong, H., Onstott, T. C., Hinman, N. W., and Li, S. M. (1998). Biogenic iron mineralization accompanying the dissimilatory reduction of hydrous ferric oxide by a groundwater bacterium. *Geochimica et Cosmochimica Acta*, 62(19-20), 3239-3257.

Freundlich, H. (1907). Über die adsorption in lösungen. Zeitschrift für physikalische *Chemie,* 57(1), 385-470.

Funkey, C. P., Latour, R. J., & Bronk, D. A. (2015). Abiotic effects on effluent dissolved organic nitrogen along an estuarine transect. *Water Environment Research*, 87(3), 258-265.

Ghasemi, E. and Sillanpää, M. (2015). Magnetic hydroxyapatite nanoparticles: an efficient adsorbent for the separation and removal of nitrate and nitrite ions from environmental samples. *Journal of Separation Science*, 38(1), 164-169.

Giri, S. (2021). Water quality prospective in Twenty First Century: Status of water quality in major river basins, contemporary strategies and impediments: A review. *Environmental Pollution*, 271, 116332.

Haig, S. J., Schirmer, M., D'amore, R., Gibbs, J., Davies, R. L., Collins, G., and Quince, C. (2015). Stable-isotope probing and metagenomics reveal predation by protozoa drives E. coli removal in slow sand filters. *The ISME journal*, 9(4), 797-808.

Hale, S. E., Arp, H. P. H., Slinde, G. A., Wade, E. J., Bjørseth, K., Breedveld, G. D., ... and Høisæter, Å. (2017). Sorbent amendment as a remediation strategy to reduce PFAS mobility and leaching in a contaminated sandy soil from a Norwegian firefighting training facility. *Chemosphere*, 171, 9-18.

Haynes, W. M. (Ed.). (2014). CRC handbook of chemistry and physics. CRC Press, Boca Raton, FL, USA.

Hijnen, W. A., Dullemont, Y. J., Schijven, J. F., Hanzens-Brouwer, A. J., Rosielle, M., and Medema, G. (2007). Removal and fate of Cryptosporidium parvum, Clostridium perfringens and small-sized centric diatoms (Stephanodiscus hantzschii) in slow sand filters. *Water Research*, 41(10), 2151-2162.

Ho, Y. S., Wase, D. A. J., and Forster, C. F. (1996) Removal of lead ions from aqueous solution using sphagnum moss peat as adsorbent. *Journal of Water Supply Association* 22(3), 219-224.

Hossain, F., Chang, N. B., and Wanielista, M. (2009). Modeling kinetics and isotherms of functionalized filter media for nutrient removal from stormwater dry ponds. *Environmental Progress & Sustainable Energy*, 29(3), 319-333.

Islam, M. T., Valencia, A., Ordonez, D., Sadmani, A. H. M. A., and Chang, N. B. (2023). The effect of green sorption media pretreatment on nanofiltration during water treatment for long- and short-chain per- and polyfluoroalkyl substances (PFAS) removal," *Sep. Purif. Technol.*, 324, p. 124548.

Jasinski, S. M. (2013). Mineral resource of the month: Phosphate rock. *Earth*.

Jeon, J., Kannan, K., Lim, B. J., An, K. G., and Kim, S. D. (2011). Effects of salinity and organic matter on the partitioning of perfluoroalkyl acid (PFAs) to clay particles. *Journal of Environmental Monitoring*, 13(6), 1803-1810.

Jeon, Y., Li, L., Calvillo, J., Ryu, H., Santo Domingo, J. W., Choi, O., ... and Seo, Y. (2020). Impact of algal organic matter on the performance, cyanotoxin removal, and biofilms of biologically-active filtration systems. *Water Research*, 184, 116120.

Ji, B., & Zhao, Y. (2023). Interactions between biofilms and PFASs in aquatic ecosystems: Literature exploration. *Science of The Total Environment*, 167469.

Jiao, W., Chen, W., Chang, A. C., and Page, A. L. (2012). Environmental risks of trace elements associated with long-term phosphate fertilizers applications: a review. *Environmental Pollution*, 168, 44-53.

Ji, J., Peng, L., Redina, M. M., Gao, T., Khan, A., Liu, P., and Li, X. (2021). Perfluorooctane sulfonate decreases the performance of a sequencing batch reactor system and changes the sludge microbial community. *Chemosphere*, *279*, 130596.

Kah, M., Oliver, D., and Kookana, R. (2021). Sequestration and potential release of PFAS from spent engineered sorbents. *Science of the Total Environment*, 765, 142770.

Kilgus-Vesely, S. (2023). Comparing Phosphorus Removal Efficiencies and Mechanisms via Two Cost-Effective Specialty Adsorbents in a Cascade Upflow Filtration System. Master Thesis, University of Central Florida.

Kim, H., Bae, H. S., Reddy, K. R., and Ogram, A. (2016). Distributions, abundances and activities of microbes associated with the nitrogen cycle in riparian and stream sediments of a river tributary. *Water Research*, 106, 51-61.

Kitidis, V., Uher, G., Woodward, E. M. S., Owens, N. J. P., and Upstill-Goddard, R. C. (2008). Photochemical production and consumption of ammonium in a temperate river–sea system. *Marine Chemistry*, 112(1-2), 118-127.

Lapointe, B. E., Herren, L. W., and Paule, A. L. (2017). Septic systems contribute to nutrient pollution and harmful algal blooms in the St. Lucie Estuary, Southeast Florida, USA. *Harmful Algae*, 70, 1-22.

Langmuir, I. (1918). The adsorption of gases on plane surfaces of glass, mica and platinum. *Journal of the American Chemical Society,* 40(9), 1361-1403.

Lagergren, S. K. (1898). About the theory of so-called adsorption of soluble substances. Sven. Vetenskapsakad. *Handingarl,* 24, 1-39.

Lee, C. G., Fletcher, T. D., and Sun, G. (2009). Nitrogen removal in constructed wetland systems. *Engineering in Life Sciences*, 9(1), 11-22.

Lei, Y., Song, B., Saakes, M., van der Weijden, R. D., and Buisman, C. J. (2018). Interaction of calcium, phosphorus and natural organic matter in electrochemical recovery of phosphate. *Water Research*, 142, 10-17.

Liao, K., Ma, S., Liu, C., Hu, H., Wang, J., Wu, B., and Ren, H. (2022). High concentrations of dissolved organic nitrogen and N-nitrosodimethylamine precursors in effluent from biological nutrient removal process with low dissolved oxygen conditions. *Water Research*, 216, 118336.

Lin, K. S., Chang, N. B., and Chuang, T. D. (2008). Fine structure characterization of zero-valent Iron nanoparticles for decontamination of nitrites and nitrates in wastewater. *Science and Technology for Advanced Materials*, 9, 025105.

Liu, C., Chen, D. W., Ren, Y. Y., and Chen, W. (2019). Removal efficiency and mechanism of phycocyanin in water by zero-valent iron. *Chemosphere*, 218, 402-411.

Liu, H., Dong, Y., Liu, Y., and Wang, H. (2010). Screening of novel low-cost adsorbents from agricultural residues to remove ammonia nitrogen from aqueous solution. *Journal of Hazardous Materials*, 178(1-3), 1132-1136.

Liu, Y., Cao, X., Yu, Z., Song, X., and Qiu, L. (2016). Controlling harmful algae blooms using aluminum-modified clay. *Marine Pollution Bulletin*, 103(1-2), 211-219.

Liu, Y., Xue, J., Gui, Z., Zhang, L., and Yao, X. (2023). Short-term photodegradation of autochthonous and allochthonous dissolved organic matter in Lake Taihu, China. *Environmental Science and Pollution Research*, 1-13.

Luk, G. K. and Au-Yeung, W. C. (2002). Experimental investigation on the chemical reduction of nitrate from groundwater. *Advances in Environmental Research*, 6(4), 441-453.

Ma, J., Lenhart, J. H., and Tracy, K. (2011). Orthophosphate adsorption equilibrium and breakthrough on filtration media for storm-water runoff treatment. *Journal of Irrigation and Drainage Engineering*, 137(4), 244-250.

Mahmood, T., Saddique, M. T., Naeem, A., Westerhoff, P., Mustafa, S., and Alum, A. (2011). Comparison of different methods for the point of zero charge determination of NiO. *Industrial & Engineering Chemistry Research*, 50(17), 10017-10023.

Martin, R. B. (1986). The chemistry of aluminum as related to biology and medicine. *Clinical Chemistry*, 32(10), 1797-1806.

MarvinSketch (2023). Marvin version 23.4, 2023, ChemAxon (http://www.chemaxon.com).” Accessed: Mar. 27, 2023. [Online]. Available: https://chemaxon.com/marvin

Maynard, H. E., Ouki, S. K., & Williams, S. C. (1999). Tertiary lagoons: a review of removal mechanisms and performance. *Water Research*, 33(1), 1-13.

McCleaf, P., Englund, S., Östlund, A., Lindegren, K., Wiberg, K., and Ahrens, L. (2017). Removal efficiency of multiple poly- and perfluoroalkyl substances (PFASs) in drinking water using granular activated carbon (GAC) and anion exchange (AE) column tests. *Water Research*, 120, 77-87.

McGowen, S. L., Basta, N. T., & Brown, G. O. (2001). Use of diammonium phosphate to reduce heavy metal solubility and transport in smelter-contaminated soil. *Journal of Environmental Quality*, 30(2), 493-500.

Merbt S. N., Auguet J. C., Blesa A., et al. (2015). Wastewater treatment plant effluents change abundance and composition of ammonia-oxidizing microorganisms in Mediterranean urban stream biofilms. *Microbial Ecology*, 69, 66-74.

Mittler, R. (2002). Oxidative stress, antioxidants, and stress tolerance. *Trends in Plant Science*, 7(9), 405-410.

Murphy, A. P. (1991). Chemical removal of nitrate from water. *Nature*, 350(6315), 223-225.

Naidu, R., Nadebaum, P., Fang, C., Cousins, I., Pennell, K., Conder, J., Newell, C., Longpré, D., Warner, S. and Crosbie, N. (2020). Per-and poly-fluoroalkyl substances (PFAS): Current status and research needs. Innovation, E.T.a. (ed), p. 100915, Elsevier.

Ordonez, D., Valencia, A., Elhakiem, H., Chang, N. B., and Wanielista, M. P. (2020a). Adsorption thermodynamics and kinetics of Advanced Green Environmental Media (AGEM) for nutrient removal and recovery in agricultural discharge and stormwater runoff. *Environmental Pollution*, *266*, 115172.

Ordonez, D., Valencia, A., Chang, N. B., and Wanielista, M. P. (2020b). Synergistic effects of aluminum/iron oxides and clay minerals on nutrient removal and recovery in water filtration media. *Journal of Cleaner Production*, 275, 122728.

Ordonez, D., Valencia, A., Pereira, B., and Chang, N. B. (2022a). Color removal for large-scale interbasin water transfer: Experimental comparison of five sorption media. *Environmental Research*, 212, 113208.

Ordonez, D., Podder, A., Valencia, A., Sadmani, A.A., Reinhart, D. and Chang, N.-B. (2022b) Continuous fixed-bed column adsorption of perfluorooctane sulfonic acid (PFOS) and perfluorooctanoic acid (PFOA) from canal water using zero-valent Iron-based filtration media. *Separation and Purification Technology,* 299, 121800.

Ordonez, D., Valencia, A., Sadmani, A.A. and Chang, N.-B. (2022c) Green sorption media for the removal of perfluorooctanesulfonic acid (PFOS) and perfluorooctanoic acid (PFOA) from water. *Science of the Total Environment*, 819, 152886.

Ordonez, D., Valencia, A., Cheng, J., and Chang, N. B. (2023). Exploring the differential effect of adsorption ingredients in three green sorption media for phosphorous removal from river water. *Journal of Water Process Engineering*, 55, 104073.

Özacar, M. and Şengil, İ. A. (2003). Enhancing phosphate removal from wastewater by using polyelectrolytes and clay injection. *Journal of Hazardous Materials*, 100(1-3), 131-146.

Pinheiro, I. G., Schmitz, P., and Houi, D. (1999). Particle capture in porous media when physico-chemical effects dominate. *Chemical Engineering Science*, 54(17), 3801-3813.

Pradhan, S., Helal, M. I., Al-Ghamdi, S. G., and Mackey, H. R. (2020). Performance evaluation of various individual and mixed media for greywater treatment in vertical nature-based systems. *Chemosphere*, *245*, 125564.

Prest E. I., Hammes, F., van Loosdrecht M. C. M., and Vrouwenvelder, J. S. (2016). Biological Stability of Drinking Water: Controlling Factors, Methods, and Challenges. *Front. Microbiol.* 7, 45.

Recht, H. L. and Masood, G. (1970). Kinetics and mechanism of precipitation and nature of the precipitate obtained in phosphate removal from wastewater using aluminum (III) and iron (III) salts. US Federal Water Quality Administration, 1970.

Ritchie, J. D. and Perdue, E. M. (2003). Proton-binding study of standard and reference fulvic acids, humic acids, and natural organic matter. Geochimica et cosmochimica acta, 67(1), 85-96.

Rotthauwe, J. H., Witzel, K. P. and Liesack, W. (1997). The ammonia monooxygenase structural gene amoA as a functional marker: molecular fine-scale analysis of natural ammonia-oxidizing populations. *Applied and Environmental Microbiology.* 63(12), 4704-4712.

Ryan, P., Wanielista, M., & Chang, N. B. (2010). Nutrient reduction in stormwater pond discharge using a chamber upflow filter and skimmer (CUFS). *Water, Air, and Soil Pollution*, 208, 385-399.

Saueia, C. H. R. and Mazzilli, B. P. (2006). Distribution of natural radionuclides in the production and use of phosphate fertilizers in Brazil. *Journal of Environmental Radioactivity*, 89(3), 229-239.

Scott, D. M., Lucas, M. C., and Wilson, R. W. (2005). The effect of high pH on ion balance, nitrogen excretion and behaviour in freshwater fish from an eutrophic lake: a laboratory and field study, *Aquat Toxicol*, 73(1), 31-43.

Sengco, M. R. and Anderson, D. M. (2004). Controlling harmful algal blooms through clay flocculation 1. *Journal of Eukaryotic Microbiology*, 51(2), 169-172.

Shammas, N. K. (2005). Coagulation and flocculation. In Physicochemical treatment processes (pp. 103-139). Humana Press, Totowa, NJ, USA.

Shrestha, P., Hurley, S. E., and Wemple, B. C. (2018). Effects of different soil media, vegetation, and hydrologic treatments on nutrient and sediment removal in roadside bioretention systems. *Ecological Engineering*, 112, 116-131.

Sima, M. W. and Jaffé, P. R. (2021). A critical review of modeling Poly-and Perfluoroalkyl Substances (PFAS) in the soil-water environment. *Science of the Total Environment,* 757, 143793.

Snoeyenbos-West, O. L., Nevin, K. P., Anderson, R. T., and Lovley, D. R. (2000). Enrichment of Geobacter species in response to stimulation of Fe (III) reduction in sandy aquifer sediments. *Microbial Ecology*, 39, 153-167.

Thomas, H. C. (1944). Heterogeneous ion exchange in a flowing system. *Journal of the American Chemical Society*, 66(10), 1664-1666.

Todisco, F., Vergni, L., and Ceppitelli, R. (2023). Modelling the dynamics of seal formation and pore clogging in the soil and its effect on infiltration using membrane fouling models. *Journal of Hydrology*, 618, 129208.

Tsushima, I., Kindaichi, T., and Okabe, S. (2007). Quantification of anaerobic ammonium-oxidizing bacteria in enrichment cultures by real-time PCR. *Water Research*, 41(4), 785-794.

Tsushima, I., Kindaichi, T., and Okabe, S. (2007). Quantification of anaerobic ammonium-oxidizing bacteria in enrichment cultures by real-time PCR. *Water Research*, 41(4), 785-794.

Valencia, A., Chang, N. B., Wen, D., Ordonez, D., and Wanielista, M. P. (2019). Optimal recipe assessment of iron filing-based green environmental media for improving nutrient removal in stormwater runoff. *Environmental Engineering Science*, 36(10), 1323-1336.

Valencia, A., Ordonez, D., Wen, D., McKenna, A. M., Chang, N. B., and Wanielista, M. P. (2020). The interaction of dissolved organic nitrogen removal and microbial abundance in iron-filings based green environmental media for stormwater treatment. *Environmental Research*, 188, 109815.

Wang, X., Wang, X., Zhao, J., Song, J., Wang, J., Ma, R., and Ma, J. (2017). Solar light-driven photocatalytic destruction of cyanobacteria by F-Ce-TiO2/expanded perlite floating composites. *Chemical Engineering Journal,* 320, 253-263.

Wang, S., Zhang, M., He, L., Li, M., Zhang, X., Liu, F., and Tong, M. (2022). Bacterial capture and inactivation in sand filtration systems with addition of zero-valent iron as permeable layer under both slow and fast filtration conditions. *Journal of Hazardous Materials*, 436, 129122.

Wanielista, M. and Chang, N. B. (2008). Alternative stormwater sorption media for the control of nutrients. Stormwater Management Academy, University of Central Florida, Orlando, FL, USA.

Wen, D. (2019). Comparative Nutrient Removal with Innovative Green Sorption Media for Groundwater and Stormwater Co-treatment. Ph.D. dissertation, University of Central Florida.

Wen, D., Chang, N. B., and Wanielista, M. P. (2020). Assessing nutrient removal in stormwater runoff for urban farming with iron filings-based green environmental media. *Scientific Reports*, 10(1), 9379.

Wen, D., Valencia, A., Ordonez, D., Chang, N. B., and Wanielista, W. P. (2020). Comparative nitrogen removal via microbial ecology between soil and green sorption media in a rapid infiltration basin for co-disposal of stormwater and wastewater, *Environmental Research,* 184, 109338.

WHO (2020). Cyanobacterial toxins: microcystins Background document for development of WHO Guidelines for drinking-water quality and Guidelines for safe recreational water environments. WHO (ed.).

Williams, K. A., Nelson, P. V., & Hesterberg, D. (2000). Phosphate and potassium retention and release during chrysanthemum production from precharged materials: I. Alumina. *Journal of the American Society for Horticultural Science*, 125(6), 748-756.

Xia, F., Wang, J. G., Zhu, T., Zou, B., Rhee, S. K., & Quan, Z. X. (2018). Ubiquity and diversity of complete ammonia oxidizers (comammox). *Applied and Environmental Microbiology* 84(24), e01390-18.

Xenopoulos, M. A., Barnes, R. T., Boodoo, K. S., Butman, D., Catalán, N., D'Amario, S. C., ... & Wilson, H. F. (2021). How humans alter dissolved organic matter composition in freshwater: relevance for the Earth's biogeochemistry. *Biogeochemistry*, 154, 323-348.

Xuan, Z., Chang, N. B., Wanielista, M., & Hossain, F. (2010). Laboratory-scale characterization of a green sorption medium for on-site sewage treatment and disposal to improve nutrient removal. *Environmental Engineering Science*, 27(4), 301-312.

Xu, C. Y., Li, J. Y., Xu, R. K., & Hong, Z. N. (2017). Sorption of organic phosphates and its effects on aggregation of hematite nanoparticles in monovalent and bivalent solutions. *Environmental Science and Pollution Research*, 24, 7197-7207.

Yan, G., Viraraghavan, T., & Chen, M. (2001). A new model for heavy metal removal in a Biosorption Column. *Adsorption Science & Technology*, 19(1):25-43.

Yang, Y., Sun, P., Padhye, L. P., & Zhang, R. (2021). Photo-ammonification in surface water samples: Mechanism and influencing factors. *Science of the Total Environment*, 759, 143547.

Yin, G., Hou, L., Liu, M., Li, X., Zheng, Y., Gao, J., ... & Lin, X. (2017). DNRA in intertidal sediments of the Yangtze Estuary. *Journal of Geophysical Research: Biogeosciences* 122(8), 1988-1998.

Yoon, Y. H., & Nelson, J. H. (1984). Application of gas adsorption kinetics I. A theoretical model for respirator cartridge service life. *American Industrial Hygiene Association Journal* 45(8), 509-516.

Yu, Z., Song, X., Cao, X., & Liu, Y. (2017). Mitigation of harmful algal blooms using modified clays: Theory, mechanisms, and applications. *Harmful Algae*, 69, 48-64.

Zhang, Y., Li, Y., Li, J., Hu, L., & Zheng, X. (2011). Enhanced removal of nitrate by a novel composite: nanoscale zero valent iron supported on pillared clay. *Chemical Engineering Journal*, 171(2), 526-531.

Zhang, Y., Zhang, R., Li, S. L., Mostofa, K. M., Fu, X., Ji, H., ... & Sun, P. (2021). Photo-ammonification of low molecular weight dissolved organic nitrogen by direct and indirect photolysis. *Science of the Total Environment*, 764, 142930.

Zhang, M., Dong, X., Li, X., Jiang, Y., Li, Y., and Liang, Y. (2020). Review of separation methods for the determination of ammonium/ammonia in natural water. *Trends Environ. Anal. Chem.*, 27, p. e00098.

Zhao, Y., Wu, X., Chang, W., Che, W., Liu, Y., & Li, Y. (2023). A novel magnetic buoyant-bead flotation method for the removal of typical microalgae from harmful algal blooms. *Journal of Environmental Chemical Engineering*, 11(3), 110170.